



## Chronology of thrust propagation from an updated tectonosedimentary framework of the Miocene molasse (western Alps)

Amir Kalifi, Philippe Hervé Leloup, Philippe Sorrel, Albert Galy, François Demory, Vincenzo Spina, Bastien Huet, Frédéric Quillévéré, Frédéric Ricciardi, Daniel Michoux, et al.

### ► To cite this version:

Amir Kalifi, Philippe Hervé Leloup, Philippe Sorrel, Albert Galy, François Demory, et al.. Chronology of thrust propagation from an updated tectonosedimentary framework of the Miocene molasse (western Alps). *Solid Earth*, 2021, 12 (12), pp.2735-2771. 10.5194/se-12-2735-2021 . hal-03534316

**HAL Id: hal-03534316**

**<https://hal.science/hal-03534316>**

Submitted on 19 Jan 2022

**HAL** is a multi-disciplinary open access archive for the deposit and dissemination of scientific research documents, whether they are published or not. The documents may come from teaching and research institutions in France or abroad, or from public or private research centers.

L'archive ouverte pluridisciplinaire **HAL**, est destinée au dépôt et à la diffusion de documents scientifiques de niveau recherche, publiés ou non, émanant des établissements d'enseignement et de recherche français ou étrangers, des laboratoires publics ou privés.



Distributed under a Creative Commons Attribution 4.0 International License

# Chronology of thrust propagation from an updated tectono-sedimentary framework of the Miocene molasse (western Alps)

Amir Kalifi<sup>1,2</sup>, Philippe Hervé Leloup<sup>1</sup>, Philippe Sorrel<sup>1</sup>, Albert Galy<sup>3</sup>, François Demory<sup>4</sup>, Vincenzo Spina<sup>2</sup>, Bastien Huet<sup>2</sup>, Frédéric Quillévéré<sup>1</sup>, Frédéric Ricciardi<sup>2</sup>, Daniel Michoux<sup>2</sup>, Kilian Lecacheur<sup>1</sup>,  
5 Romain Grime<sup>1</sup>, Bernard Pittet<sup>1</sup>, Jean-Loup Rubino<sup>2</sup>

<sup>1</sup> Univ Lyon, Univ Lyon 1, ENSL, CNRS, LGL-TPE, F-69622, Villeurbanne, France.

<sup>2</sup> Total SA, CSTJF, Avenue Larribau, 64000 Pau, France.

<sup>3</sup> CRPG, 15 rue Notre Dames des Pauvres, 54500 Vandœuvre-lès-Nancy, France.

<sup>4</sup> Aix Marseille Univ, CNRS, IRD, INRAE, Coll France, CEREGE, Aix-en-Provence, France

Correspondence to: Amir Kalifi ([kalifi.amir@gmail.com](mailto:kalifi.amir@gmail.com))

**Abstract.** After more than a century of research, the chronology of the deformation of the external part of the western Alpine belt (France) is still controversial for the Miocene epoch. In particular, the poor dating of the foreland basin sedimentary  
15 succession hampers a comprehensive understanding of the deformation kinematics. Here we focus on the Miocene Molasse deposits of the northern subalpine massifs, southern Jura, Royans, Bas-Dauphiné, Crest and La Bresse sedimentary basins through a multidisciplinary approach to build a basin-wide tectono-stratigraphic framework. Based on sequence stratigraphy constrained by biostratigraphical, chemostratigraphical (Sr-isotopes) and magnetostratigraphical data between the late Aquitanian (~21 Ma) and the Tortonian (~8.2 Ma), the Miocene Molasse chronostratigraphy is revised with a precision of ~0.5  
20 Ma. The Miocene Molasse sediments encompass four different paleogeographical domains: (i) the oriental domain, outlined by depositional sequences S1a to S3 (~21 to ~15 Ma), (ii) the median domain characterized by sequences S2 to S5 (~17.8 to ~12 Ma), (iii) the occidental domain, in which sequences S2a to S8 (~17.8 to ~8.2 Ma) were deposited and, (iv) the Bressan domain, where sedimentation is restricted to sequences S6 to S8 (~12 to ~8.2 Ma). A structural and tectono-sedimentary study is conducted based on new field observations and the reappraisal of regional seismic profiles, thereby allowing the  
25 identification of five major faults zones (FZ). The oriental, median and occidental paleogeographical domains are clearly separated by FZ1, FZ2 and FZ3, suggesting strong interactions between tectonics and sedimentation during the Miocene. The evolution in time and space of the paleogeographical domains within a well-constrained structural framework reveals syntectonic deposits and a westward migration of the depocenters, allowing to propose the succession of three deformation phases at the western alpine front: (i) A compressive phase (P1) corresponding to thrusting above the Chartreuse Orientale  
30 Thrust (FZ1), which was likely initiated during the Oligocene and rooted east of Belledonne. This tectonic phase generated reliefs that limited the Miocene transgression to the east; (ii) a ~W-WNW/E-ESE-directed compressive phase (P2) lasting between 18.05 +/- 0.25 Ma and ~12 Ma, with thrusts rooted in the Belledonne basal thrust. Thrusts were activated from East to west: the Salève (SAL) and Gros Foug (GF) thrusts and then successively FZ2, FZ3, FZ4 and FZ5. Along two E-W balanced cross-section the amount of horizontal shortening is of ~6.3 to 6.7 km corresponding to average shortening rates of ~1.2 km



35  $\text{Ma}^{-1}$ , and migration of the deformation toward the west at a rate of  $\sim 2.9 \text{ km Ma}^{-1}$ . During  $\sim 6 \text{ Myr}$ , the Miocene Sea was forced  
to regress rapidly westwards in response to westward migration of the active thrusts and exhumation of piggy-back basins atop  
the fault zones. Phase P2 thus deeply shaped the Miocene paleogeographical evolution of the area, and appears as a prominent  
compressive phase at the scale of the western Alps from the Swiss Molasse basin to the Rhodano-Provençal one. (iii) a  $\sim 300\text{m}$   
phase of uplift in the Bas-Dauphiné (P3) of probable Tortonian age ( $\sim 10 \text{ Ma}$ ), which would have induced southward sea-  
40 retreat, and be coeval with the folding of the Jura in the north and possibly with back-thrusting east of the Chartreuse massif.

## 1 Introduction

Foreland basins result from the flexural warping of the lithosphere in response to the orogenic load induced by a continental  
collision (Dickinson, 1974; Beaumont, 1981). Along the flexural profile of the foreland basin, the accommodation space  
increases progressively towards the orogeny and is maximal near the deformation front (DeCelles and Giles, 1996). As the  
45 deformation front advances, the entire flexural profile is forced to migrate, and additional secondary controls interact with the  
flexural migration. Thrust systems are activated synchronously with the sedimentary infill between the deformation front and  
the inner part of the orogenic wedge. There, small-scale basins are carried on top of growing thrusts and constitute “piggy-  
back basins” (Ori and Friend, 1984). As a result, foreland basin strata (including piggy-back basins, DeCelles and Giles, 1996)  
are among the most reliable witness of the geometry and kinematics of growing structures (Suppe et al., 1992) and thus, of the  
50 advance of the deformation front.

The arcuate form of the Western Alps results from a N-NW-directed continental collision from Eocene to earliest Oligocene  
(Ford and Lickorish, 2004; Dumont et al., 2008, 2011, 2012) then W directed motion driven by extrusion of the internal  
Western Alps, leading to the radially propagating arc (Butler, 1992a; Dumont et al., 2011, 2008). This evolution was recorded  
in the foreland basin strata. From the Oligocene to the Aquitanian, the larger flexural basin was located in the North Alpine  
55 Foreland Basin (NAFB, Fig. 1A) where Molasse deposits are very thick (up to 4 km; Bonnet et al., 2007; Burkhard and  
Sommaruga, 1998). During the middle to late Miocene, the NAFB was uplifted (Ford and Lickorish, 2004), and the depocenter  
migrated to the west along the western Alpine Foreland basin in France (Allen and Bass, 1993; Lamiriaux, 1977) (Fig. 1A).  
The present study focuses on the transitional area between these two domains (Fig. 1A), which correspond to the southern  
prolongation of the NAFB (southern Jura synclines) constituted by lower Miocene strata, and the northern termination of the  
60 western Alpine Foreland basin (Bas-Dauphiné basin) constituted mainly by middle to upper Miocene deposits (Latreille, 1969;  
Nicolet, 1979; Kwasniewski et al., 2014). The Bas-Dauphiné basin is located in front of the Vercors and Chartreuse subalpine  
massifs and southern Jura synclines (Fig. 1B) where Miocene deposits outcrop in piggy-back basins above NNE-SSW trending  
Miocene thrusts that root in a basement thrust below the External Crystalline Massifs (ECM) (Laubscher, 1992; Bellahsen et  
al., 2014; Deville and Chauvière, 2000; Deville et al., 1994, 1992). In the NAFB and the southern Jura synclines, Miocene  
65 syntectonic deposits date from the late Burdigalian (e.g. Allen and Bass, 1993; Beck et al., 1998; Deville et al., 1994;  
Garefalakis and Schlunegger, 2019) and a westward depocenter migration occurred between the early and the middle Miocene

(Lamiriaux, 1977; Bass, 1991). Further south, in the Vercors-Chartreuse and Bas-Dauphiné basins, syn-tectonic deposits are, however, still insufficiently described. Hence this hampers a comprehensive understanding of the onset, and the chronology, of the Alpine deformation over the Miocene.

70 This study aims at reappraising the Miocene deformation history of the Western Alpine foreland basin. Based on  $^{87}\text{Sr}/^{86}\text{Sr}$  dating combined with new sedimentological fieldworks, new sequence stratigraphy interpretations for upper Aquitanian to lower Langhian sedimentary successions outcropping in piggy-back basins of the subalpine massifs and the southern Jura synclines have been proposed (Kalifi et al., 2020). Here, we complete this work with data from the Bas-Dauphiné, Crest and La Bresse basins, and propose an updated chronostratigraphy for the whole area based on integrated biostratigraphical, magnetostratigraphical and new chemiostratigraphical dating of well-logs and field sedimentological sections. A new structural analysis is also conducted based on fieldwork data along with a re-interpretation of available seismic lines, geological maps and published cross-sections. Taken together, the sedimentological, chronostratigraphical and structural approaches enable an updated calendar of the Subalpine massifs and Southern Jura deformations and shortening phases, as a response to the western propagation of the Alpine orogen during the Miocene.

## 80 2 Geological setting

The western Alpine foreland basin corresponds to a part of the peripheral foreland basin of the Cenozoic Alpine orogeny (Fig. 1A). The Alpine orogeny originates from the closure of the Tethyan Ocean and subsequent continental collision between Eurasia and Adria (or Apulia) (Nicolas et al., 1990; Pfiffner et al., 1997; De Graciansky et al., 2011). The study area (Fig. 1B) includes (i) the subalpine massifs (i.e., Vercors, Chartreuse and Bauges massifs) and the French southern Jura, where the Miocene “Molasse” deposits are preserved within synclinal structures and constitute the infill of piggy-back basins; (ii) the Bas-Dauphiné, La Bresse and Crest basins (Fig. 1B), where deposits are poorly deformed and constitute the infill of the foreland basin. These deposits generally lie unconformably on the thick Mesozoic substratum, or conformably on Oligocene continental deposits (Bass, 1991; Butler, 1992b; Kalifi et al., 2020; Allen and Bass, 1993; Gidon and Arnaud, 1978), and result from the second shallowing-upward cycle of the western alpine foreland basin overfilled phase (Sinclair and Allen, 1992). During this cycle, the regional paleogeography corresponded to a narrow and shallow seaway that connected the Mediterranean Sea (ex-Tethys) to the NAFB (ex-ParaTethys, Allen and Bass, 1993; Bass, 1991; Demarcq, 1970; Rubino et al., 1990).

In the study area, the Cenozoic chronostratigraphical framework is still poorly constrained and relies mainly on lithostratigraphical subdivisions (Giot, 1943; Pelin, 1965; Bocquet, 1966; Latreille, 1969; Lamiriaux, 1977; Mortaz-Djalili, 1977; Mortaz-Djalili and Perriaux, 1979; Nicolet, 1979; Mujito, 1981; Bass, 1991; Allen and Bass, 1993; Berger, 1985, 1992), since biostratigraphical data are scarce. The main compressive phase has been commonly dated to the end of the Miocene (i.e., Tortonian to Messinian; ~11–5 Ma) (Butler, 1989, 1992b; Gidon et al., 1978). However, seismic data from the southern Jura synclines (Deville et al., 1994; Beck et al., 1998), as well as field observations (Blanc, 1991; Kalifi et al., 2020), suggest that

deformation started much earlier with syntectonic sedimentation of the earliest marine deposits (Burdigalian-Langhian; 20–14 Ma).

100  $^{87}\text{Sr}/^{86}\text{Sr}$  and sedimentological analyses (Kalifi et al., 2020) defined a new and well-constrained sequence stratigraphy for the lower Miocene (with depositional sequences S1, S2 and S3 deposited from the late Aquitanian [ $\sim 21.3$  Ma] to the early Langhian [ $\sim 16$  Ma]) in piggy-back basins (e.g., the subalpine massifs and the southern Jura area). The upper Burdigalian onset of the deformation is evidenced by the sedimentary transition of flexural subsiding distal deposits to syntectonic proximal deposits (Kalifi et al., 2020). This transition corresponds to the westward progressive migration of the orogenic wedge towards  
105 the foreland basin and is materialized by: (i) a shallowing-upward sedimentation defined by shallow-marine successions capped by gravel-rich fan delta (marine to continental) and continental (fluvial) deposits; (ii) growth strata relationships, and (iii) abnormally-thick sediment accumulations induced by an increased subsidence due to the migration of the depocentre located in front of the adjacent thrust belt and their piggy-back basins.

In the study area, the principal structures correspond to cover folds and thrusts striking NNE-SSW. The thrusts juxtapose  
110 Mesozoic units over Cenozoic or Upper Cretaceous units and accommodate the last  $\sim$ WNW-ESE shortening phase of the Alpine collision wedge (Mugnier et al., 1990; Doudoux et al., 1982; Bellahsen et al., 2014; Menard and Thouvenot, 1987). On one hand, based on geophysical data, most of the authors propose that the thrusts are rooted in basement thrust(s) below the Belledonne massif (Guellec et al., 1990; Deville et al., 1994; Deville and Chauvière, 2000; Bellahsen et al., 2014). On the other hand, Gidon (2001) stress out that there is no clear field evidence for such thrust below belledonne, but rather for  
115 shortening and thrusting affecting the Mesozoic grabens within Belledonne. Balanced sections of the sedimentary cover document that horizontal shortening increases from the Vercors ( $\sim 6$  km) to the Chartreuse ( $\sim 22$  km) (Mugnier et al., 1987; Bellahsen et al., 2014; Philippe et al., 1996, 1998).

The easternmost major thrust has large, up to 10 km offsets (Deville and Chauvière, 2000). To the north, at the front of the Bauges and Bornes massifs (Fig. 1B), this thrust corresponds to the “*chevauchement des nappes inférieures*” of Doudoux et al. (1982), and the “*chevauchement frontal des Bauges*” ( $\phi\text{B}$ , Fig. 1B) of Gidon (1999). The thrust extends southwards in the Chartreuse massif, and was named differently by various authors (Gidon, 1964; Butler and Bowler, 1995; Gidon and Arnaud, 1978; Gidon et al., 1978; Deville and Chauvière, 2000; Philippe et al., 1998). The southern prolongation of this fault beyond the Isère valley is contentious, but possibly corresponds to the “Moucherotte thrust” ( $\phi\text{Mo}$ , Fig. 1B) (Debelmas, 1965; Gidon, 1981; Donzeau et al, 1993), whose geometry and structural interpretation are still debated (Gignoux and Moret, 1952;  
125 Debelmas, 1953, 1966; Gidon, 1981). We discuss that point in more details below (§ 4.3).

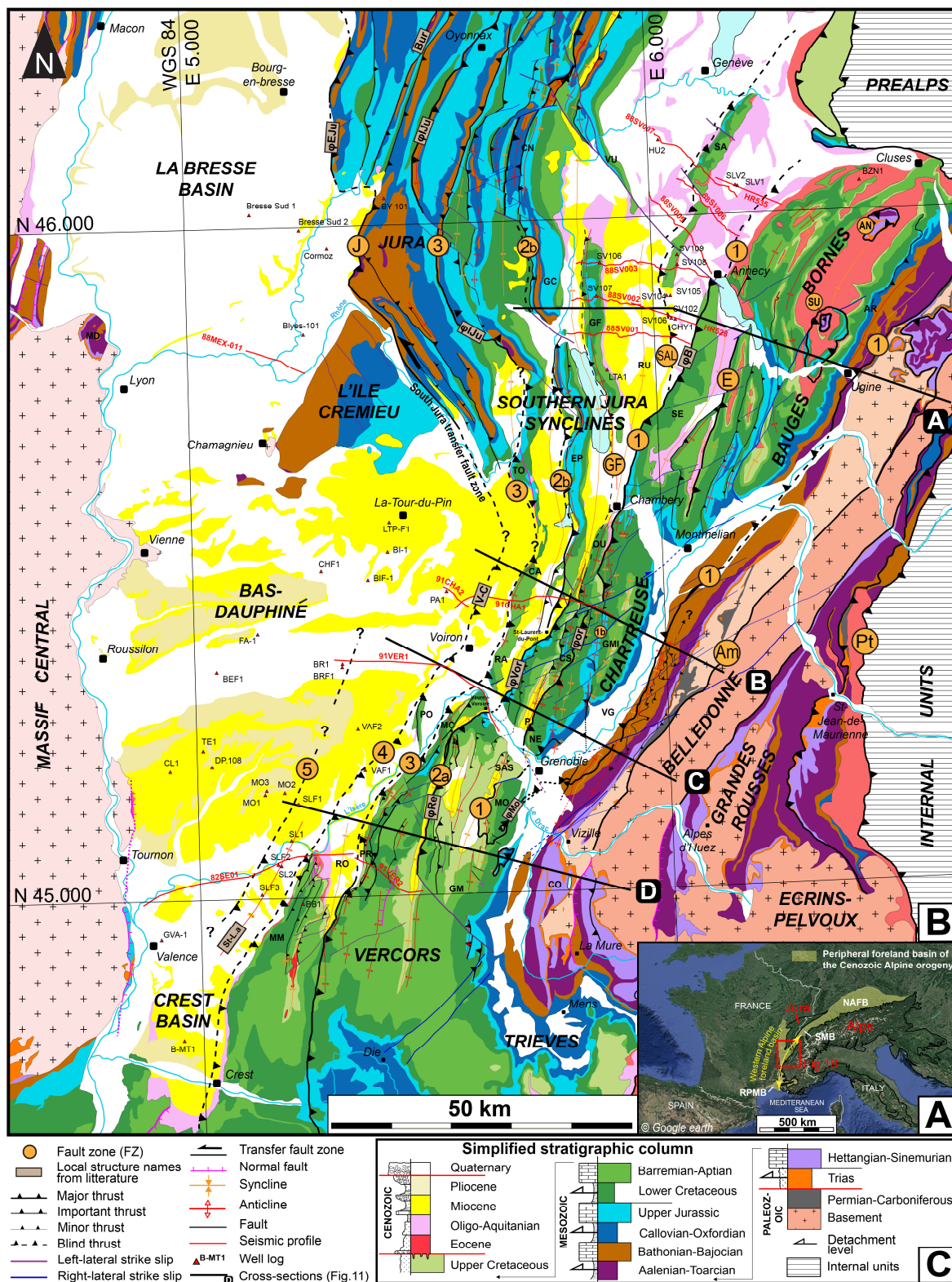


Figure 1: (A) Location of the western Alpine foreland basin and the study area. NAFB= North Alpine foreland basin. SMB= Swiss Molasse basin. RPMB= Rhodano-Provençal Molasse basin. (B) Structural map of the subalpine massifs, the southern Jura and adjacent basins (Bas-Dauphiné, Crest, La Bresse). Names of the main faults are indicated within orange circles: 1 to 5 are Fault Zones (FZ) defined in this study; PT= Penninic thrust; Am= Internal Belledonne thrust; E= Entrevignes thrust; SAL = Saleve thrust; J= Jura thrust; SU= Sulens klippen; AN= Annes klippe. Local fault names from the literature:  $\phi$ B= Bauges thrust;  $\phi$ EJu= External Jura thrust;  $\phi$ IJu= Internal Jura thrust;  $\phi$ Mo= Moucherotte thrust;  $\phi$ or= Oriental Chartreuse thrust;  $\phi$ vor= Voreppe thrust;  $\phi$ Re= Rencurel thrust; Bur= Buron thrust; St-L.a= Saint Lattier anticline; V-C= Voiron-Chirens fault. Local ranges and structures names: AR= Aravis ; CA= Chailles ; CN= Crête du Nu ; CO= Conest ; EP= Epine ; GC= Grand Colombier ; GM= Grande Moucherotte ; GMI= Grand Manti ; GF= Gros Foug anticline; MC= Montaud col; MD= Monts-d'or ; MM= Monts-du-Matin ; MO= Moucherotte ; NE= Néron ; P= Proveyzieux anticline ; PO= Poliénas ; PR= Pont-en-Royans anticline ; OU= Outherans ; RA= Ratz ; RO= Royans ; RU= Rumilly syncline ; SA= Salève ; SAS= Sassenage ; SE= Semnoz ; TO= Tournier ; VG= Grésivaudan valley ; VU= Vuache. Seismic profiles appear as red lines and wells as red triangles. (C) Simplified synthetic stratigraphic column of the area stressing out the main unconformities (red lines) and potential detachment levels (arrows). Same colours as for Figures 3, 7, 8, 9, 10, 11, 14, S1.

West of this thrust zone, other major thrusts involve Miocene Molasse deposits. In the Vercors massif, from east to west, these thrusts are: (i) the “*Rencurel thrust*” ( $\phi$ Re, Fig. 1B) or the “*thrust zone 3*” (Watkins et al., 2017). In the South, the thrust originates at the tip of a NW-SE left-lateral ramp (Barfèty et al., 1967; Gidon, 1964), and can be followed to the north until the Montaud col (MC, Fig. 1B). Its northward prolongation is still disputed: the thrust is connected either to the northern part of the “*thrust zone 2*” (Watkins et al., 2017) (see below), or to the “*Voreppe thrust*” in the Chartreuse Massif ( $\phi$ Vor, Fig. 1B) (Gidon, 2018; Gidon and Arnaud, 1978); (ii) the tectonic front of the Vercors massif, which partly corresponds to the “*thrust zone 2*” of Watkins et al. (2017), (iii) the “*thrust zone 1*” (Watkins et al., 2017) at the western border of the Monts-du-Matin massif (MM, Fig. 1B); (iv) the “*St-Lattier anticline*” (St-L.a, Fig. 1B) (Deville et al., 1992).

In the Chartreuse massif, at least three thrust zones exist west of the “*Chevauchement de la Chartreuse orientale*” ( $\phi$ Or, Fig. 1B). From east to west they are: (i) the “*Voreppe thrust zone*” ( $\phi$ Vor, Fig. 1B) (Butler and Bowler, 1995; Gidon, 1994), also named the “*Voreppe fault*” (Gidon et al., 1978; Gidon and Arnaud, 1978) or the “*chevauchement  $\phi$ 1 de la Chartreuse occidentale*” (Gidon, 1988; or “*F1*”, Gidon, 1964). From St-Laurent-du-Pont northwards, the prolongation of this accident becomes unclear (Butler, 1992a); (ii) the Ratz anticline (RA, Fig. 1B) corresponding to the tectonic front of the Chartreuse massif and, (iii) the “*Voiron-Chirens*” fault (V-C, Fig. 1B) indirectly deduced from a 100m vertical offset of middle Miocene deposits (Nicolet, 1979).

Further north, west of the Bauges and Bornes massifs, the southern Jura synclines widen progressively northwards. The synclines are separated by anticlines that develop in the hangingwalls of blind thrust (Beck et al., 1998; Doudoux et al., 1982; Lickorish et al., 2002). From west to east, these anticlines are: (i) the Salève mountain (SA, Fig. 1B) (Gorin et al., 1993; Mastrangelo and Charollais, 2018) and (ii) the Gros Foug mountain (GF, Fig. 1B). Further west, in the Jura massifs, three main thrust systems exist from east to west: (i) the thrust involving the Grand-Colombier anticline (GC, Fig. 1B); (ii) the “*chevauchement interne du Jura*” ( $\phi$ IJu, Fig. 1B) (Philippe, 1995) which corresponds to the northern prolongation of the thrust involving the Tournier anticline (TO, Fig. 1B) and, (iii) the “*chevauchement externe du Jura*” ( $\phi$ EJu, Fig. 1B) (Philippe, 1995).

At the latitude of Chambéry, the transition between widely spaced and more closely spaced thrusts and folds (Fig. 1B) has been attributed to the presence of a more efficient décollement level in the Triassic layers in the north (Philippe, 1995; Philippe et al., 1996).

As mentioned above, the detailed chronology of these thrusts is poorly constrained. Moreover, Miocene deposits were poorly investigated in the Vercors and Chartreuse massifs. As a result, the main compressive phase could have started during the late Miocene (Gidon et al., 1978; Gidon ([www.geol-alp.com](http://www.geol-alp.com)); Butler, 1989b, 1989a, 1992a, 1992b). However, this is off-phase with the observations to the north, in the southern Jura, where detailed investigation of lower Miocene deposits in seismic profiles and field observations revealed seismites and growth-strata relationships which suggests that a compressive phase started during the early Miocene (Deville et al., 1994; Beck et al., 1998; Blanc, 1991; Rangheard et al., 1990).

### 3 Material and methods

Sedimentological and stratigraphical analyses were conducted from 35 well-outcropping sections of the Miocene Molasse deposits (sections 4, 5, 13, 16, 22 are detailed in Kalifi et al., 2020), and from partially preserved sections (<40m) outcropping in adjacent localities. Sedimentary successions, up to 1050 m-thick, were logged at the decimeter (dm) to meter (m) scale resolution in the field. Using the combined analyses of textural characteristics, clastic and biogenic components, bed thickness, bed organization and geometry, sedimentary structures and paleocurrent measurements, 25 facies grouped into 11 facies associations (FA) were previously defined by Kalifi et al. (2020). Building on these results and using the same methodology, depositional sequences were identified based on facies associations evolution and the main stratigraphical surfaces (Embry, 1993, 1995). Depositional sequences identified, using Posamentier and Allen (1999) methodology on spontaneous potential (SP) and gamma-ray logs (GR) data from 28 well-logs located in the Bas-Dauphiné basin.

Three dating approaches have been combined in order to constrain the ages of the depositional sequences. The results have been calibrated on the GTS2016 chronostratigraphic chart (Ogg et al., 2016).

Biostratigraphical dating was conducted on field and well-log samples using calcareous nannofossils (calibrated using Young et al., 2017), dinoflagellate cysts (using Hardenbol et al. (1998) biozonation and calibrated using TimeScale Creator 7.4), and foraminifera (calibrated using BouDagher-Fadel (2015), Lirer et al. (2019) and Wade et al. (2011) biozonations; see Kalifi, 2020 for details). Calcareous nannofossils, foraminifera and mammal dating available in the literature were also implemented (21 mammal localities were calibrated on the GTS 2016 using Time scale Creator 7.4, see Kalifi, 2020 for details).

Strontium (Sr) isotopes dating was performed on samples collected in the field, as well as on a few well-log samples. To the 57 samples published by Kalifi et al. (2020) we add 72 new samples (Table S1). The Sr isotope ratios were measured on marine carbonate skeletons (oysters and pectens) at CRPG (Centre de Recherches Pétrographiques et Géochimiques) in Nancy. A thorough inspection of shells was preliminarily conducted at TOTAL using (i) cathodoluminescence, in order to select shells yielding a pristine structure as well as to avoid recrystallized structures; (ii) and/or stable isotope ratios ( $\delta^{13}\text{C}$  and  $\delta^{18}\text{O}$ ), in order to evaluate possible diagenetic disturbance (Hudson, 1977; Nelson and Smith, 1996; Hudson, 1975). The maximum

confidence zone corresponds to  $\delta^{13}\text{C}$  values between + 3.5 ‰ and – 1 ‰, as the global ocean  $\delta^{13}\text{C}$  during Miocene was between 0 and + 2.5 ‰ (Hayes et al., 1999) and an additional margin of about +/- 1 ‰ must be applied for epicontinental seas (Saltzman and Thomas, 2012). Samples with  $\delta^{13}\text{C}$  values lower than -5 ‰ are excluded as they are considered as diagenetized (Kalifi, 2020). Corresponding ages are derived from measured  $^{87}\text{Sr}/^{86}\text{Sr}$  ratios using the LOWESS non-parametric regression curve of McArthur et al. (2012). A mean value was calculated where more than one sample was available for one stratigraphic level. The average of the  $^{87}\text{Sr}/^{86}\text{Sr}$  ratios was converted to ages using the LOWESS 5 table (McArthur et al., 2012). The average uncertainty corresponds to the largest value between the values defined by 2 standard errors or s.e. (= 2 x the standard deviation of isotopic ratios divided by the square root of the number of data involved) and the individual minimum error of the sample (taking into account the measurement error and the standard error). More details about the geochemical analyses used in this study are given in Kalifi (2020) and Kalifi et al. (2020).

Paleomagnetic results were obtained for 84 samples. 33 and 51 oriented cores or blocks were retrieved from the Forezan (24 layers) and Grésy-sur-Aix (48 layers) sedimentary sections 4 and 5. Samples were subjected to stepwise alternating field (AF) demagnetization, thermal demagnetization or a composite procedure (Thermal up to 350°C and then AF) of the Natural Remanent Magnetization (NRM). All remanent magnetizations were measured using the Superconducting Rock Magnetometer SRM 760R (2G Enterprises) of the CEREGE (Aix-en-Provence, France). AF online and thermal experiments were performed using the magnetically-shielded oven MMTD80 (Magnetic Measurements Ltd.). All paleomagnetic results (directions, treatment and statistics) are archived in Table S1. According to the moderate quality of the paleomagnetic results (especially for the Grésy-sur-Aix section) and the rather low values of bedding dips, no fold test could be calculated. The magnetic component most resistant to the demagnetization protocols was considered to be (or be close to) the directional geomagnetic signal acquired during just after deposition of magnetic particles.

The structural study was carried out by a systematic reappraisal of published structural maps and cross-sections at the light of new field data. Published geological maps at 1:50000 scale (BRGM), as well as local structural observations and cross-sections (i.e. <http://www.geol-alp.com> and references therein) were used together with new field observations (stratification and fault measurements, observation of panoramas, study of stratigraphic successions) in key areas at 821 locations (Fig. S1) to determine the geometry of the structures and their continuity. Bedding measurements are listed in Table S6. Seismic profiles (Fig. 1B) that partially penetrate the front of the subalpine chains are located on the western edge of the Vercors and Chartreuse massifs (91CHA1-2, 91VER1, 82SE01-91VER2, published in Deville, 2021) and on the western edge of the Bauges and Bornes massifs (88SV01, 88SV02-HR528, 88SV03, 88SV05, 88SV06, 88SV07-HR535; Gorin et al., 1993; Signer and Gorin, 1995; Beck et al., 1998; available at BRGM) and were reinterpreted by using the stratigraphic column presented in Figure 1 and by integrating new field data. Interpretations may differ from those of Deville (2021) published after the realization of this study. Further information has been obtained from well-logs in the southern Jura synclines, the La Bresse and Bas Dauphiné basins (Fig. 1B). The combined analysis of these data allows us to propose a new structural map of the area (Fig. 1B) along with four regional cross-sections (A to D). The cross-sections B and C in the Chartreuse massif were balanced and restored backward taking in consideration the timing of deformation provided by this study, using the “flexural slip algorithm” of the

230 Move software. In order to ensure realistic fault geometries, the restoration was performed using the top of the most laterally continuous pre-thrusting unit (i.e. Barremian-Aptian limestones).

## 4 Results and interpretations

### 4.1 Dating

#### 4.1.1 Chemostratigraphy

235 129 Sr dating results are compiled in this study (Table S2). 12 samples display evidence for diagenetic alteration with  $\delta^{13}\text{C}$  values  $< -5\text{‰}$  (Table S2) and cathodoluminescence imagery exhibiting recrystallization patterns. Since their stable isotopes data exhibit no evidence of diagenetic bias ( $\delta^{13}\text{C} > -5\text{‰}$ ) but the obtained ages are older than the age of the stratigraphic level four samples were further interpreted as reworked samples, and considered as outliers (Table S2). Excluding those 16 recrystallized or outlier samples, the  $^{87}\text{Sr}/^{86}\text{Sr}$  ratios range between 0.708338 and 0.708914 corresponding to stratigraphic ages  
240 between 21.45  $\pm$  0.30 Ma (late Aquitanian) and 8.58  $\pm$  1.78 Ma (Tortonian), thereby allowing to date 113 stratigraphic levels.

#### 4.1.2 Magnetostratigraphy

For the Forezan and Grésy-sur-Aix sections (respectively sections 5 and 4, Fig. 2; locations in Fig. 3), the NRM intensity ranges between  $1.53 \cdot 10^{-5}$  and  $8.43 \cdot 10^{-3} \text{ Am}^{-1}$  with an average of  $1.12 \cdot 10^{-3} \text{ Am}^{-1}$ , and between  $3.19 \cdot 10^{-5}$  and  $3.95 \cdot 10^{-3} \text{ Am}^{-1}$  with  
245 an average of  $8.83 \cdot 10^{-4} \text{ Am}^{-1}$ , respectively. The Forezan section (enriched in clayey facies) presents slightly higher NRM intensities and better paleomagnetic results probably due to finer and more abundant ferromagnetic grains. Orthogonal projection of paleomagnetic results exhibits different patterns: (i) a stable reverse polarity slightly overprinted by a normal polarity (Fig. S2A) in many samples of the Forezan sedimentary section, (ii) a large normal overprint with a path toward reverse polarity (Fig. S2B) for many samples of the Grésy sedimentary section, (iii) rarely stable normal polarity (Fig. S2C)  
250 attributed to full normal remagnetization, or eventually a subchron, and (iv) in the 868-870m interval of the Grésy section (for 2 neighboring samples), a stable normal polarity affected by a post-lock tilting (Fig. S2D). Declination and inclination of the stable magnetization, or the direction displayed in the very last steps of demagnetization, were plotted together with the reversal angle (Fig. S3A, B). Due to large normal magnetic overprints, the reversal angle, which is the angle between the calculated direction and the expected direction for the normal geomagnetic polarity, helps to determine geomagnetic polarity scale  
255 especially in carbonates affected by partial but intense remagnetizations (e.g. Demory et al., 2011). The entire Forezan sedimentary section displays very high reversal angles (Fig. S3A) attributed to the record of the reverse geomagnetic Chron C5Cr according to the age frame inferred from Sr dating (Fig. 2). Most of the Grésy-sur-Aix section is characterized by reverse polarities except from the normal polarity recorded at 772 m, which may be attributed to Subchron C5Dr.1n., and tilted normal



polarities (Fig. S2D and Fig. S3B) located at 868 m - just below a major unconformity – that may be related to the record of  
 260 Chron C5Dn (Fig. 2). In the case of post-lock tilting, the reversal angle is higher than expected for normal polarity.

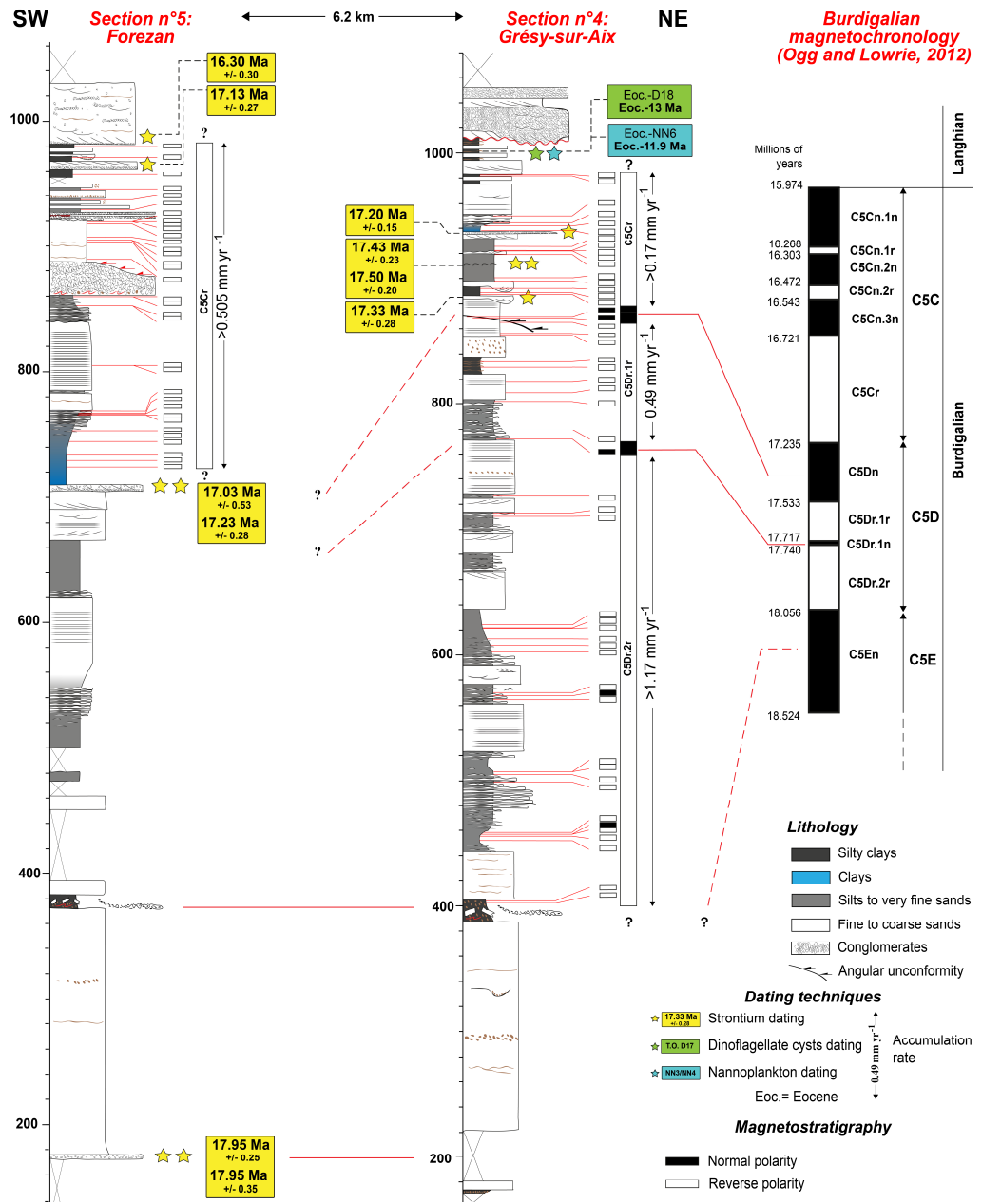


Figure 2: Magnetostratigraphy of the Forézán and Grésy-sur-Aix sections, integrated with Strontium and biostratigraphic dating.

### 4.1.3 Biostratigraphy

34 out of 74 analyzed samples enabled the biostratigraphical dating of sedimentary sections based on nannofossil assemblages  
 265 (Table S3). Species that allowed precise stratigraphical calibrations are *Coccolithus miopelagicus* (NN5–NN8; 14.91–10.55

Ma), *Helicosphaera ampliaperta* (middle part of NN2–top NN4; 20.4–14.91 Ma), *Helicosphaera scissura* (upper NN2–NN5; 20.1–14.91 Ma), *Helicosphaera stalis* (NN6–NN11; 13.53–5.59 Ma), *Sphenolithus belemnoides* (base NN3–top NN3; 19–18 Ma), *Sphenolithus heteromorphus* (base NN4–top NN5; 18–13.5 Ma).

21 out of 34 analyzed samples allowed biostratigraphical constraints from dinoflagellate cyst assemblages (Table S4). Species that allowed precise stratigraphic calibrations are *Cousteaudinium* sp. (upper D16–top D17; 20.5–14.8 Ma), *Ectosphaeropsis burdigalensis* (lower D16–lower D18; 23.2–13.8 Ma), *Hystriospheropsis obscura* (lower D17–top D19 ;18.65–7.5 Ma), and *Systematophora placacantha* (Eocene–D18; Eocene–13 Ma).

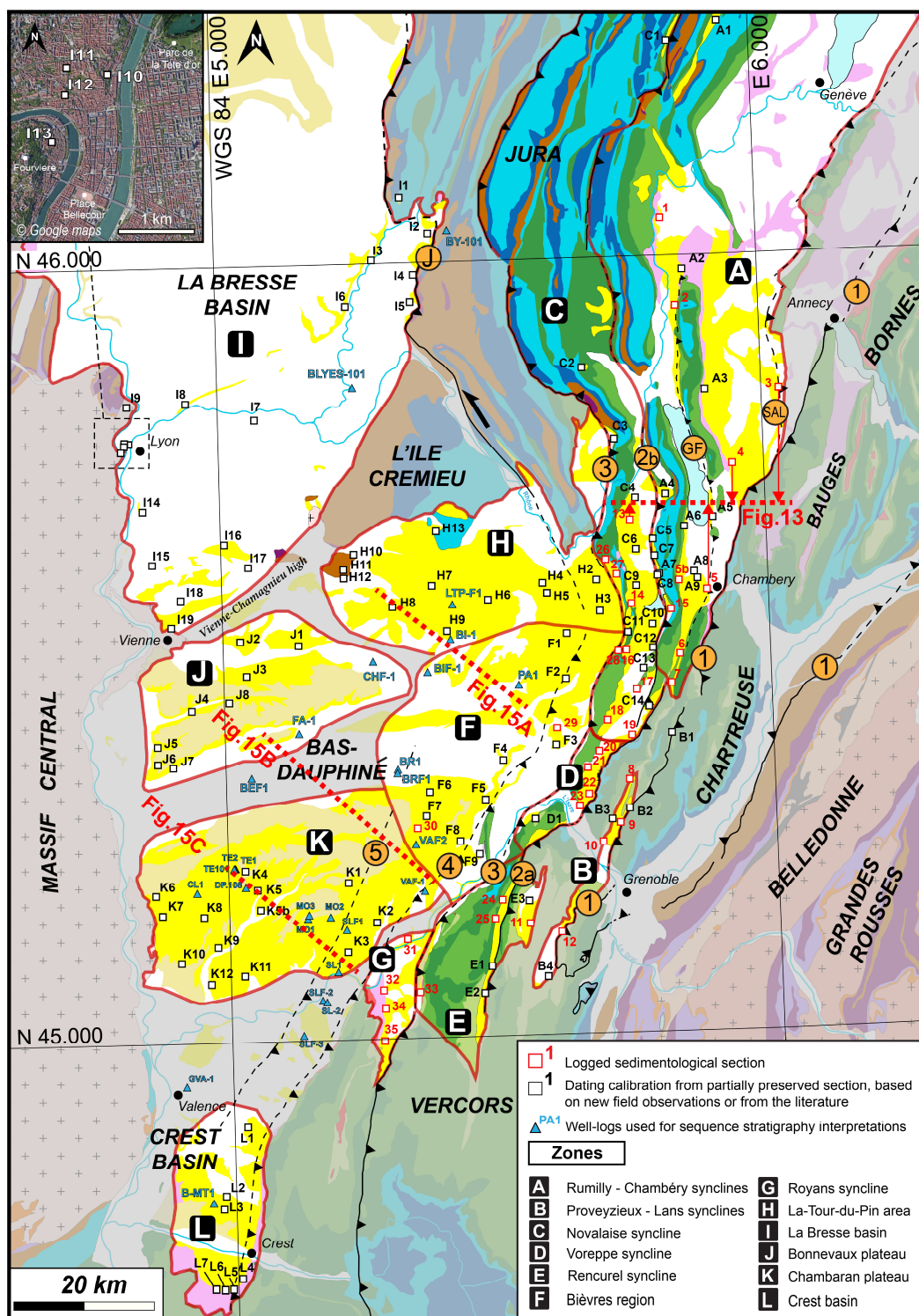
Only 2 out of 40 analyzed samples provided a biostratigraphical dating of sedimentary sections based on foraminiferal assemblages (Table S5). In addition, 13 foraminiferal assemblages were already available from the literature (Lamirault, 1977; Latreille, 1969; Mein, 1985; Aguilar et al., 2004) and were implemented in this study using recent biostratigraphical charts (Table S5). The species allowing firm stratigraphical constraints are *Globigerinoides sicanus* (MMi4a–MMi4c; 16.1–14.87 Ma sensu Lirer et al., 2019), *Paragloborotalia bella* and *Praeorbulina circularis* (respectively N5b–N9; 20.4–14.0 Ma and N8b–N9a; 15.9–14.5 Ma; sensu BouDagher-Fadel, 2015).

21 mammal assemblages available from the literature (Fig. S4; see also Kalifi (2020) and references therein for more details) also revealed to be useful to constrain the age of the sea retreat (Fig. S5 to Fig. S17) between Zones MN6 and MN9 (15.2–9.5 Ma).

The Figure S4 compiles a synthesis of the Miocene biostratigraphy chart of the study area.

## 4.2 Sequence stratigraphy

Absolute and relative dating calibrations were crucial to constrain the timing of the sequence stratigraphy interpretations arising from the 35 sedimentological sections and 28 well log data (Fig. 3 for location; see also Kalifi (2020) for sedimentological and stratigraphical detail) integrated in this study. To add more timing constraints on these sections and well-logs, 84 dating calibrations obtained from partially preserved successions outcropping in adjacent localities complete here the previously published data (Kalifi et al., 2020; Fig. 3, Fig. S5 to Fig. S17). These additional points derive from new field observations and data from the literature (Kalifi, 2020 and references therein). Taken together, the whole dataset allowed the establishment of 11 marine depositional sequences between the late Aquitanian (S1a) and the early Tortonian (S7), capped by a continental upper Tortonian sequence (S8) (Fig. 4A). The Sr-based ages obtained in the basal transgressive deposits coincide with eustatic sea-level rises (Fig. 4B, C), suggesting that the depositional sequences are eustatically-driven (see also Kalifi et al., 2020), except for sequence S8 (Fig. 4A, B). Twelve paleogeographical zones (A to L, Fig. 3) with distinct infill histories were identified based on their specific sedimentological and chronostratigraphical records (Fig. S5 to Fig. S17). The error bars of the Sr-based ages obtained in the basal transgressive deposits do not allow the identification of diachronic transgressions from one paleogeographic zone to the other (Fig. 4C). Therefore, we assume that each transgression occurred sub-synchronously at the scale of the study area, and that the eustatic sea-level rise age (Fig. 4B) will be used to: (i) constrain in time depositional sequences without dating controls and/or, (ii) homogenize the age of the sequence at the basin scale.



300 **Figure 3:** The 12 paleogeographical zones of the Miocene basin of the subalpine massifs, southern Jura and adjacent basins (Bas-Dauphiné, La Bresse, Crest). Sedimentological and chronostratigraphical records of each zone are provided in Fig. S5 to Fig. S17.

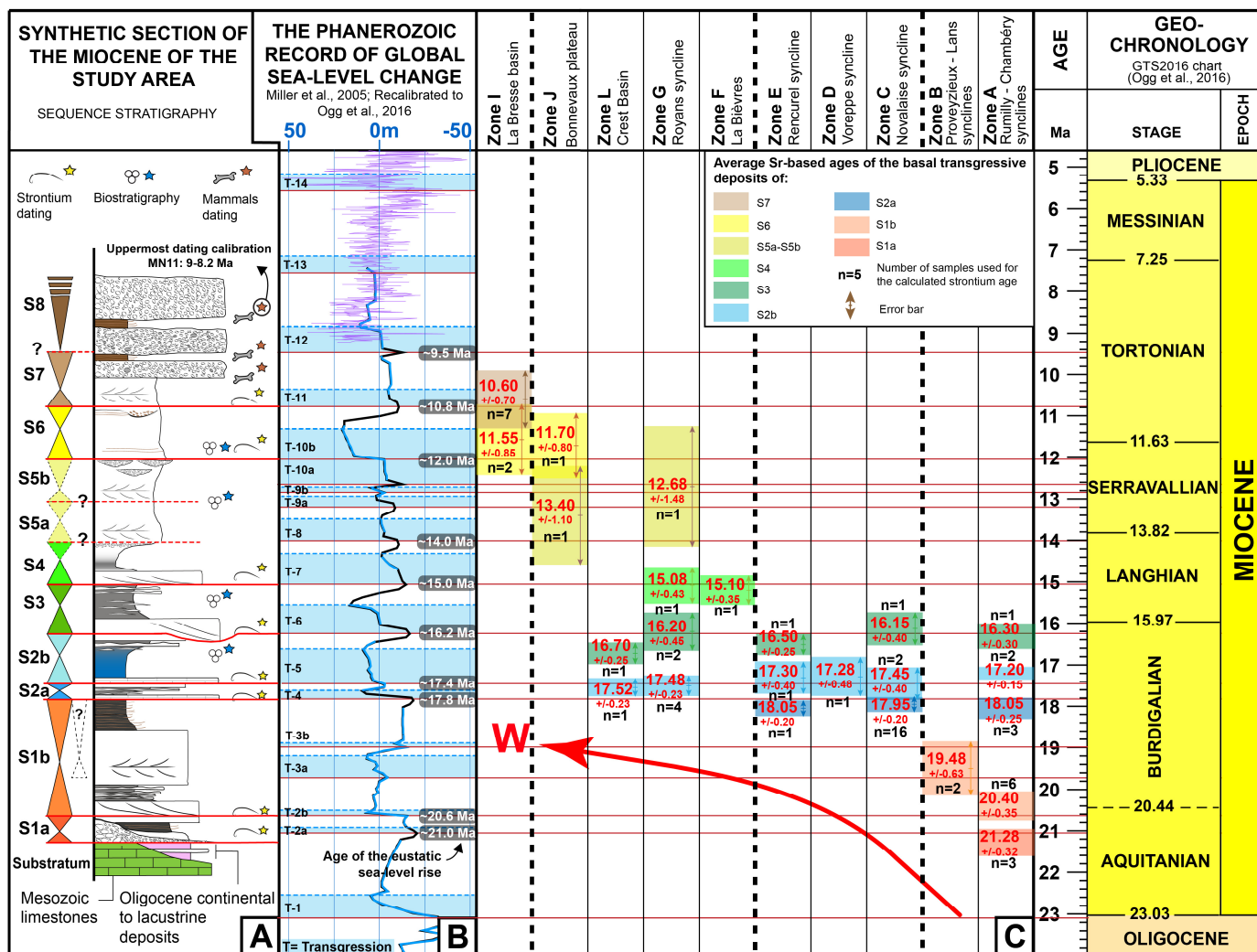


**Figure 4: The Miocene chronostratigraphy of the subalpine massifs, southern Jura and adjacent basins (Bas-Dauphiné, La Bresse, Crest). (A) Synthetic section of the Miocene of the study area and the 11 Miocene depositional sequences. Legend in Fig. 5; (B) The eustatic curve of Miller et al. (2005) recalibrated with the Global Time Scale (GTS) of Ogg et al. (2016); (C) Average Sr-based ages of the transgressions in the paleogeographical zones. n: number of age values. Only ages of samples with  $\delta^{13}\text{C}$  values  $> -1$  ‰ (Table S2) are considered here (maximum confidence zone). Red curved arrow= Westward migration of the marine deposits during the lower Miocene.**

The 12 Miocene paleogeographical zones can be grouped in four domains based on our chronostratigraphy (Fig. 5):

- (i) Oriental domain:** this depositional area corresponds to the Rumilly-Chambéry synclines (Zone A) and the Proveyzieux-Lans synclines (Zone B). Located in the easternmost part of the subalpine chains, they are characterized by the occurrence of the lower marine Burdigalian sequences (S1a and S1b). The upper Burdigalian (S2a and S2b sequences) is also very thick (~800 m in the zone A) and is characterized by distal marine deposits in the North (zone A) and coarse-grained deltaic deposits in the South (zone B) (Fig. 5). The S3 (+S4?) sequences is on the other hand very poorly developed (<50 m), and corresponds to coarse-grained deltaic to continental deposits. The middle Miocene and younger deposits are absent in this domain.



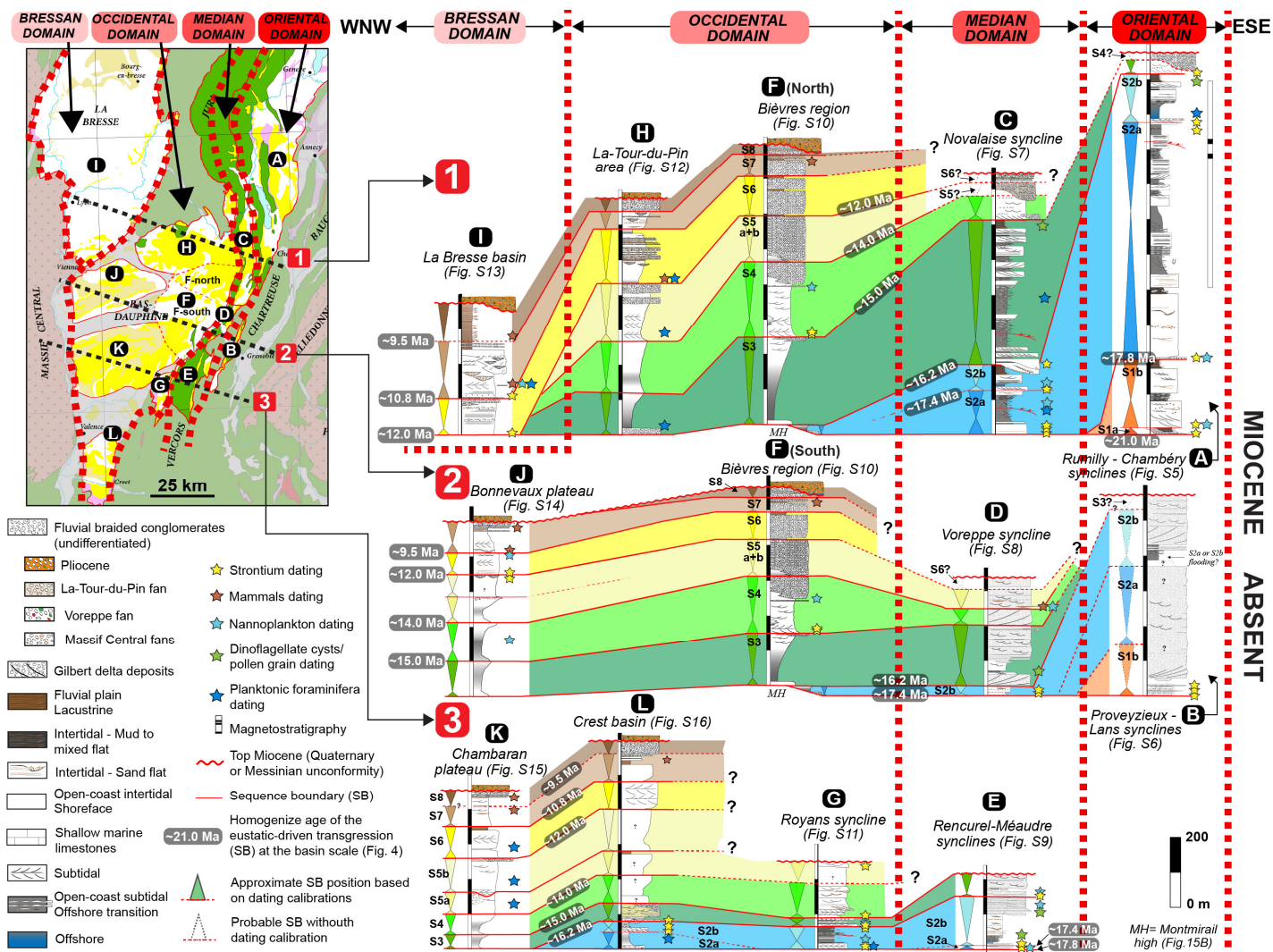


**Figure 5: Spatio-temporal distribution of the Miocene depositional sequences of the sub-alpine massifs, southern Jura synclines, Bas-Dauphiné, Crest and La Bresse, which highlight the four depositional domains resulting from the sequence stratigraphical interpretation of the 12 paleogeographical zones (presented in details in Fig. S5 to Fig. S17).**

320 **(ii) Median domain:** from north to south, this depositional domain encompasses the Novalaise (zone C), Voreppe (zone D) and Rencurel-Méaudre synclines (zone E). The lower Burdigalian (S1a and S1b sequences) is absent in this domain set in the westernmost position of the subalpine chains (Fig. 5). The first deposit corresponds to the marine upper Burdigalian (S2a and S2b sequences), which is about 100 to 200 m thick. Sequence 3, on the other hand, is much thicker in this domain (~400 m in zone C). The S4 and S5 depositional sequences of the middle Miocene do not exceed 150 m in thickness and are characterized by coarse-grained deltaic to continental deposits (Fig. 5). The upper Miocene (above S5) is in turn rarely recorded, thin or not expressed at all.

325

(iii) **Occidental domain:** This domain concerns the Tour-du-Pin area (H), Bièvres region (F), Bonnevaux plateau (J), Chambaran plateau (K), Royans syncline (G) and Crest basin (L). These areas are characterized by the absence of the lower Burdigalian (S1a, S1b) and the discontinuous occurrence of the upper Burdigalian (S2a and S2b sequences). The Langhian and Serravalian depositional sequences (S3 to S6 sequences), however, are remarkably well developed (Fig. 5). The thickest upper Miocene deposits (S7 and S8 sequences), mainly containing continental sediments, are also found in this domain (Fig. 5).

(iv) **“Bressan” domain:** this domain concerns solely the Bresse basin (I), where lower and middle Miocene (S1 to S5 sequences) marine sediments are absent (Fig. 5). This zone was only flooded during the major eustatic transgression of the S6 sequence. Upper Miocene deposits (S7 and S8 sequences) are particularly thick in this domain and mainly made of continental products.

### 4.3 Overall structure and main thrust zones

Structural maps and cross-sections have been reappraised with the aim to produce a new regional structural map (Fig. 1B). West of the Belledonne external crystalline range, the Mesozoic cover is affected by numerous thrusts, nearly all dipping to the east. The uppermost thrust sheet is the Penninic thrust outcropping at the base of the Sulens and Les Annes klippen (Fig. 1B). This thrust roots east of Belledonne and was active during the Oligocene (Simon-Labric et al., 2009; Dumont et al., 2008, 2011, 2012; Doudoux et al., 1982). To the West, in the footwall of the Penninic thrust, five main NNE-SSW striking fault zones, locally offset by NE-SW right-lateral faults, straddle the Vercors and Chartreuse massifs. We describe below these fault zones in more detail, from East to West. We also evaluate the continuity of the fault zones between the southern area (Vercors and Chartreuse massifs) where folds and thrusts are closely spaced, and the northern area where folds and thrusts are more widely spaced.

#### 4.3.1 “Chartreuse orientale thrust” or Fault Zone 1 (FZ1)

Within the Chartreuse massif, a major thrust bringing Lower Cretaceous units on top of younger Cretaceous units has long been distinguished in the literature. It runs from Chambéry to the west of Grenoble and was successively referred to the “*Chevauchement de la Chartreuse orientale*” (Gidon, 1964, 1995) (φOr, Fig. 1B), the “*Central Chartreuse thrust zone*” (Butler and Bowler, 1995), the “*chevauchement subalpin principal*” (Gidon and Arnaud, 1978; Gidon et al., 1978), the “*Subalpine front*” (Deville and Chauvière, 2000), and the “*Chartreuse orientale thrust*” (Philippe et al., 1998). Here we refer to this thrust as the Chartreuse orientale thrust (φOr, Fig. 1B). It shows a large offset of about ten kilometres (Deville and Chauvière, 2000) at the latitude of Chambéry. Along its southern portion this thrust brings the Néron syncline affecting “Urgonian” (=Barremian-Aptian) limestones on top of the Proveyzieux syncline filled with Miocene deposits. In its central part, it brings Mesozoic sediments on top of the Charmant Som anticline (CS, Fig. 1B), while further north Cretaceous strata are found over Oligocene deposits (Doudoux et al., 1992a, b; Gidon and Barfèty, 1969). The Chartreuse orientale thrust is

affected by numerous right-lateral NE-SW faults (Fig. 1B). North of Chambéry, the thrust connects with the western front of the Bornes and Bauges massifs characterized by Mesozoic units thrust over Oligocene and Miocene deposits ( $\phi B$ , Fig. 1B).

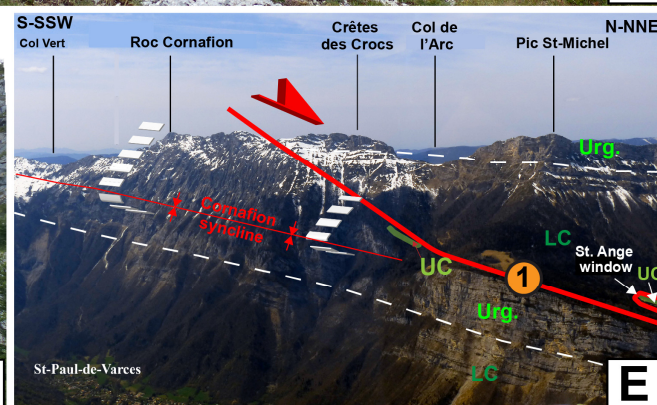
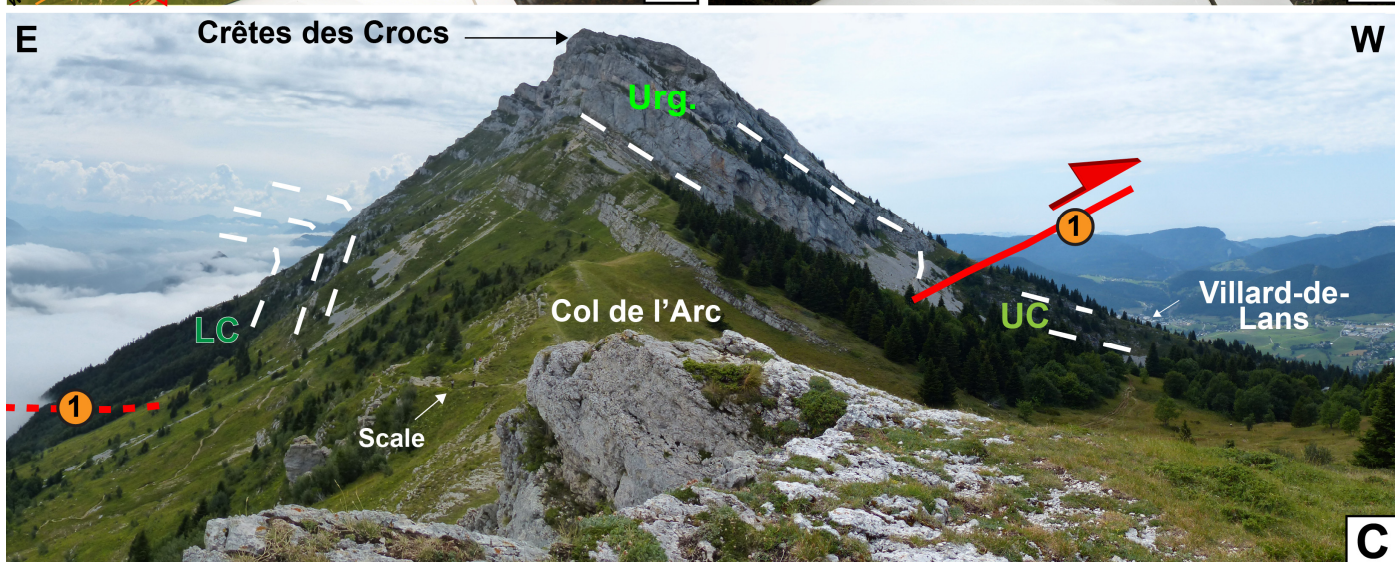
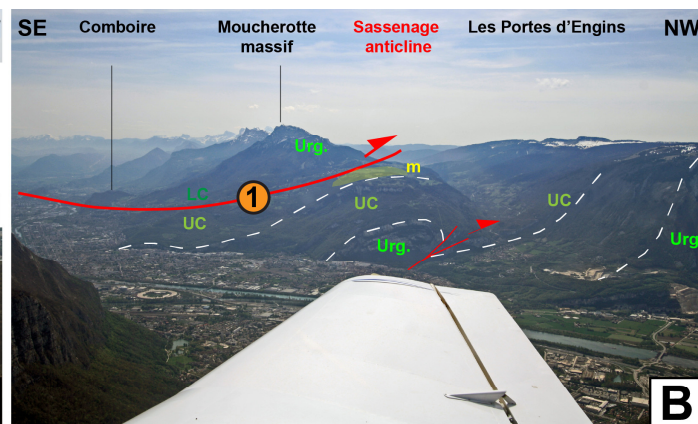
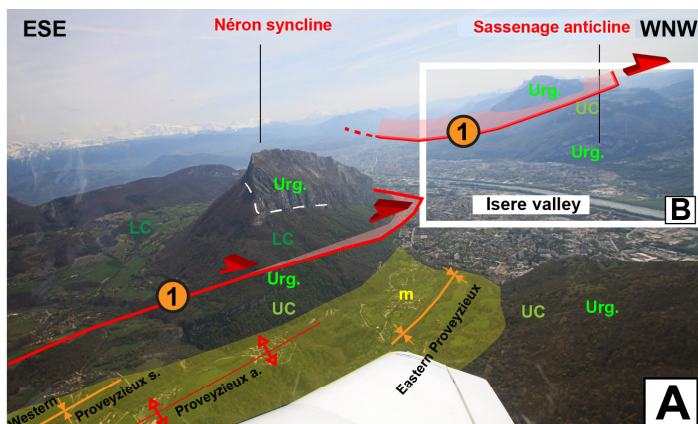
360 The prolongation of this thrust towards the south across the Isère valley is more contentious. The valley has been sometimes interpreted as the location of either a fold saddle (e.g. Gignoux and Moret, 1952) or possibly a fault (Gidon and Arnaud, 1978) that would offset the structures outcropping on both sides. The most recent detailed study concluded that there is no offset in the downstream part of the valley, but possibly a tear fault in the upstream (Gidon, 1995). South of the valley, the Moucherotte Thrust that brings Cretaceous sediments atop Miocene of the Villard-de-Lans syncline has a complex 3D geometry, connecting

365 with the poorly exposed Perrières Fault through the Bruzier right lateral fault (Debelmas, 1965; Gidon, 2020b) (Fig. 7A). We combine new field observations with the published geological maps and other publications to produce a new structural map, with corresponding cross-sections (Fig. 7) and interpretation. North of the Isère valley, the Proveyzieux syncline is a complex structure since it corresponds in fact to two synclines separated by a pinched anticline (the Proveyzieux anticline in Fig. 6A; Fig. 7A). South of the Isère valley, the Sassenage fold is also an anticline conformably capped by Miocene deposits (Fig. 6B).

370 On each side of the Isère valley, the two anticlines have close axis direction: N198°, 03° for Proveyzieux and N181°, 06° for Sassenage (Fig. 7A). In both cases, the eastern limb of the anticline is overthrust by Cretaceous sediments including “Urgonian” limestones (Moucherotte thrust in the south, Néron thrust in the north) strongly suggesting that the thrust system is continuous across the Isère valley (Gidon, 1965) (Fig. 7A; Fig. S18B). Therefore, we propose that the Proveyzieux and Sassenage anticlines correspond to the same structure. The precise trace of the thrust is unclear, hidden by Quaternary

375 sediments, but the Moucherotte – Bruzier – Perrières thrust appears to be offset from the Néron thrust by ~2km along a left-lateral NW-SE strike-slip fault along the Isère valley (Fig. 7A; Fig. S18B). Such a fault is compatible with the general direction of shortening (~E-W). A major thrust thus appears to be continuous from the western front of the Bauges massif to the western front of the Moucherotte range (from north to south  $\phi B$ ,  $\phi Or$ ,  $\phi Mo$ ), and is referred here as the Fault Zone 1 (FZ1) (Fig. 1B).







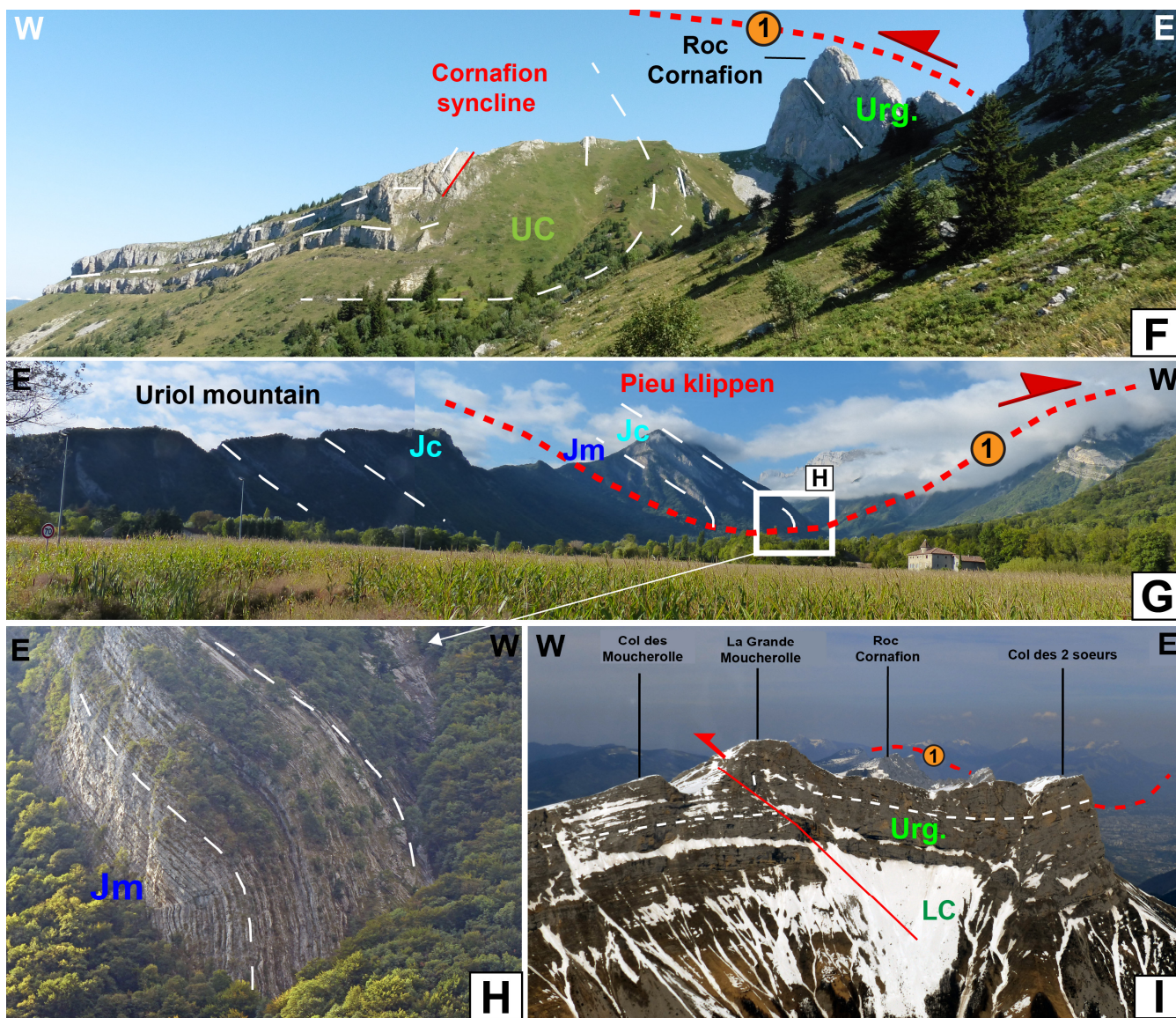
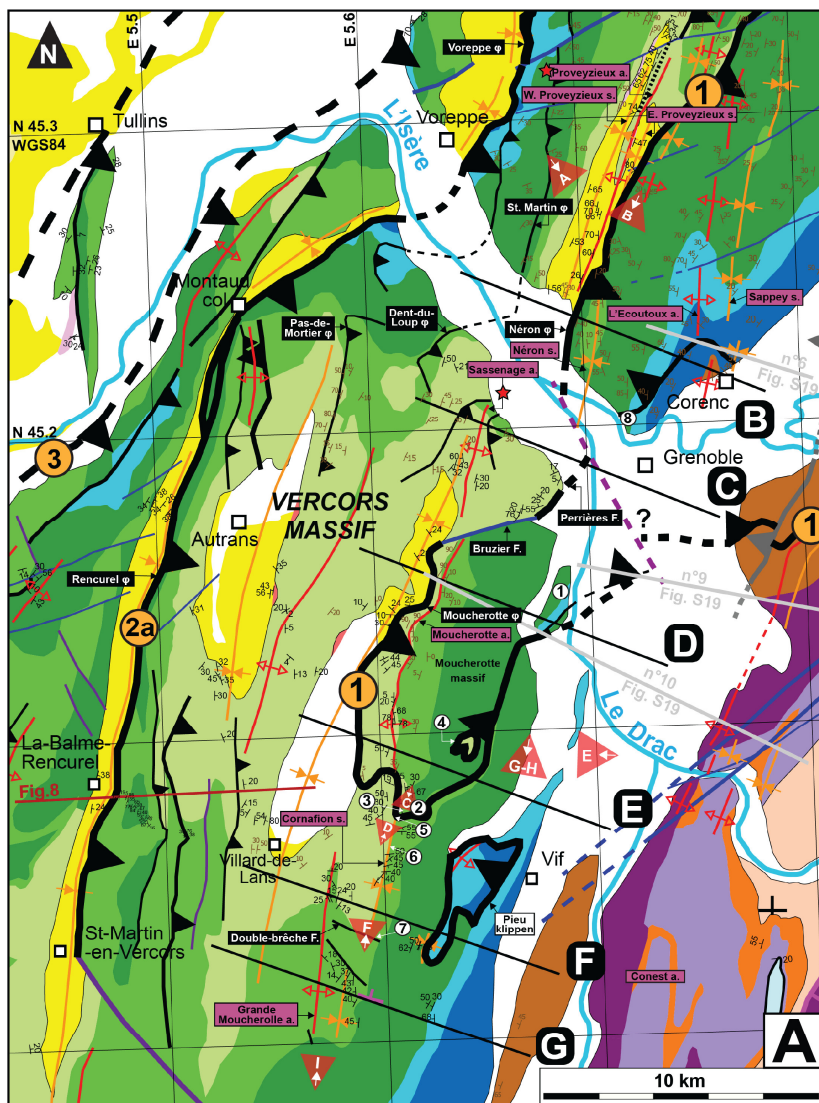


Figure 6: Field and aircraft pictures of the Chartreuse Orientale and Moucherotte thrusts (FZ1) in southern Chartreuse and northern Vercors. See viewpoints A to I locations in Fig. 7A. m= Miocene; UC= Upper Cretaceous; Urg. = Urgonian (Barremian-Aptian limestones); LC= Lower Cretaceous; Jc= Upper Jurassic limestones; Jm= Upper Jurassic marls. Dashed white lines underline the stratifications. Thrust faults in red. Orange circle= Fault zone (FZ). (A, B) Néron and Moucherotte thrusts, aerial views from the N. The Provezieux Miocene deposits are underthrust below the Néron syncline. Beyond the Isère valley, the Sassenage fold capped with Miocene deposits is underthrust below the Moucherotte massif. Note that Provezieux syncline corresponds to two synclines separated by an anticline. (C) View towards the south of the Col de l'Arc and the Crête des Crocs: the folded Urgonian is thrust above the Upper Cretaceous. (D) Urgonian limestones of the Moucherotte anticline in the FZ1 hangingwall. (E) View towards the west of the eastern flank of the Moucherotte massif with the FZ1 geometry. (F) View towards the north of the Cornaifion syncline. The Urgonian is overturned, in the FZ1 footwall. (G) Duplication of the Jurassic series in the Pieu klippen, view from the North; (H) Zoom on the anticline on the hangingwall of the FZ1 in the Pieu klippen. (I) View towards the north of the Grande Moucherolle, where autochthonous series are weakly deformed.





### ★ Proveyzieux anticline

Western limb  
ALV88, ALV163, ALV165,  
ALV175, ALV176, ALV200,  
ALV205, ALV206, ALV207,  
ALV255 (Table S6)

Eastern limb

ALV79, ALV80, ALV81,  
ALV82, ALV83 (Table S6)

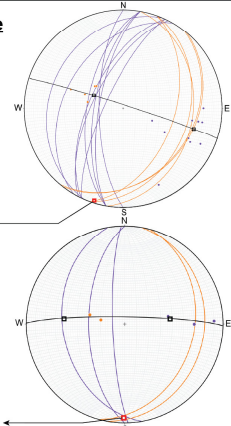
Fold axis: N198, 03°

### ★ Sassenage anticline

Western limb  
M444, M445, M446 (Table  
S6)

Eastern limb  
ALV12, M443 (Table S6)

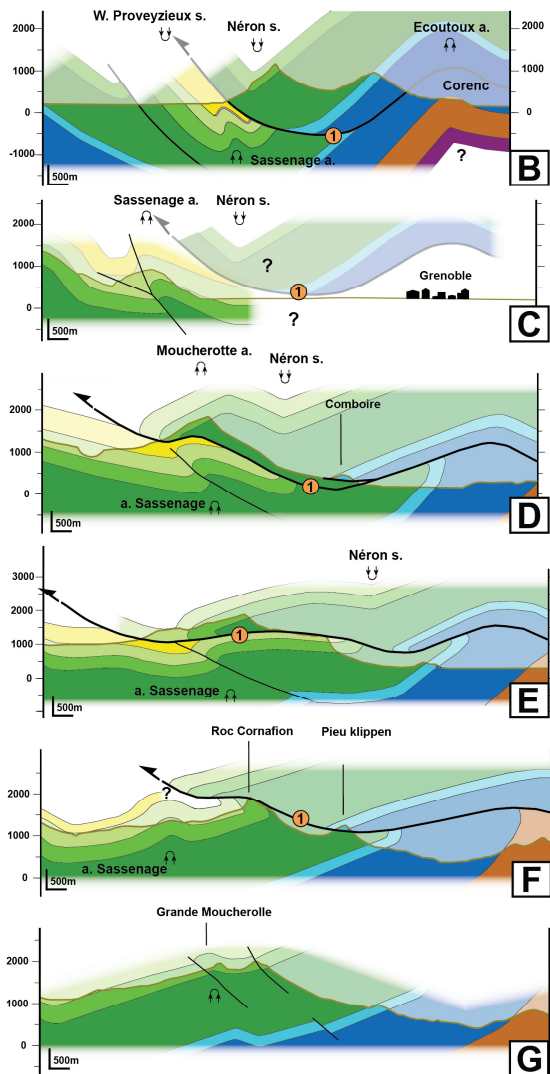
Fold axis: N181, 06°



- Major thrust
- Back thrust
- Important thrust
- Minor thrust
- Blind thrust
- Left-lateral strike slip
- Right-lateral strike slip
- Normal fault
- Syncline
- Anticline
- Fault zone (FZ)
- Thrusts (=φ) and faults (=F.)
- Folds (anticline = a.; syncline = s.)
- Cross-sections (B to G)

WNW

ESE



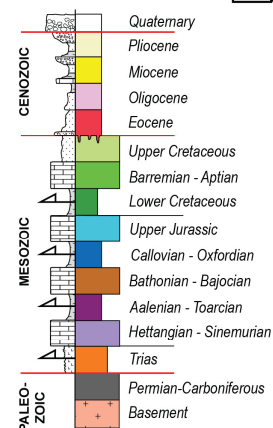
Cross-sections adapted  
from Barféty and Gidon  
(1996) (Fig. S19)  
View point (Fig. 6)

### Bedding strike and dip measurement

- 10 From this study
- 10 From geological maps

### ① Localities

1. Comboire
2. Col de l'arc
3. Crête des Crocs
4. St-Ange window
5. Pierre Vivari
6. Roc Cornafion
7. Double Brèche
8. Corenc-Jalla



395 **Fig. 7: Structure of the Chartreuse orientale thrust (FZ1) in northern Vercors and southern Chartreuse. See Fig. 1 for legend of the stratigraphy. (A) Structural map. Fig. 6 viewpoints A to I are located. (B-G) Geological cross-sections (see location in A). The two stereo diagrams (Stereonet software, Cardozo and Allmendinger, 2013) at the lower left are plots of the stratifications and their poles in order to calculate the anticline axis.**

Although the westward Moucherotte thrust has long been described, its detailed geometry is still discussed. We conducted a detailed mapping based on field observations at 210 stations (Table S6) combined with a detailed analysis of previous maps and publications and one aircraft flight, in order to constrain the 3D geometry of the Moucherotte range geology.

On the western flank of the Moucherotte range, the Cretaceous beds of the Moucherotte anticline are thrust on top of the Miocene of the Villard de Lans syncline, above the Sassenage anticline (Fig. 6B and Fig. 7D) (Gidon, 1981). In the Comboire range, at the foot of the eastern flank of the Moucherotte massif (locality 1, Fig. 7A), gently dipping to the west Upper Jurassic strata rest above marls. These marls, previously mapped as Jurassic (Vif geological map; Barféty et al., 1967), are rather Early Cretaceous in age based on the occurrence of *Berriasella* (Gidon, 2020a). This implies a duplication of the Mesozoic series and thus the emergence of a west-dipping thrust. This thrust most probably connects in depth with the Moucherotte thrust, making the Moucherotte range a klippen (Fig. 7D).

A few kilometers further south, near the “Col de l’Arc” (locality 2 Fig. 7A), the Cretaceous series are also duplicated. To the west, Urgonian beds of the Moucherotte anticline rest on top of the Upper Cretaceous (Fig. 6C, Fig. 7E). The hanging wall structure is complex with a syncline of Upper Cretaceous sediments in the footwall and a boxed anticline overlain by a monocline in the hangingwall (Fig. 6D). To the east of the Col de l’Arc, below the “Crête des Crocs” (locality 3, Fig. 7A), the Lower Cretaceous dips steeply to the east (~70°, Fig. 6C), and is allochthonous above more gently dipping Urgonian limestones. Further to the north the Urgonian limestones and Upper Cretaceous are seen below the Lower Cretaceous through the “st Ange” window (locality 4, Fig. 7A) (Fig. 6E) (Barféty et al., 1967). The top of the Moucherotte range is thus a klippen that can be traced ~1 km farther to the south to the “Pierre Vivari” (locality 5, Fig. 7A).

Further south, the Moucherotte klippen has been completely eroded, and the Cornafion summit (locality 6, Fig. 7A) corresponds to the inverted eastern limb of a N10° trending syncline in the footwall of the thrust (Fig. 6E, 7F), while further east the Upper Jurassic and Lower Cretaceous series are duplicated, constituting the Pieu klippen (Fig. 6G; Fig. 7F) (Barféty et al., 1967). At the western edge of this klippen, Upper Jurassic limestone allochthonous strata form a bent-fault anticline above the autochthonous Jurassic and Cretaceous strata (Fig. 6H) suggesting thrusting toward the west. We interpret this klippen as the southern/lower extension of the Moucherotte one (Fig. 7F).

The Moucherotte klippen did probably not extend south of the Double Brèche fault (locality 7, Fig. 7A), south of which the footwall syncline is no more observed (Fig. 7A). Further south, the Mesozoic formations are weakly deformed, locally exhibiting west-verging anticlines such as the “Grande Moucherolle” (Fig. 6I, Fig. 7G).

No evidence of the west verging Moucherotte thrust is found east of the Pieu klippen implying that it roots east of the Conest range, which is the southwestern prolongation of the external Belledonne cover (Fig. 7A, D, E, F; Fig. 1B; Fig. 11D). Such geometry, resulting in apparent normal motion along the west dipping portions of the thrust (i.e., east of the Pieu klippen and Comboire range), strongly suggests that the thrust was folded after its activity.

Apparent offsets measured along NW-SE cross sections increase from south to north: 1.1 km along the Pieu section (Fig. 7F),  
430 3.3 km along the Pic St-Michel and Moucherotte sections (Fig. 7E, D).

As discussed above, we interpret the Moucherotte thrust as the prolongation of the “Chartreuse orientale thrust”, or FZ1, locally  
call the “Néron thrust”, across the Isère valley. In the same way, the “Corenc-Jalla” folded-thrust system (locality 8, Fig. 7A)  
(Blanchet and Chagny, 1923; Gignoux and Moret, 1952), also termed “ $\phi c$ ” in the geological map of Grenoble (Gidon and  
Arnaud, 1978) probably corresponds to the northern prolongation of the eastern flank of the Moucherotte thrust outcropping  
435 in Comboire south of the Isère valley (Gidon, 1981) (Fig. 7A, B). This thrust system has been affected by the Ecoutoux  
anticline, a late east verging fold that also affects the autochthonous units (Blanchet and Chagny, 1923; Gidon, 1981) (Fig.  
7A; Fig. 7B). Apparent offset of the base of the Lower Cretaceous across the Néron – Conrenc thrust (FZ1) measured along a  
NW-SE cross section amounts to 2.8 km (Fig. 7B).

Barfély and Gidon (1996) further consider that the FZ1, that they termed “ $\phi 1$ ”, is a major thrust which re-emerges to the east  
440 of the Isère valley, on the western edge of the Belledonne massif (Fig. S19A, D). There, along the Grésivaudan valley on top  
of the Belledonne basement,  $\phi 1$  dips 20-40° to the west being sub-parallel to the Mesozoic series it affects, and duplicates the  
Dogger (Barfély and Gidon, 1996) (Fig. S19A, D).  $\phi 1$  thus appears as a top to the west fault with an apparent normal motion,  
but that is an additive contact, and thus more probably a tilted thrust (Deville et al., 1994; Barfély and Gidon, 1996). Further  
to the north, at the eastern edge of the Bornes massif, the Dogger and Lias are tightly folded in a top-to-the-west ~4 km thick  
445 shear zone (Barfély and Barbier, 1983; Barfély and Gidon, 1996; Doudoux et al., 1982, 1999) that also possibly corresponds  
to a thrust tilted by the later uplift of the Belledonne range (Doudoux et al., 1999) (Fig. S19A, B, C).

Whilst further field study would be necessary to warrant this interpretation, we propose that the Chartreuse Orientale thrust  
(FZ1) runs continuously from the western front of the Bornes to the west Moucherotte thrust in the south, and from the east of  
Moucherotte to east of the Bornes, defining a ~120km long thrust nappe (Fig. 1B). This thrust sheet was termed the Aravis-  
450 Mt Granier unit (Bellahsen et al., 2014) or the Subalpine nappe (Pfiffner, 2014). These authors further suggested that this thrust  
roots in the basement east to the Belledonne massif, which would have been uplifted after motion along the thrust ended (also  
see Lacassin et al., 1990; Menard and Thouvenot, 1987).

#### 4.3.2 Voreppe thrust or Fault Zone 2 (FZ2)

In the Vercors massif, the main thrust west of the FZ1 is the “Rencurel thrust” ( $\phi Re$ , Fig. 1B; Fig. 7A) which outcrops near  
455 “La-Balme-Rencurel” (Fig. 8A). There, the thrust exhibits Barremian-Aptian limestones thrust above overturned Miocene  
Molasse deposits (Fig. 8B). The apparent offset for the top of the Urgonian is of 1.5 km along this section (Fig. 8C). Miocene  
strata are limestones bearing *Chlamys praescabrusculus*, which are upper Burdigalian in age (Fig. S9). At this location, the  
fault strikes N3°, 40°E with slickensides having a pitch of 80°S (Fig. 8B) indicating an almost pure reverse faulting. Analysis  
of the dips in the Lower Cretaceous marls indicates that the hangingwall of the fault is characterized by two anticlinal structures  
460 separated by a syncline (Fig. 8C). Further east, two other thrusts, with smaller offsets (0.8 and 0.9 km), are observed parallel  
to the Rencurel thrust (Fig. 8C). According to the published geological map (Barfély et al., 1967), the thrust extends southwards

for 6 km until it branches at the tip of a NW-SE left-lateral fault (Fig. 1B). Towards the north, the thrust is continuous until the “Col de Montaud” (MC, Fig. 7A), with Miocene deposits observed in the footwall. At this location, it was proposed that the thrust connects with the thrust at the western front of the Vercors (Watkins et al., 2017). However, the fault does not cut across the footwall Miocene deposits (Gidon and Arnaud, 1978), but more likely turns from N-S to NNE-SSW to reach Veurey-Voroize where Upper Jurassic sediments are found thrusting atop the Miocene (Fig. 1B; Fig. 7A). N-E of the Isère valley, we suggest that the “Rencurel thrust” prolongates to the “Voreppe thrust” across the Isère valley (Fig. 7A). Indeed, the seismic profile 91VER1 that follows the Isère valley (Fig. 9A) reveals a major thrust at this location (Fig. 9C) with a 1.5 km apparent offset of the basal Lower Cretaceous reflector. Hence, we interpret the Rencurel and Voreppe thrusts as the same tectonic structure as previously proposed by Gidon et al. (1978) and Dumont and SPIA (2020).

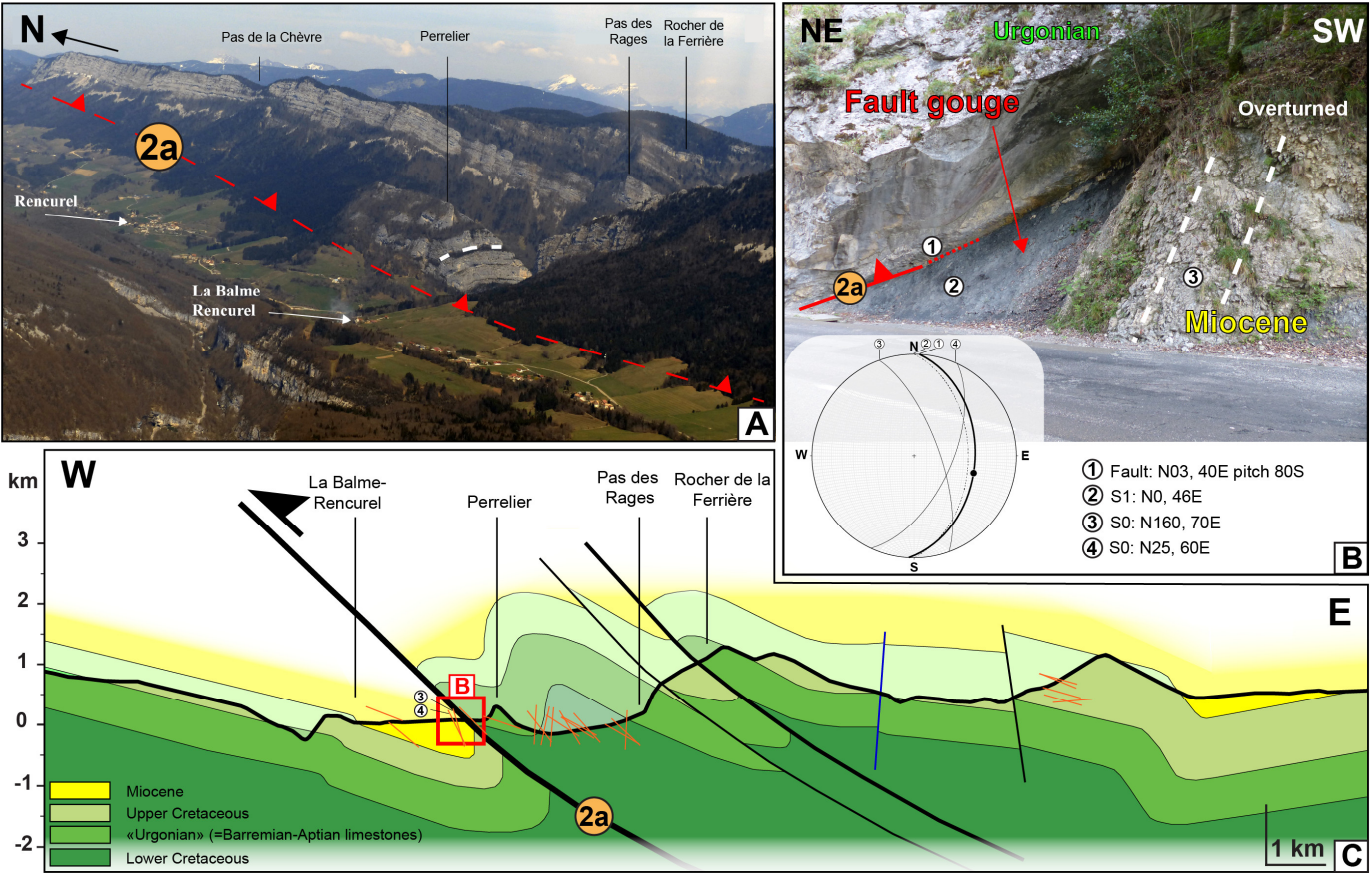


**Figure 8: The Rencurel thrust in the Vercors massif. Orange lines= projected dip measurements. Blue line = Right-lateral strike slip fault. Black line = Thrust. (A) The N-S Rencurel thrust that juxtaposes Cretaceous units on top of Miocene Molasse deposits. (B) Outcrop of the Rencurel thrust along the D103 road, SE to the La Balme-Rencurel village, exhibiting Barremian-Aptian limestones thrust on top of overturned Miocene deposits. Corresponding stereographic diagram (lower hemisphere) at the bottom. (C) E-W cross-section along the “gorges de la Bourne”. See Fig. 7A for location of the cross-section and dip measures on map view.**

Further north, the Voreppe thrust is mapped as a continuous structure bringing Jurassic sediments on top of Miocene deposits of the Voreppe syncline (Fig. 1B) (Gidon and Arnaud, 1978). North of St Laurent-Du-Pont, this thrust terminates, but other



thrusts continue further to the north: to the west two faults merge together before bounding the western limb of the l'Épine anticline (EP, Fig. 1B), while to the east Miocene and Cretaceous deposits are vertical in the western flank of the Outherans (OU) anticline (Fig. 1B). The seismic profile 91CHA1 stands across the four faults (Fig. 9A, B). Its interpretation suggests that the two western faults (2b and 2c) merge at depth just above the basement, and that they could also merge with the Voreppe thrust (2a) just east of the eastern limit of the seismic profile (Fig. 8B). We thus interpret the western faults [2b and 2c] as the northern prolongation of the Voreppe thrust [2a], with a 8 km long left-lateral step over (Fig. 1B). Within the step over, short NW-SE left-lateral faults are reported on the 1/50 000 map (Gidon, 1970a) (Fig. 1B) that may concur to the westward shift of the shortening from the Voreppe thrust to the l'Épine thrust. Based on the basal Lower Cretaceous reflector, the apparent offsets are 2.2 km for the Voreppe thrust [2a], 2.3 km for the fault [2b] and 1.1 km for the fault [2c] (Fig. 9B). Following this interpretation, the FZ2 thrust system would be shifted westwards, and continues northward as the [2b] thrust bordering the western flank of the "Épine" [EP], "Grand Colombier" [GC] and "Crêt du Nu" anticlines (Fig. 1B).

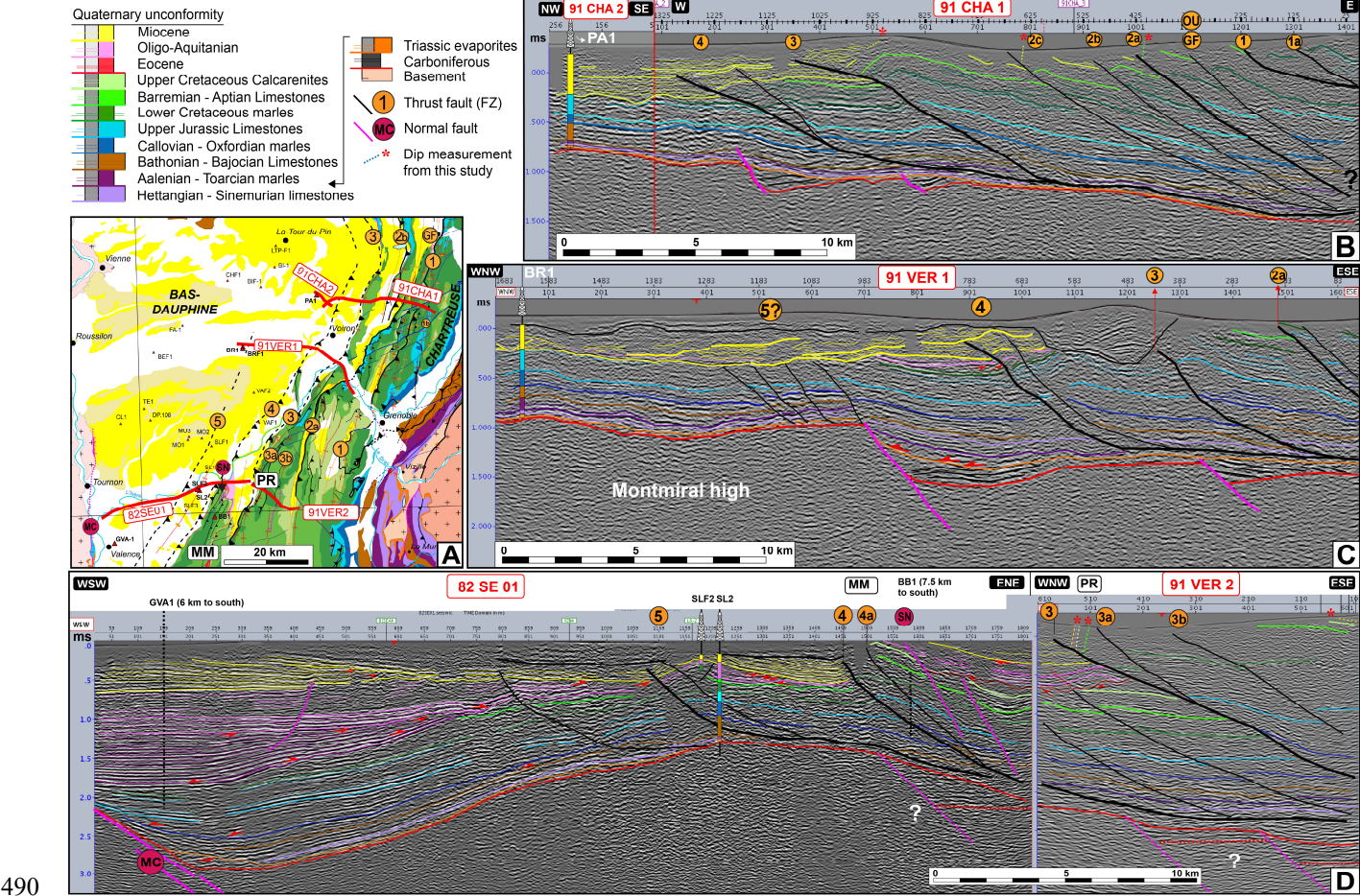
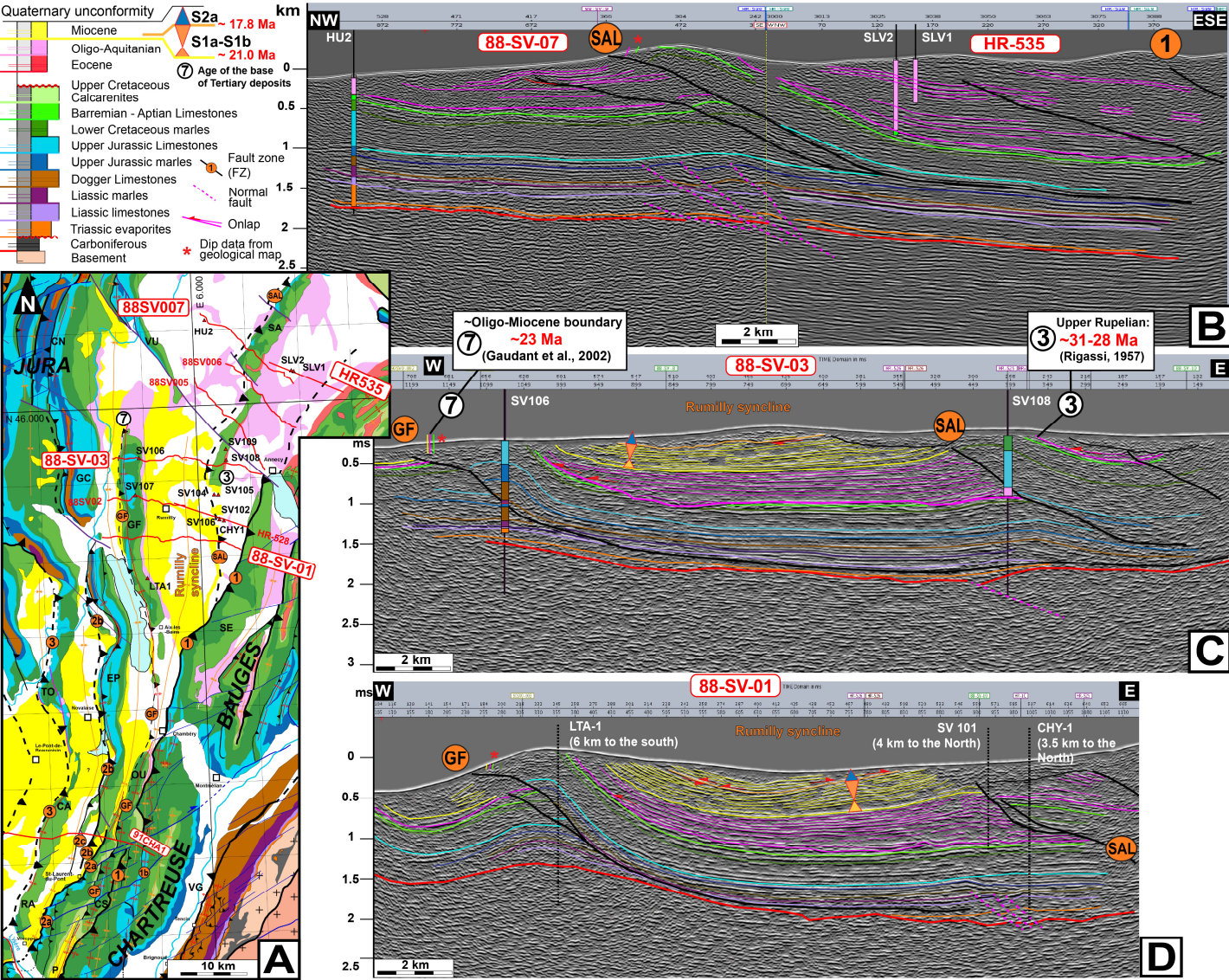


Figure 9: Seismic profiles along the Vercors and Chartreuse massifs (seismic lines published by Deville (2021) and reinterpreted). (A) Geographical and geological locations of the interpreted seismic lines. (B) Seismic profiles 91CHA1 and 91CHA2. Interpretation is proposed using PA-1 well data and fieldwork data. Note that the Outherans blind thrust [OU] corresponds further north to the



495 GF thrust. (C) Seismic profiles 91VER1. Interpretation is proposed using BR-1 well data and fieldwork data. (D) Seismic profiles 82SE01-91VER2. Interpretation is proposed using SLF-2, SL-2 and extrapolated BB1 and GVA-1 well data and fieldwork data.



**Figure 10: The salève (SAL) and Gros Foug (GF) faults between the Chartreuse massif and the Jura synclines (A, legend in Fig. 1) as based on seismic profiles 88SV07+HR-535 (B), 88SV03 (C) and 88SV01 (D).**

The seismic profile 91CHA1 shows that the western flank of the Outherans anticline is bounded by the Outherans blind thrust [OU] which is almost parallel to the three other ones and has a 1.3 km apparent offset (Fig. 9B). To the south, the Outherans (OU) anticline corresponds to the Chartreuse median anticline of Gidon (1964, 1990) (CS, Fig. 1B, Fig. 10A), while to the North it most likely connects with the Gros Foug (GF) anticline across the Chambéry valley (Fig. 1B). The geometry of the Gros Foug (GF) anticline can be observed on seismic profiles 88SV01 and 88SV03 (Fig. 10C, D), and supports a east-dipping

500

Gros Foug (GF) thrust with an apparent offset between 2 and 2.5 km of the basal Upper Jurassic limestones reflector. This thrust appears to root in the Triassic detachment level above the basement (Fig. 10C, D) and is probably the northern extent of the Outherans thrust in between the Chartreuse Orientale (FZ1) and the Voreppe thrust (FZ2) (Fig. 10A).

The seismic profiles also reveal another thrust fault between FZ1 and FZ2: the Salève (SAL) thrust bounding the Salève (SA) anticline (Fig. 1B, Fig. 10A, B) that also roots above the basement in the Triassic. The apparent offset of SAL fault is evaluated to be 2.5 km based on the basal Barremian-Aptian limestones reflector in seismic profile 88SV01 (Fig. 10D), and on the basal Upper Jurassic limestones reflector in seismic profile SV03 (Fig. 10C). The seismic profiles do not allow to visualize the connection between FZ1 and the SAL faults, and two hypotheses have been proposed: (i) the FZ1 and the SAL faults are connected at depth (Deville and Sassi, 2006; Beck et al., 1998); (ii) the FZ1 and the SAL faults are distinct (Guellec et al., 1990; Doudoux et al., 1982).

#### **4.3.3 The Royans - Ratz thrust or Fault Zone 3 (FZ3)**

The western edge of the Vercors and Chartreuse massifs corresponds to open anticlines characterized by steep west-dipping forelimbs and gently dipping back-limbs. Such anticlines are continuous from Pont-en-Royans in the Vercors massif (PR) to the Chailles anticline in the Chartreuse massif (CA), with the Ratz (RA) anticline in an intermediate position (Fig. 1B). Seismic profiles crossing these structures (Fig. 9A) reveal that these anticlines formed in the hanging wall of a major thrust zone: the Royans - Ratz thrust (FZ3). This thrust zone corresponds to a single fault bringing Barremian-Aptian to Upper Jurassic limestones above Miocene strata. According to the basal Upper Jurassic limestones reflector, the apparent offset is estimated to be 1.5 km along the 91CHA1-2 and 91VER1 seismic profiles (Fig. 9B, C). Alternatively, the seismic profile 82SE01 (Fig. 9D) shows that the main fault (FZ3) has an apparent offset of 4.5 km, but that other minor faults also occur. The FZ3 roots in the Triassic detachment level above the basement (Fig. 9). According to the published geological maps the Chailles anticline appears to connect in the north with the Tournier anticline (TO) (Fig. 1B), suggesting that the FZ3 could connect with the Jura internal thrust ( $\phi$ IJu) (Fig. 1B).

#### **4.3.4 The Monts du matin – Voiron thrust or Fault Zone 4 (FZ4)**

To the west of FZ3, seismic profiles reveal a blind thrust system, with two thrusts likely connected at depth, here referred as the FZ4, with a total apparent offset of the basal Upper Jurassic limestones reflector of ~100-300 m in the north (91CHA1-2; 91VER1, Fig. 9B, C) and ~1.24 km in the south (82SE01, Fig. 9D). To the south, this thrust system bounds the Mont-du-Matins anticline (MM, Fig. 9A). The thrusts crosscuts inherited normal faults (i.e. the Saint-Nazaire fault [SN], Fig. 9D) as already reported by Deville et al. (1992), and roots in the Triassic detachment level (Fig. 9).

#### **4.3.5 The St Lattier thrust or Fault Zone 5 (FZ5)**

West of the FZ4, the seismic profile 82SE01 (Fig. 9D) highlights the presence of an additional blind thrust system that corresponds to the St-Lattier anticline (St-La, Fig. 1B) (Deville et al., 1992), here referred as the FZ5. The extension of FZ5



535 to the north is not well constrained, but may coincide with thrusts exhibiting small offsets (<100 m) that are rooted on an inherited normal fault seen along profile 91VER1 ~40 km further north (Fig. 9C). FZ5 is not observed on the seismic profile 91CHA1-2, in the north (Fig. 9B).

#### 4.3.6 Summary of the structure of the subalpine and South Jura domains and regional cross sections

540 Five main west verging thrust zones have been indentified that all mostly trend NNE-SSW on an updated structural map of the subalpine ranges (Fig. 1B) and presented on four regional cross sections (Fig. 11). Folds in between the thrusts have the same general trend and the cross-sections have been drawn in a WNW-ESE direction.

More specifically, sub-surface data and surface data (field observations and geological maps at 1:50 000) were used to build cross-section A west of FZ1, while east of FZ1, the construction of the cross-section relies on the analysis of 1:50 000 scale geological maps and the ECORS-CROP profile (Guellec et al., 1990; Roure et al., 1990; Mugnier and Marthelot, 1991) recently  
545 revised by Pfiffner (2014). The Cenozoic filling consists of Oligocene and Eocene deposits and is involved in superposed nappes (Doudoux et al., 1982). In the north part of the zone, west of Cluses, the Upper Jurassic limestones are found vertically three times along the BZN1 borehole (Fig. 1B for location) (Charollais and Jamet, 1990). Seismic imaging suggests the presence of a thrust uplifting the Brizon basement high (Guellec et al., 1990). To the east, we have also integrated the Montjoie valley synthetic section of Gidon (2019) (Fig. S19A, B, C) for the Aravis and Belledonne chains relationships. In order to  
550 build the westernmost part of section B up to the FZ1, sub-surface data and surface data (field observations and geological maps at 1:50 000) were used. Between FZ1 and the summit of the Grand Manti (Fig. 11B), the construction of the cross-section relies on detailed analyses of 1:50 000 geological maps. To the east of the Grand Manti, the data originate from the northernmost section available in Barf  ty and Gidon (1996). The results presented in Fig. 6, Fig. 7 and in Barf  ty and Gidon (1996) (Fig. S19A, D) were used to build sections C and D (Fig. 10C, D) east of FZ2, while sub-surface data (Fig. 9C, D) and  
555 results presented in Fig. 7 (for section D) were used to the west of FZ2. Sections B and C have been balanced and restored using the Move software (Fig. 18).

In this interpretation, the FZ1 has been refolded and roots east of external Belledonne with large parts of the subalpine ranges (Moucherotte, East Chartreuse, Beauges, Bornes) being klippen. West of FZ1, FZ2 (2a, 2b, 2c) runs from South to North from the Vercors to the l'Epine and the Grand Colombier – Cr  t du Nu. Seismic profiles (Fig. 9B) and structural mapping (Fig. 1B)  
560 highlight that FZ2 has not been refolded as FZ1, but most probably branch at the top of the basement on a flat decollement in the Triassic evaporites that roots further east below external Belledonne massif, in the Belledonne basal thrust (Doudoux et al., 1982; Bellahsen et al., 2014, 2012; Butler, 2017; Deville and Chauvi  re, 2000; Deville et al., 1992, 1994). FZ1 and FZ2 are only 4 to 9 km apart in the Vercors-Chartreuse, but 39 km apart in the Jura-Bauges (Fig. 1B). Such widening is the combination of a fan-like map-shape of the folds and offsets by left-lateral NW-SE faults. The greater distance between the  
565 thrust and the inner part of the belt in the Jura is likely to represent a more efficient d  collement in the North, where Triassic evaporitic series are thicker (Philippe et al., 1996; Lickorish et al., 2002; Deville, 2021). Anticlines are found in FZ2 hangingwall and thus in FZ1 footwall (Fig. 1B, Fig. 11), but related to the activity of FZ2 according to Guellec et al. (1990)

and Doudoux et al. (1982). FZ3 is continuous from the Vercors to the western Chartreuse. Further north, according to published geological maps, it appears to turn to the west and merge with the “chevauchement majeur du Jura interne” (φIJu, Fig.1B) (Philippe, 1995). The map pattern is similar to that of the FZ2 and interpreted in the same way. As there is no significant basement culmination between FZ2 and FZ3, FZ3 is interpreted to follow the same décollement level and to root underneath the Belledonne external massif as FZ2. FZ4 is only documented from seismic profiles and its apparent offset decreases toward the north. The general fault pattern might suggest that FZ4 could connect with the “chevauchement majeur du Jura externe” (φEJu, Fig.1B) through the NW-SE Jura transfert zone followed by the Rhône river (J, Fig. 1B) (Philippe, 1995). FZ5 is only documented west of the Vercors. As there is no significant basement culmination between FZ5 and FZ2, FZ5 and FZ4 are interpreted to follow the same décollement level and to root underneath the Belledonne external massif. East verging thrusts are locally described. East of the Royans (RO, Fig. 1B) in the Vercors and in the crêt du Nu in the Jura (CN, Fig. 1B), they appear to be linked with the underlying west verging decollement (Philippe, 1995). In Grenoble (Ecoutoux anticline, Fig. 7A, B; Fig. 11C), they appear as related to a late deformation phase (Barfěty and Gidon, 1996).

As described above, the NW-SE (N145°) left-lateral South Jura transfert zone appears to offset FZ3 and possibly FZ4 (Fig. 1B). The step over between the Voreppe (2a) and the Epine (2b) thrusts stands in the prolongation of this zone and shows small NW-SE left-lateral faults (Fig.1B) suggesting that it is linked to the same process. Other similar faults are only found at the southern tip of the Rencurel thrust (2a, N140°), and possibly along part of the Isère valley near Grenoble offsetting FZ1 (Fig. 1B). Numerous NE-SW (~N65°) right-lateral faults affect the southern Bauges, the Chartreuse and the northern Vercors (Fig. 1B). These faults offset FZ1 and possibly FZ2 but not FZ3 (Fig. 1B). Both the left-lateral and the right-lateral faults are compatible with an ~ESE-WNW compression as the main trusts and folds.

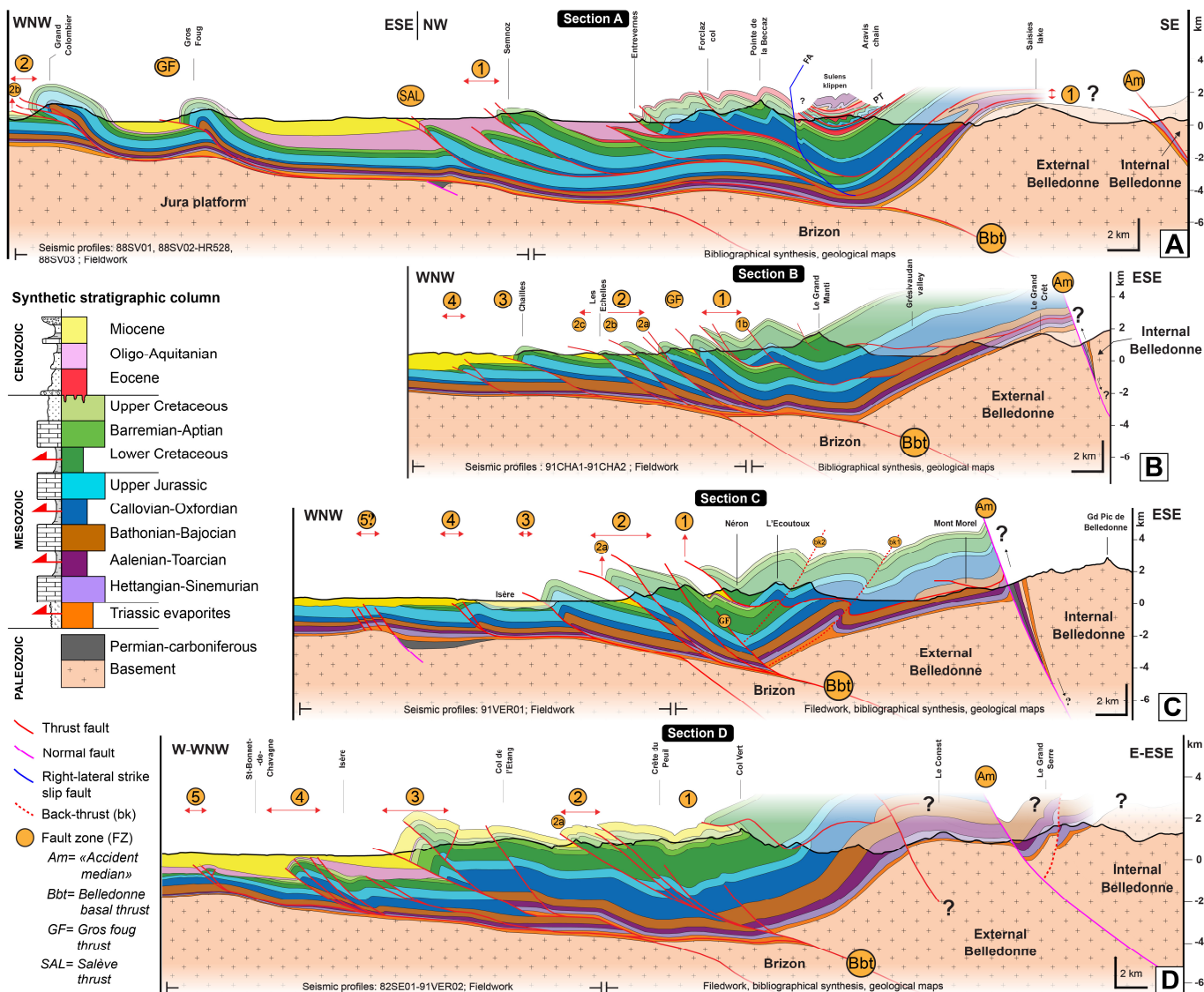


**Figure 11: Regional cross-sections of the study area. Cross section location on the Fig.1. A) cross section A through the eastern Jura and the Bornes. PT= Penninic thrust. AF= Arcalod fault. B) Cross section B through central Chartreuse and Belledonne. C) Cross section C through southern Chartreuse and Belledonne. D) Cross section D through Vercors and southern Belledonne.**

## 4.4 Relationships between sedimentation and tectonics

### 4.4.1 The Rumilly syncline

In the footwall of the FZ1, in the Rumilly syncline located to the north of the oriental domain (Zone A, Fig. 5), the Oligo-Miocene succession starts with sub-concordant onlaps on the Mesozoic substratum, according to seismic profiles (Fig. 10).

The thickness of the Oligo-Aquitainian continental deposits decreases westward (Fig. 10C, D). Indeed, these deposits are ~200 m thick west of the Rumilly syncline (Fig. 9C, D) (Enay et al., 1970; Gidon, 1970b), while to the east, they reach 1838 m

between the footwall of the FZ1 and the hangingwall of the SAL fault (SLV2 well data, Fig. 10A, B), and 1716 m at the footwall of the SAL fault (SV-101 well data, Fig. 10A, D). Thus, on both sides of the SAL fault, which appears west of the FZ1 (Fig. 10B), the thickness of Oligocene deposits is relatively similar (Fig. 10B, D), suggesting that the Oligo-Aquitania depocenter was located in the footwall of FZ1. This, along with sub-concordant Oligocene strata on the Mesozoic substratum, suggests that the SAL fault likely activated after the deposition of both Oligocene and Early Miocene sediments (21-18 Ma). This is further consistent with field analyses revealing that the basal Miocene Molasse deposits (upper Aquitanian-lower Burdigalian) are conformably lying on continental Aquitanian deposits dipping vertically in the eastern flank of the Rumilly syncline (Alby-sur-Chéran, 3, Fig. 3). Altogether, this implies that both Oligocene and Miocene sediments were deformed by the SAL fault after deposition, then after the early Burdigalian.

#### 4.4.2 Grésy-sur-Aix section

To the south of the Rumilly syncline, in the Grésy-sur-Aix sedimentological section (4, Fig. 3), (Fig. 12A) the sequence S2a basal boundary (dated to 18.05 +/- 0.3 Ma based on correlation with the Forezan section (5), see Fig. 2; Fig. 3 for location) was extrapolated along-strike to the north. In the 88SV01 and 88SV03 seismic profiles (Fig. 9D, C), this major stratigraphic surface coincides with a high amplitude reflector. This reflector is characterized by low-angle toplaps and onlaps that either suggest: (i) an angular unconformity, which would materializes the onset of a tectonic phase; or (ii) an erosive surface above the underlying deposits, which corresponds to a classic feature for sequences boundaries.

The Grésy-sur-Aix section outlines three examples of syntectonic sedimentation within sequence S2a (Fig. 12). First, sequence S2a is abnormally thick and has a very high sedimentation rate of 0.72 +/- 0.32 mm y<sup>-1</sup> (~750 m of sediments deposited over ~0.85 Myr between 18.05 +/- 0.25 [base] to 17.2 +/- 0.15 Ma [top]. For the top of the S2a sequence which was recorded during the Chron C5Cr, the calculation excludes an age older than the Chron C5Cr starting at 17.23 Ma), compared to the underlying sequences S1a-S1b, that is only 200 m thick has an average sedimentation rate of 0.06 +/- 0.01 mm y<sup>-1</sup> (deposited over ~3.5 Myr between 21.45 +/- 0.3 and 18.05 +/- 0.25 Ma) (Fig. 12A). This suggests a significant increase of accommodation space at the initiation of sequence S2a, likely related to a regional tectonic event. Second, a 15m-thick interval (390-405m, Fig. 12A) with a regional-scale continuity (also described 18 km to the south, in section 5, at ~380 m, Fig. 2) containing disorganized monogenic clasts of various sizes (cm to pluri-m, Fig. 12C) and 'ball and pillow' structures (Fig. 12D), suggest an earthquake-disturbed layer (i.e. seismites, F25 sensu Kalifi et al., 2020). Third, the occurrence of an angular unconformity observed in tidal flat deposits (Fig. 12A, B), as characterized by a decrease in bedding dip from 18° to 7° up-section and an erosive surface exhibiting westward-directed onlaps above it. This angular unconformity argues for a compressive tectonic event.

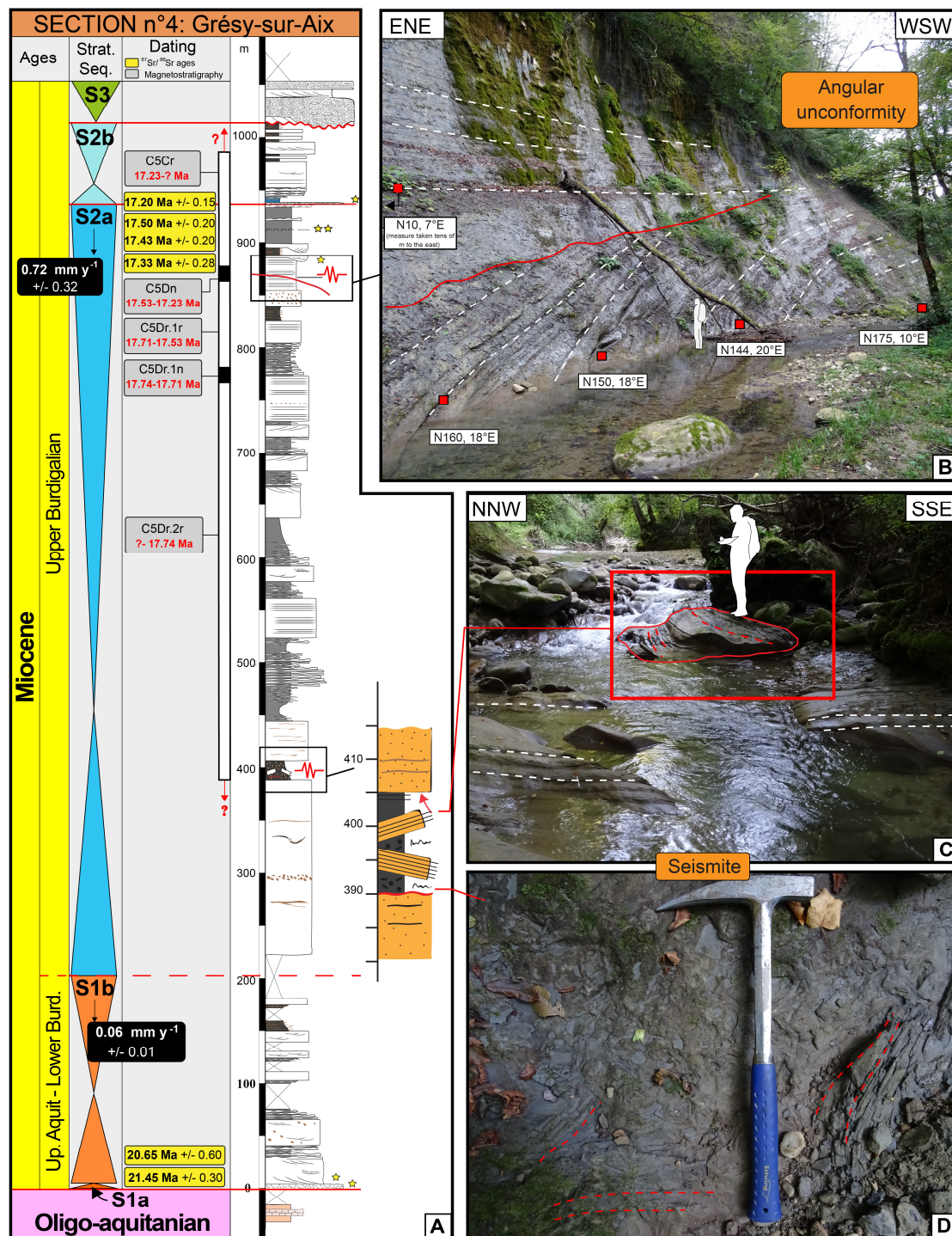


Figure 12: (A) Grésy-sur-Aix sedimentological section with sequence S2a syntectonic deposits indicated: seismite near the bottom (see also C and D) and angular unconformity near the top (see also B). The S2a sequence boundary was observed and dated in the Forezan section (5, Fig. 2). Legend in Fig. 5. Black box= Average sedimentation rate of the sequence; (B) The angular unconformity has established between 17.53 and 17.23 Ma within Chron C5Dn. White dashed lines = bedding. Red line = erosive surface. Red



630 square = Dip measure; (C) Seismite disturbing 15 m of sediments in S2a, with plurimetric blocks tilted in situ and slump balls; (D)  
Detail of an intensively disturbed sedimentary level.

The timing of the angular unconformity is further well-constrained by magnetostratigraphy, and has been associated to Chron  
C5Dn at 17.35  $\pm$  0.15 Ma (Fig. 2). Thus, sequence S2a most probably records the onset of a compressive phase. In this  
interpretation, in the 88SV01 and 88SV03 seismic profiles (Fig.9D, C), the sequence S2a sequence boundary characterized by  
635 low-angle toplaps and onlaps is a tectonic-driven angular unconformity, and thus, dates the initiation of compression at 18.05  
 $\pm$  0.25 Ma.

#### 4.4.3 Southern Jura synclines

Strontium, biostratigraphical and magnetostratigraphical dating were applied on sedimentological sections 3, 4, 5 (oriental  
domain, zone A) and 13 (median domain, zone C) from the southern Jura synclines immediately north of Chambéry (Fig. 3).  
640 Sequence stratigraphy interpretations enable E-W correlations in lower Miocene deposits between section 3 and section 13  
(Fig. 13), by using sequence boundaries and maximum flooding surfaces. The thicknesses of sequences S1a-S1b do not exceed  
200 m in sections 3, 4 and 5 (Fig. 13), and are even absent to the west, in section 13 (Fig. 13). During sequence S2a, the  
maximum thickness is  $\sim$ 750 m and is recorded in section 4 (Fig. 13), while to the west, in section 13 (Fig. 13), sequence S2a  
is 145 m thick. Furthermore, in section 4 (Fig. 13), the average sedimentation rate increases sharply from 0.06  $\pm$  0.01 mm y<sup>-1</sup>  
645 <sup>1</sup> during sequences S1a-S1b, to 0.72  $\pm$  0.32 mm y<sup>-1</sup> during sequence S2a (Fig. 12A). This firmly demonstrates that a  
depocenter localized close to section 4 (Fig. 13) appeared during sequence S2a. Subsequently, the thickest accumulation of  
the following sequence (S2b) lies further west at the Forezan locality (275 m, section 5, Fig. 13). This lateral variation of the  
thickness is associated with significant lateral facies variation characterized by a dominance of proximal marine deposits to  
the east (950-1015 m, section 4, Fig. 13), while to the west, sequence S2b is mainly represented by distal marine deposits (700-  
650 920 m, section 5, Fig. 13), thereby suggesting a westward migration of the depocenter between sequences S2a and S2b. This  
is also consistent with a progressive decrease of accommodation rates from ca. 1.17 mm yr<sup>-1</sup> to 0.17 mm yr<sup>-1</sup> between sequences  
S2a and S2b in section 4 to the east (Fig. 13). Finally, the maximum thickness of sequence S3 is recorded west of the section  
5 (Fig. 13), at section 13 (Fig. 13). There, the sequence S3 is 390 m-thick, while in the Rumilly-Chambéry synclines area (Fig.  
13), the sequence S3 was probably much thinner. Furthermore, during deposition of sequence S3, lateral variation of the  
655 thickness is associated with significant lateral facies variation. At Loisieux (section 13, Fig. 13; Fig. S7), sequence S3 is mainly  
characterized by distal marine deposits, while it exhibits coarse-grained deltaic deposits to the east (sections 4, 5, Fig. 13; Fig.  
S5). These proximal deposits suggest that the Rumilly-Chambéry synclines area was progressively exhumed, which is also  
suggested by the continuation of the progressive decrease of accumulation rates recorded between sequences S2a and S2b.  
Thus, the S3 depocenter is most-probably located in the Loisieux locality (section 13, Fig. 13), further highlighting the  
660 westward migration of the depocenter (Fig. 13).

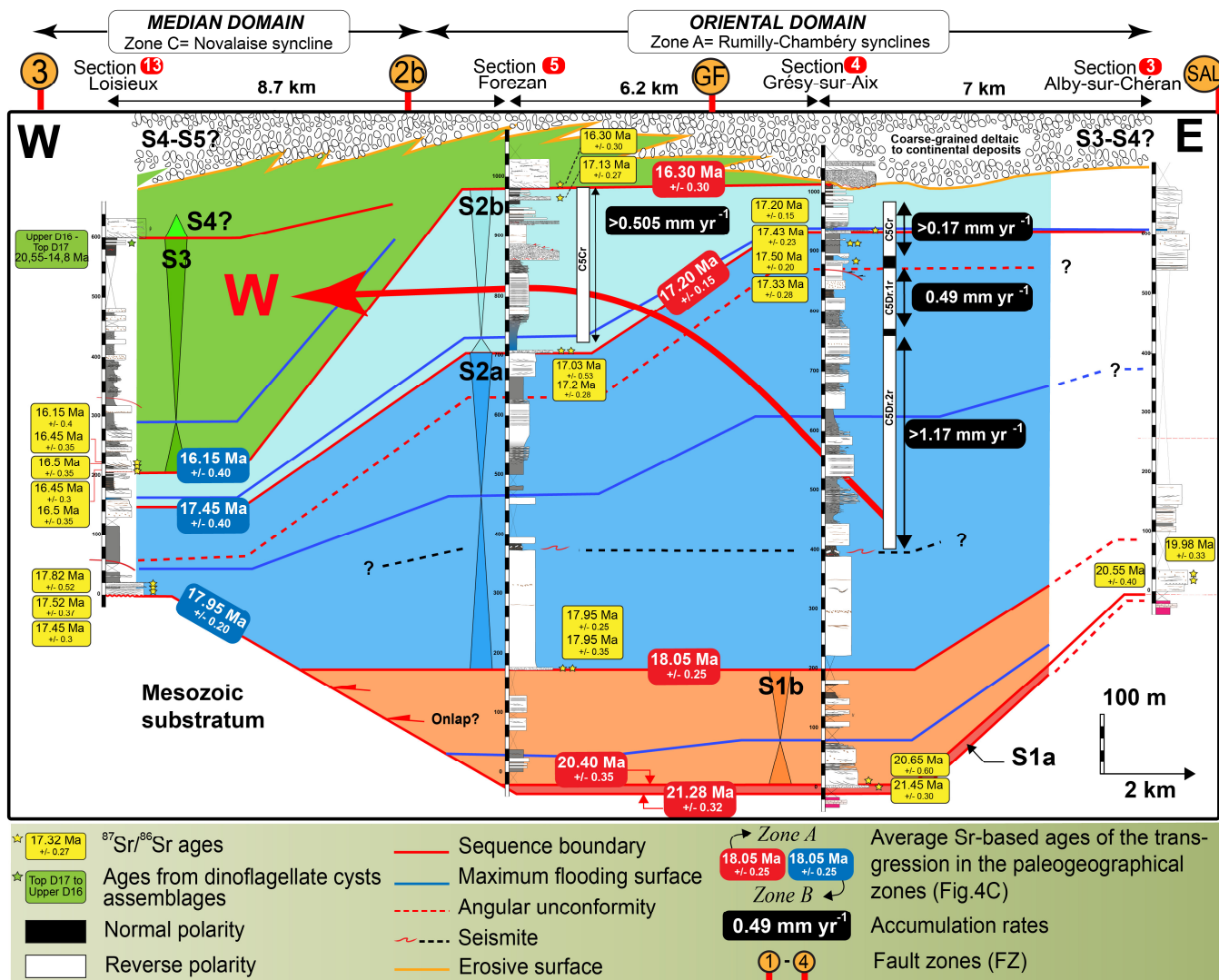


**Figure 13: Westward migration of the depocenter during the lower Miocene (red curved arrow). The sedimentological sections were projected on a E-W axis, which corresponds to a direction orthogonal to the thrusts. See Fig. 3 for location of the transect and sedimentological sections. Red squares = sedimentological sections quoted in the text and used for correlations. The dashed red line corresponds to the angular unconformity presented in Fig. 12B.**

#### 4.4.4 Western Chartreuse

In the 91CHA1-2 seismic profile (Fig. 14A), the Miocene sequences were calibrated using the PA-1 well-log (Fig. 14B, C). The thicknesses of sequences S4 and S5 increase from the hangingwall to the footwall of the FZ4, which is likely associated with a decrease in bedding dip up-section (Fig. 14A) suggesting growth-strata in response to FZ4 activity. On the other hand, the underlying S3 deposits are isopacheous both in the footwall and the hangingwall of FZ4 giving an initiation of FZ4 after the deposition of sequence S3. The end of tectonic activity on FZ4 is not so well constrained since seismic data do not allow a detailed observation of S6 deposits, although sequence S6 apparently seals (conformably) the underlying deposits, that might

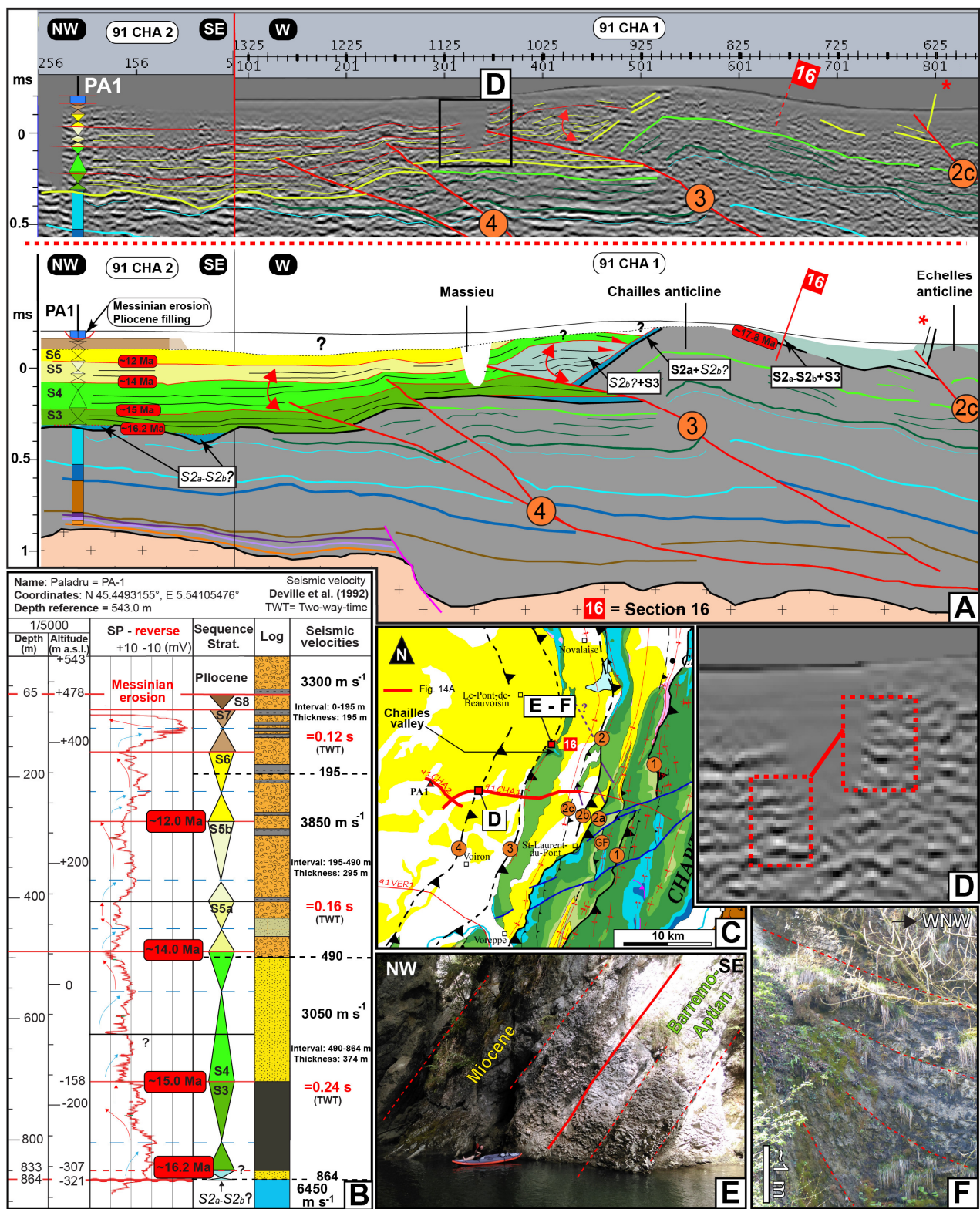
suggest the end of tectonic activity. This could be in accordance with the fact that the FZ4 offsets solely S4 deposits, while S5 deposits are simply folded that probably indicates a progressive decrease in the tectonic activity from sequences S4 to S5.

675 Alltogether, these observations suggest that the FZ4 activity was recorded by the sequences S4 and S5 (~15.0 to ~12.0 Ma). Further east, beyond the artefact located at the emergence of FZ3 (Massieu, Fig. 14A), the identification of sequence S4 is proposed based on similar seismic facies (Fig. 14D). In the hangingwall of FZ3, the basal Miocene deposits are conformably lying on the Mesozoic bedrock (on top of the Chailles anticline). This is consistent with fieldwork observations made 5 km to the north, in the Chailles gorges (Fig. 14A, C), where the basal Miocene Molasse deposits have been attributed to sequence

680 S2a (Fig. 14E) suggesting that FZ3 was inactive during deposition of the sequence S2a. On the FZ3 hangingwall, the overlying sequences (S2b? -S3) geometries are observed on the 91CHA1-2 seismic profile (Fig. 14A), and their thicknesses decrease gradually when approaching the Chaille anticline together with a decrease in bedding dip. In the up section, S2b?, S3 and S4 sequences are also characterized by eastward-directed onlaps on the folded S2a deposits (Fig. 14A), thus suggesting growth-strata related to FZ3 activity, between these sequences. Downstream to the Chailles valley (Fig. 14C), above the S2a sequence,

685 high in the cliff, growth strata (Fig. 14F) are again suggested based on apparent eastward-directed onlaps onto S2a deposits, in agreement with the interpretation of the seismic profile. However, these outcropping onlaps does not allow to identify more precisely the timing of the growth strata.





690 **Figure 14: Growth strata relationships inferred for FZ3 and FZ4 based on the 91CHA1 and 91CHA2 seismic profiles, sequential interpretation of the PA-1 well and fieldwork observations. The ages in red boxes correspond to the homogenized ages of the eustatic-driven transgressions (Fig. 4B). Orange circle = Fault zone (FZ). (A) Seismic profiles 91CHA1 and 91CHA2 depicting the Miocene reflectors and geometrical relationships associated with FZ3 and FZ4. The red double curved arrows point the growth stratas. Legend in Fig. 9. (B) Sequential interpretation of the PA-1 well and conversions of sedimentary thicknesses into seismic velocities (Deville et al., 1992). Legend in Fig. 15. SP-reverse= Reversed spontaneous potential curve (in response to water saturation), in millivolts (mV). (C) Geographical and geological locations. Legend in Fig. 1. (D) Zoom on the Massieu area (see location on A) showing similar seismic facies on both sides of the Massieu artefact and suggesting positive offset across FZ3. (E) Tilted concordant Urgonian-Miocene basal conglomeratic contact (S2a). (F) Growth-strata relationships at approximately 20 and 30 m above the river level, corresponding to S2b or S3 deposits according to regional correlation lines.**

695

#### 4.4.5 Bas Dauphiné basin

700 In the Bas-Dauphiné basin (Fig. 1B), the Miocene Molasse deposits are poorly deformed and only the upper part of the Miocene succession crops out. So, the three SE-NW transects (Fig. 3) presented here are proposed using the interpretation of borehole data using sequence stratigraphy (Fig. 15) and our updated chronostratigraphy. Correlations are proposed by using the main sequence boundaries elevation (in m a.s.l.= meters above sea level).

The Bas-Dauphiné basin is separated into two tectonic zones. West of the Montmiral high (Fig. 15B, C), no compressive structures were found (Kalifi, 2020; Couëffé and Tourlière, 2008). On the other hand, FZ4 and FZ5 blind thrusts are found to the east of the Montmiral and L'île Cremieu highs (Fig. 15A, B, C). In this area, the S2a, S2b and S3 sequences exhibit very few thickness variations (~100 m for S2a-b sequences between VAF-1 and VAF-2 wells, Fig. 15B, and ~50-70 m for S3 sequence between SLF-1, MO-1, MO-2 and MO-3 wells, Fig. 15C), despite the presence of the FZ5 thrusts within transect C and possibly B. On the western edge of the Bas-Dauphiné basin, the absence of S2a-S2b deposits (to the northwest of PA-1, VAF-2 and MO-3 wells, Fig. 15A, B, C) and the thickness variations of the S3 sequence to the west of the Montmiral high (Fig. 15B, C) are attributed to a complex inherited paleo-topography (Kalifi, 2020) along the Oligocene West European Rift (Debelmas 1974; Curial 1986; Bergerat 1987; Ziegler 1988, 1990, 1994; Bergerat et al. 1990; Sissingh 2003).

705

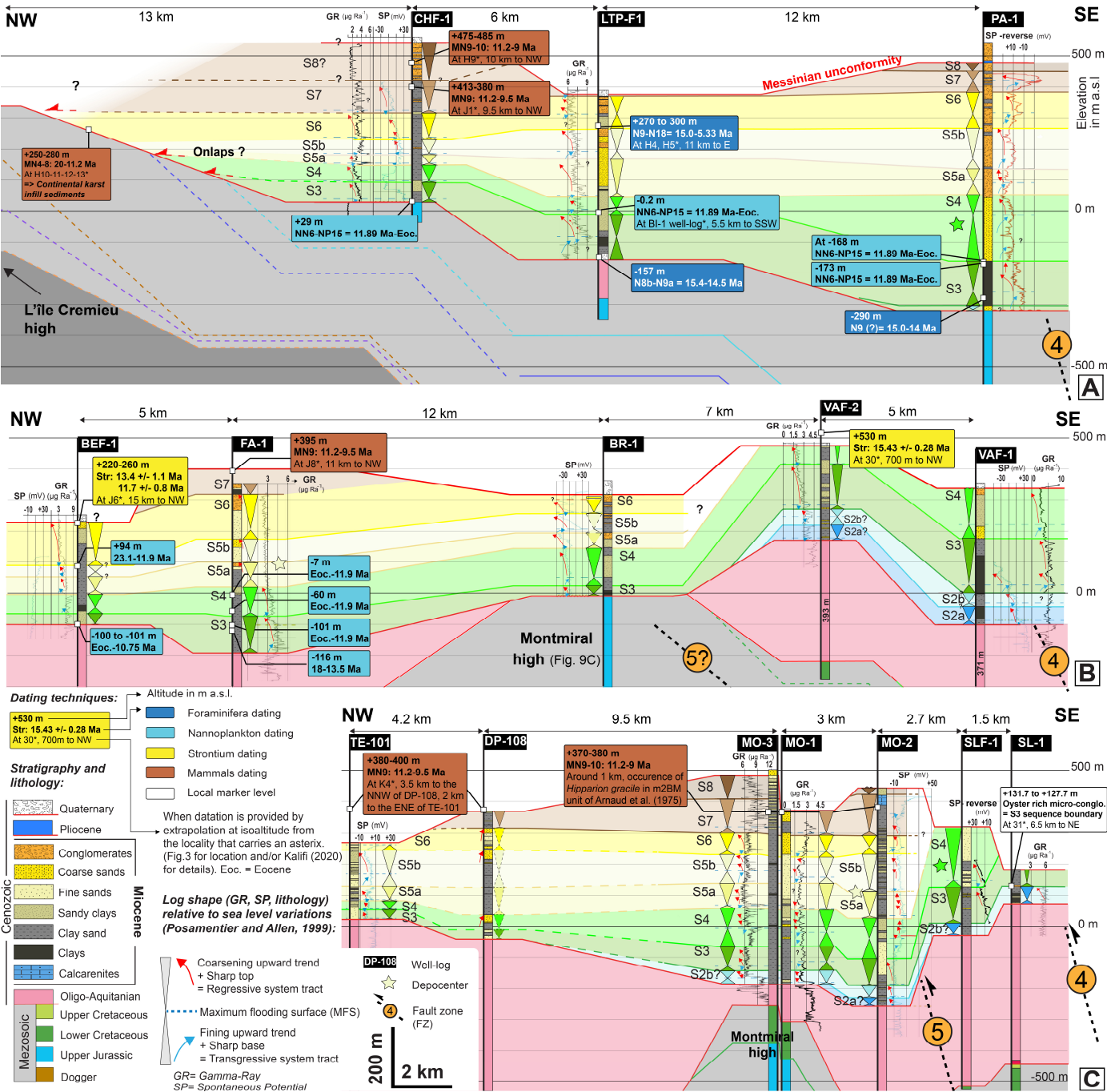
East of the Montmiral high, significant variations in depositional thickness are observed for S4 sequence with a maximum located in the footwall of the FZ4. In the transect A (Fig. 15 A), a S4 sequence maximum thickness of 215 m is recorded in the PA-1 well, while to the west, the sequence S4 thickness decreases progressively, reaching 53 m in the CH-1 well. In the transect B, sequence S4 maximum thickness is recorded in the VAF-1 well, with a thickness of at least 161 m (since its top is eroded), while to the west, sequence S4 is 118 m-thick in the BRI-1 well, above the Montmiral high (Fig. 15B). In the transect C, sequence S4 maximum thickness is recorded in the SLF-1 well, with a minimum of 190 m (eroded top), while to the west, sequence S4 is 129 m and 116 m, respectively, in the MO-2 and MO-3 wells (Fig. 15C).

715

720 The sequences S5a-S5b also exhibits variation in thickness. In the transect A, a S5a-S5b maximum thickness of 210 m is recorded in the PA-1 well, while it decreases progressively to the west reaching 82 m in the CH-1 well (Fig. 15A). In the transect B, sequences S5a-S5b maximum thickness is difficult to estimate because the top of the VAF-1 and VAF-2 successions are eroded to the east of the Montmiral high (Fig. 15B). However, a probable depocenter is located to the west of the FZ5, in the FA-1 well, with a thickness of 153 m (Fig. 15B). In the transect C, sequences S5a-S5b depocenter can be located between the Montmiral high and the FZ5, in the MO-2 well (Fig. 15C). There, the sequences S5a-S5b are 204 m-thick, while to the

725

west, it is ~165 m-thick above the Montmiral high (MO-2 and MO-3 wells, Fig. 15C). To the west, the interpretation of the DP-108 well is difficult as only lithological data are available but might suggest another depocenter with a thickness of 205 m (Fig. 15C).



730 **Figure 15: Spatio-temporal distribution of Miocene Molasse deposits along SE-NW transects of the Bas-Dauphiné basin. Correlations are proposed based on sequence stratigraphy interpretations using stacking pattern methodology on SP (Spontaneous potential), GR (Gamma ray) and lithological data from well logs. Fig. 3 for location of transects.**

No significant thickness variations are observed for the S6 sequence, which is ~105m-thick along the transect A (Fig. 15A), ~145 m-thick along the transect B (Fig. 15B), and ~70 m-thick along the transect C (Fig. 15C). The variation in thickness for  
735 S7 and S8 sequences cannot be estimated as they are rarely present in well-logs (Fig. 15).

#### 4.4.6 Bresse basin

To the east, the La Bresse basin is bordered by the l'île Cremieu high, in the south, and by the N-S striking Jura thrusts in the North (Fig. 1B). In the La Bresse basin, the lower Miocene is absent, and the area is finally flooded at ~12.0 Ma only during S6 sequence (Fig. S13). The S6 sequence (~12.0 to ~10.8 Ma, Fig. 4B) and the transgressive deposits of the S7 sequence  
740 (~10.8 to ~10 Ma, Fig. 4B) are characterized by marine deposits, while the regressive systems tract of the sequences S7 and the S8 exhibit purely continental deposits implying a major regression starting during sequence S7.

At the Jura front, the BY-101 well-log (Fig. 3) shows Mesozoic units thrusting atop Miocene deposits (Dumont, 1983). The same Miocene succession outcrops at the eastern border of the La Bresse basin, at Jujurieux (Dumont, 1983; I2, Fig. 3), and corresponds to marine deposits of sequences S6 and S7 based on Sr ages (Table S2), which are consistent with the magneto-  
745 biostratigraphical results of Aguilar et al. (2004). Therefore, the sequences S6 and S7 are thrusting by the Jura thrust, at the BY-101 locality. Thus, the onset of the Jura thrust is either synchronous, or younger than the deposition of S6-S7 marine deposits (~12 to ~10 Ma).

At the Jura front, the continental deposits, belonging to the S8 sequence according to mammal-based datings (I4, I5, I6 localities; Fig. 3), could also be partly deposited during the S7 regressive tract, and are characterized by a 200 m-thick  
750 continental clay and marl succession (Demarcq, 1970). This important thickness may suggest the existence of a tectonic-controlled depocenter in the footwall of the Jura thrust.

## 5 Discussion

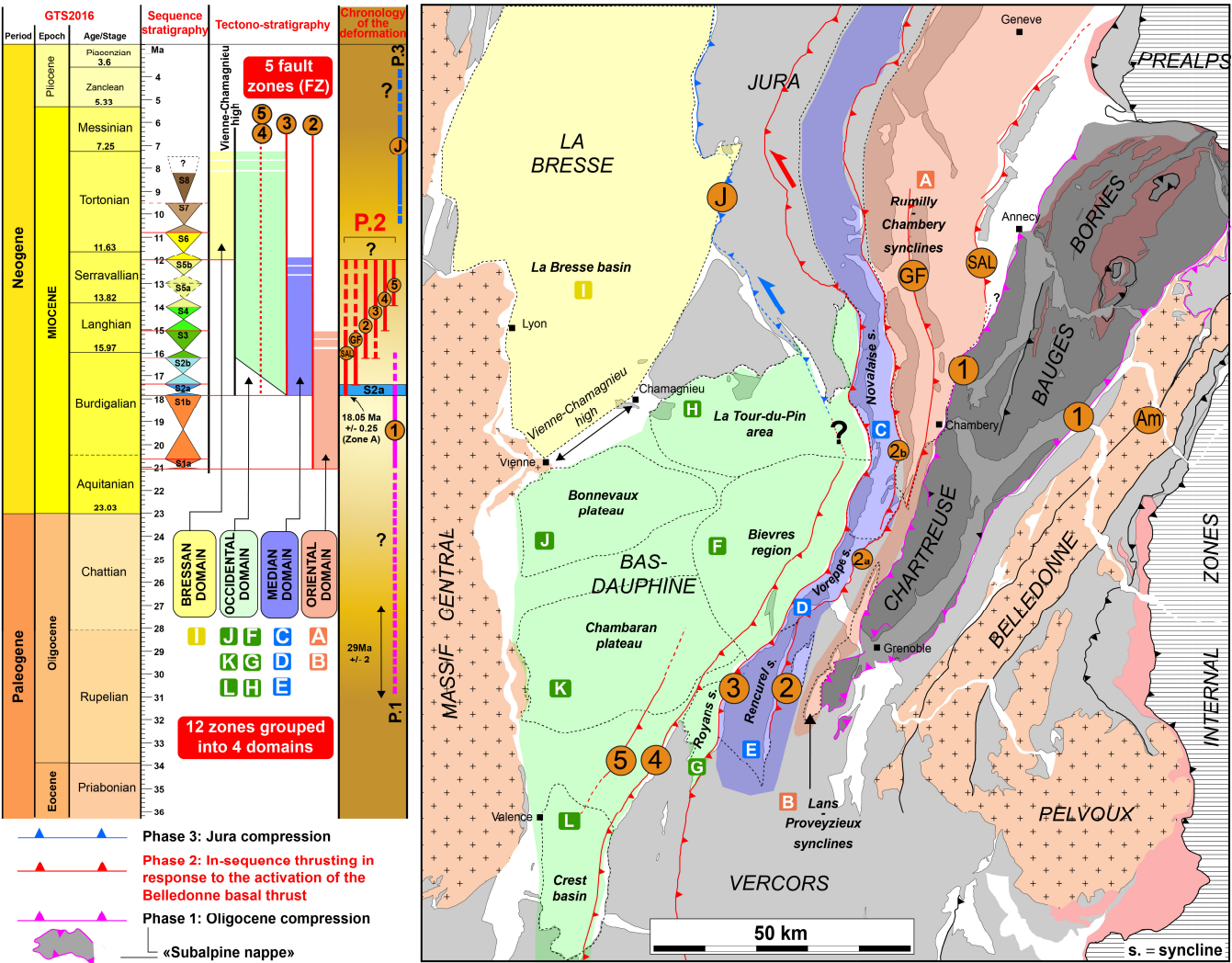
### 5.1 Genetic relationships between the stratigraphical domains and the fault zones (FZ)

The different depositional sequences depict a conspicuous spatial organization at the regional scale defining four depositional  
755 domains (Fig. 5). The Oriental and Median domains correspond to narrow longitudinal north-south bands, which are orthogonal to the general ~ESE-WNW direction of shortening linked to the alpine compression. The age of the basal sequence becomes younger toward the west, indicating a westward migration of the depocenters (Fig. 4C). A similar migration can be deduced from the thickness variation of the sequences (e.g., S2a-S2b, S3 and S4) (Fig. 5). The Oriental, Median and Occidental domains are respectively bounded to the east by the FZ1, FZ2 and FZ3 (Fig. 16). Such correspondence between the localisation



760 of the sedimentologic and the structural boundaries suggests a genetic relationship between thrusting, accommodation space creation and sediment infill.

The presence of angular unconformities and seismites within Burdigalian deposits of the southern Jura synclines (Fig. 1B) were already mentioned by Beck et al. (1998), Blanc (1991), and Deville et al. (1994), although the chronostratigraphic framework was still sketchy at that time. The present study, integrating evidence for syntectonic deposits, growth strata  
765 geometries and depocenter migration at the basin scale within a well-constrained chronostratigraphy, allows to depict the Miocene tectono-sedimentary evolution as follow.



770 Figure 16: Summary of the structural, chronostratigraphical and tectonostratigraphic results of this study. The 11 sedimentary sequences revealed 12 paleogeographical zones, themselves grouped into 4 paleogeographical domains. 5 fault zones (FZ1-5) were identified. Based on the established tectono-sedimentary evolution, three compressive phases were identified. The main phase corresponds to Phase 2, which involved the progressive onset, from east to west, of the SAL fault to FZ5 in response to the onset of the Belledonne basal thrust.

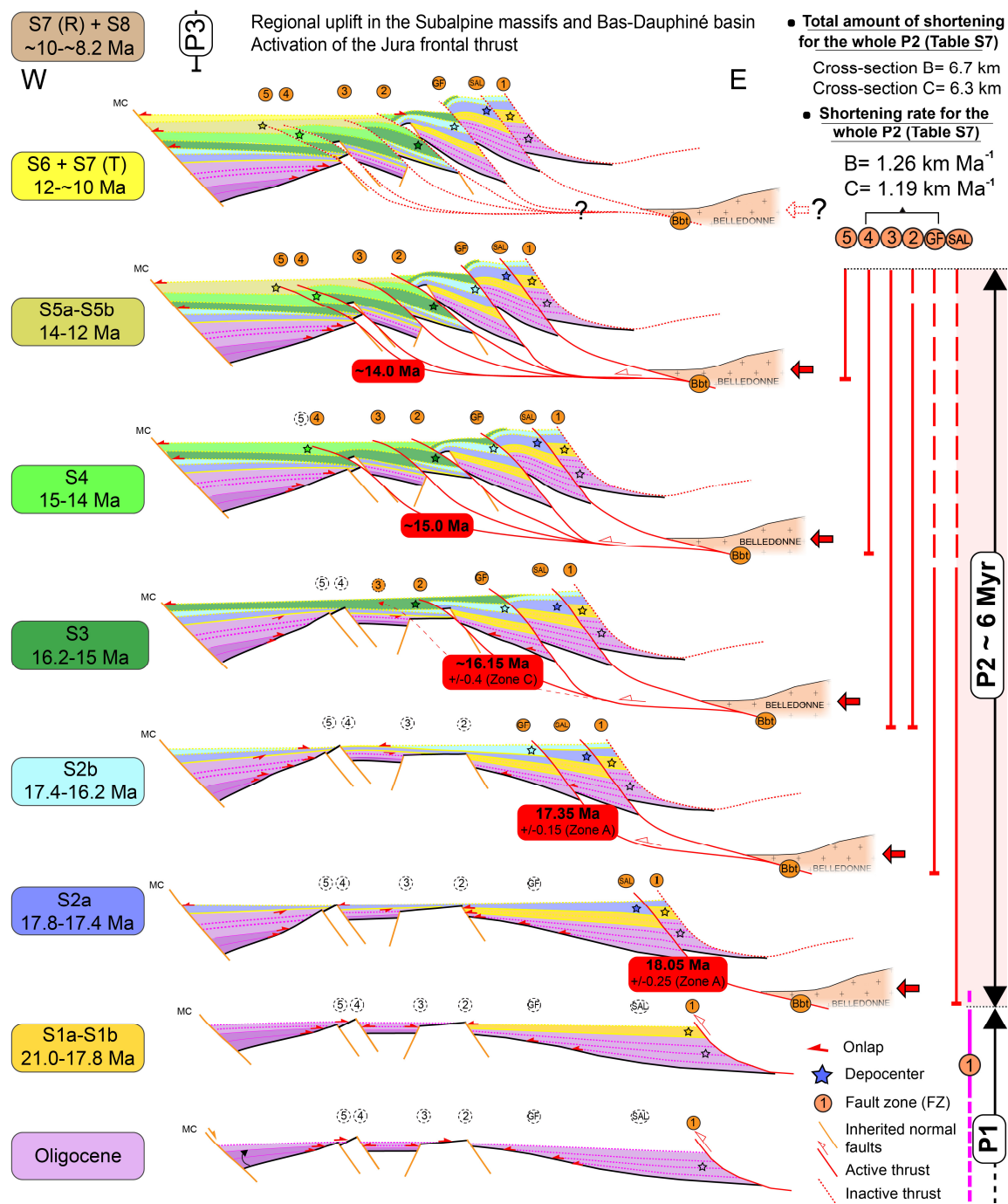
### 5.1.1 The FZ1 activity (Phase 1)

The westward thinning of the Oligocene and Miocene S1a-S1b succession (~21.0 to ~18 Ma) observed in the Rumilly syncline implies a regular subsiding area between ~29 +/- 2 Ma (Rigassi, 1957; base of the Oligocene deposits dated by palynostratigraphy westwards of Annecy, locality 3; Fig. 10A, C) and 18.05 +/- 0.15 Ma (S2a sequence boundary, Fig. 10A, C). Moreover, the westward-directed onlaps on the Mesozoic substratum, as well as the younger age of the base of the Oligocene sediments at the west of the Rumilly syncline (~23 Ma based on mammals, Gaudant et al., 2002, locality 7; Fig. 10A, C), suggest a regular and slow westward migration of the depocenter. In a foreland basin, this geometry is consistent with a foredeep depozone located between the poorly subsiding proximal flank of the forebulge and the footwall of the active (tectonic) orogenic front, where the maximum of subsidence is recorded in response to the interplay between topographic loads and long-wavelength lithospheric deflection in relation with subduction process (DeCelles and Giles, 1996; Schlunegger and Kissling, 2015). The progressive decrease of depositional thicknesses towards the west might imply the proximity to the forebulge, whereas the maximum depositional thickness recorded to the east of the Rumilly syncline suggests the proximity to the orogenic front. This interpretation is consistent with that of Deville et al. (1994), who previously interpreted the Oligocene sedimentary succession in this area as deposited in a passive foreland flexural basin. The upper Oligocene-lower Miocene tectonic front is therefore located east of the Rumilly syncline. Since marine Miocene deposits have never been described east of FZ1, we believe that it already formed a morphostructural barrier during the first marine sequences (S1a-S1b; 21.0 to ~18 Ma, Fig. 4B, C) and was thus active at least between ~21.0 and 18 Ma, and possibly as early as 29±2 Ma. However, in the early stage, the active front could as well have been located east of FZ1, for example along the Entrevernes thrust [E] (Fig. 1B) or even further east, and other arguments are still needed to decipher the ante-21.0 Ma structural history.

### 5.1.2 Onset of the SAL, GF and FZ2 faults (begining of Phase 2)

Southwest of the Rumilly syncline, the E-W correlation between sedimentological sections 3, 4, 5 and 13 (Fig. 3) highlights important thickness variations (Fig. 13), leading us to propose the following chronology. At 18.05 +/- 0.25 Ma, sequence S2a exhibits a prominent acceleration in accumulation rates especially at the Gresy-sur-Aix locality (section 4, Fig. 13), suggesting the rapid production of accommodation space probably linked to a regional tectonic event. Interestingly, the occurrence of seismites involving a major earthquake is observed within the S2a transgressive tract (Fig. 12). Seismic profiles from the Rumilly syncline (Fig. 10) outline that the S2a basal sequence boundary corresponds to high-amplitude reflectors characterized by low-angle S1 toplaps and S2 onlaps, thereby advocating for an angular unconformity. Together, this suggests a tectonic event associated with the activation of the SAL thrust at 18.05 +/- 0.25 Ma, since the sequence S2a depocenter is located at the footwall of this fault (Fig. 17). Subsequently, the angular unconformity highlighted in tidal flat deposits, and associated to Chron C5Dn (17.53-17.23 Ma, Fig. 12A, B) recovered at the top of the S2a regressive tract, most probably reflects another regional tectonic event with the depocenter abruptly migrating westwards at that time, at the footwall of the GF fault (section 5, Fig. 13). These two lines of evidence, therefore, support the hypothesis of the onset of the GF fault during Chron C5Dn

805 (Fig. 17). At ~16.2 Ma (S3 transgression), the depocenter migrated westwards again and lies at the footwall of FZ2 (section 13, Fig. 13). There, during deposition of sequence S3, thick distal marine deposits were sedimented, whereas coarse-grained deltaic deposits prevailed to the east of FZ2 (sections 4, 5, Fig. 13), suggesting a more proximal and uplifted area. Thus, FZ2 was activated during deposition of sequence S3 (Fig. 17).



810 **Figure 17: Schematic framework summarizing the main phases of thrust propagation at the western alpine front, and their**  
**chronology, based on a thorough revision of the regional chronostratigraphy between the Oligocene and the late Miocene. The**  
**horizontal and vertical scales are not respected. MC= Massif Central; P= Tectonic phase; T= Transgressive deposits; R= Regressive**  
**deposits. The colored boxes on the left side correspond to the homogenized ages of the eustatic-driven depositional sequences (Fig.**  
815 **4A, B). Red boxes highlight the timing of fault initiation deduced from depocenter migration (Fig. 13). Vertical lines on the right**  
**represent the proposed timing of activity for each fault.**

### 5.1.3 Onset of FZ3, FZ4 and FZ5

At the hangingwall of FZ3, the base of sequence S2a is concordant on the folded Urgonian suggesting that folding did not start before the deposition of S2a sequence. Sequences (S2b?)-S3 exhibit growth-strata geometries suggesting a westward thickening of sedimentary deposits (Fig. 14C, D), which can be attributed to an anticline formation in the hangingwall of FZ3.

820 Without further stratigraphic constraints, however, we can only speculate that FZ3 is active at least since deposition of sequence S3 (~16.2 Ma, Fig. 17). On the eastern edge of the Bas-Dauphiné basin, at the footwall of FZ4, the presence of growth-strata geometries between sequences S4 and S5 (Fig. 14A), as well as the occurrence of a sequence S4 depocenter between FZ4 and FZ5 (Fig. 15), implies a flexural subsidence at the footwall of the active FZ4, therefore constraining the activity of FZ4 between the onset of sequence S4 and the end of sequence S5, so between ~15.0 and ~12.0 Ma (Fig. 4A, B;

825 Fig. 17). This is also in agreement with the underlying S2 and S3 deposits, and the overlying S6 deposits, which all appear isopachous (Fig. 14, Fig. 15), and thus suggests the absence of tectonic activity during deposition of these sequences. In the FZ5 footwall the presence of a sequences S5a-S5b depocenter (~14.0 to ~12.0 Ma) (Fig. 15C) suggests a continuous westward migration of the depocenters (Fig. 17), that could be controlled by the FZ5 activity at that time. This hypothesis is consistent with the general trend observed since the base of S2a at the zone A, 18.05 +/- 0.3 Ma ago, which shows the successive activation

830 of the fault zones from east to west (SAL fault, GF fault, FZ2, FZ3, FZ4 and finally FZ5). Thus, the thrusts that are interpreted to root below the Belledonne massif in the Belledonne basal thrust were activated in-sequence (Fig. 17).

### 5.1.4 Timing of the end of deformation

In the Rumilly-Chambéry synclines the thick S2a and S2b sequences (18.05 +/- 0.15 to 16.3 +/- 0.3) marine deposits of the depocenter developed in the footwall of the SAL and GF (sections 4, 5, Fig. 13, Fig. S5) are capped by a rapid shallowing

835 upward succession, followed by S3 gravel-rich braided-river deposits (Fig. S8). This evolution suggests a final emersion linked with the fold and thrust propagation (Heller et al., 1988; DeCelles & Giles, 1996; Sinclair, 1997), and thus that the SAL and GF faults were active during the S2 and S3 sequences (until ~15 Ma). However, the lack of timing control within the S3 and overlying sequences at this location preclude any precise constraint on the timing of end of motion on SAL and GF (Fig. 13, Fig. S8).

840 In the footwall of FZ2 near Grenoble (zone D, 20, 22, Fig. 3), the sedimentary succession of the S4-S5 sequences of the Voreppe syncline is characterized by three stacked Gilbert deltas (GD). The GD1a and GD1b, 25 and 40 m-thick respectively, belong to the S4 (~15.0 to ~14.0 Ma), and the GD2 belong to the S5 (~14.0 to ~12.0 Ma) (Fig. S8). As these stacked gilbert deltas attest for a continuous, creation of slope and accommodation space (Ricketts and Evenchick 2007) we interpret them



as reflecting continuous activity of the FZ2, thus until at least ~12 Ma (Kalifi et al. 2021). GD2 is much thinner than GD1b (20 m against 40 m, respectively), and shows an abrupt transition between foresets and ~10 m-thick topsets themselves overlain by ~5m-high foresets interpreted as a mouth bar in a distal deltaic position suggesting a final transgression corresponding to S5b (Kalifi et al. 2021) (Fig. S8). This unit is finally overlain by 50m of planar-stratified conglomerates interpreted as braided-fluvial deposits likely evolving from deltaic to fluvial hydrodynamics. This transition could correspond to the final shallowing-up succession of the Gilbert deltas stacking pattern thus suggesting the progressive decrease of the FZ2 activity until the end of the S5 sequence (~12.0 Ma) (Kalifi et al. 2021).

To the west, in the footwall of the FZ3 and FZ4, the sequence S6 deposits have a constant thickness in the Bas-Dauphiné basin (Fig. 15) and the sequence S6 seals the underlying S4 and S5 growth strata (Fig. 14A). This suggests an end of the FZ3 and FZ4 activity in Vercors and Chartreuse massifs at ~12.0 Ma (top S5 sequence).

## 5.2 Sequence of shortening of the Southern Jura and Subalpine massifs

To further quantify the amount and history of shortening, cross-sections B and C (respectively, northern and southern Chartreuse, Fig. 11B, C) were balanced and restored to the initial geometry before the alpine shortening. Such reconstruction takes into account the relative timing of the various faults and yields a reconstruction of the deformation through time as well as an initial state. The cross sections have been drawn perpendicular to the main thrusts and fold axis (Fig. 1B), N118° for cross-section B and N114° for cross-section C. Total horizontal shortening along the cross-section B is 22.24 km (33.9 %) and 13.72 km (22.5 %) along the cross-section C (Fig. 18). These values are somehow approximate since they result from the hypothesis of a planar strain along a single and uniform direction of deformation for each section. They are in agreement with the previous finding of an increase in the shortening toward the north (Menard and Thouvenot, 1987; Sinclair, 1997; Philippe et al., 1998) that is interpreted as reflecting a larger amount of convergence (Bellahsen et al., 2014).

The sequential reconstruction allows to calculate the shortening related to each fault and fold and our chronological constraints on the thrusts bounds the quantification of some deformation rates. The amount of horizontal shortening for the whole Phase 1 (i.e., FZ1 horizontal shortening), is 14.1 km along the cross-section B and 5.8 km along the cross-section C, (Fig. 18A, B, Table S7). Note that the backthrusts visible in the east of section C corresponding to ~1.6 km of shortening (bk1 and bk2, Fig. 11C; Fig. 18B) are excluded from that calculation as they are only seen along that section and interpreted as related to a later tectonic phase. The amount of horizontal shortening for the whole Phase 2 (i.e., GF thrust, FZ2, FZ3 and FZ4 horizontal shortening) is of 6.7 km in cross-section B and 6.3 km in cross-section C (Fig. 18A, B, Table S7). In the Chartreuse massif, the SAL fault is not present along section B (Fig. 1B), and phase 2 is assumed to last from the onset of the GF (17.35 ± 0.15 Ma) to the end of deformation on FZ4 and 5 (~12 Ma), thus for ~5.3 Ma. This implies a migration of the deformation toward the external parts (west) at a rate of ~2.9 km Ma<sup>-1</sup> along sections B and C. This also corresponds to average shortening rates of 1.26 km Ma<sup>-1</sup> for cross-section B and 1.19 km Ma<sup>-1</sup> for cross-section C.

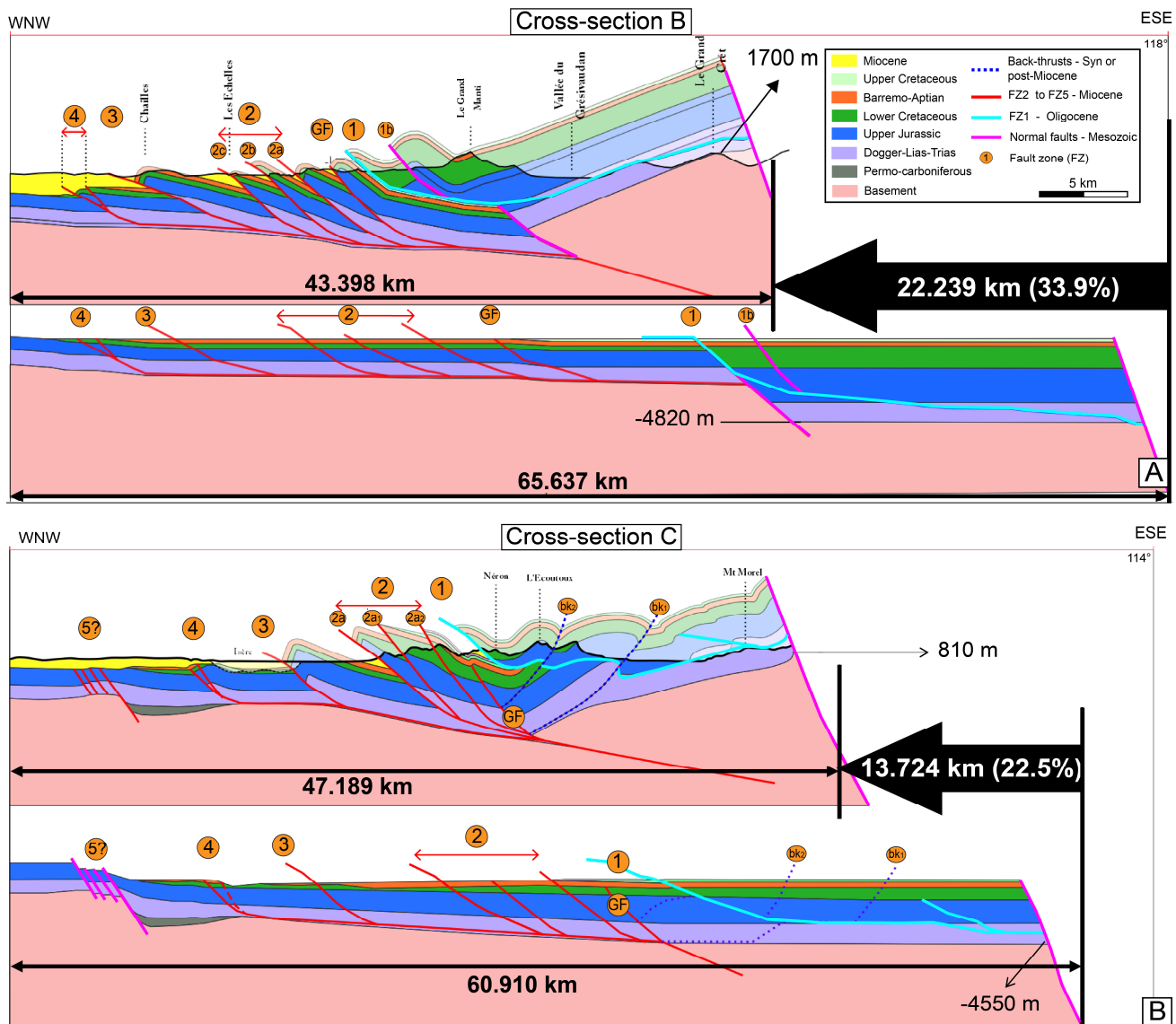


**Figure 18: Balanced cross-sections throughout the Chartreuse massif using the Move software, assuming that the ZF2 to ZF4 are rooted below a single Belledonne basal thrust. (A) Cross-section B (Fig. 11B). (B) Cross-section C (Fig. 11C). See Fig. 1B for locations. Note that the backthrusts visible in the east of section C (bk1 and bk2, Fig. 11C; Fig. 18B) are interpreted as related to a late tectonic phase, see text for details. Corresponding shortening amounts and rates are listed in table S7.**

### 5.3: Comparison of deformation phases affecting the Miocene molasse in western Alps

In Chartreuse and Vercors we thus document the phase of ~WNW-ESE shortening shaping the subalpine ranges (Phase 2) as starting at  $18.05 \pm 0.25$  Ma (SAL fault), or  $17.35 \pm 0.15$  Ma further south (GF fault). Then, surface thrusting propagated to the west at a rate of  $\sim 1.2 \text{ km Ma}^{-1}$ , with the successive onset of FZ2, FZ3, FZ4 and FZ5, with FZ5 initiation occurring at  $\sim 14$  Ma and the deformation ending at  $\sim 12$  Ma (Fig.16 and Fig. 17).

885 In the southern Jura, east of the La Bresse basin, in drillhole BY-101 (Fig. 1B) the sequences S6 and S7 marine deposits (~12 to ~10 Ma, Fig. S13) are overthrust by the Mesozoic sediments along the external the Jura thrust (J and  $\phi$ EJuE, Fig. 1B) indicating that the onset of the Jura thrust is either synchronous, or younger than sequences S6-S7. Due to the occurrence of abnormally thick Tortonian sequences S7 and S8 continental deposits (~10 to ~8.2 Ma) at the footwall of the Jura thrust that suggest a tectonically-controlled depocenter, we propose that the Jura frontal thrust (J, Fig. 1B) was active during sequence S8  
890 (~ 9.5 Ma; Fig. 4A), even perhaps coeval with the deposition of sequence S7 continental sediments (~ 10 Ma). This hypothesis is supported by earlier chronostratigraphical studies based on mammals, suggesting that the activity of the Jura frontal thrust (J, Fig. 1B) started between the Serravalien (~11 Ma) and the Pliocene (Bolliger et al., 1993; Steininger et al., 1996; Kälin, 1997). U-Pb ages of syntectonic calcite mineralizations sampled from the nearby Buron thrust (Bur, Fig. 1B) give an age of  $10.6 \pm 0.5$  Ma (Smeraglia et al., 2021). Paleontological evidence combined with tectonic evidence suggest a termination of  
895 Jura thin-skinned foreland tectonics between 9 and 4 Ma (Becker, 2000).

To the Northeast, the whole Swiss Molasse basin (SMB, Fig. 1A) lie in the prolongation of the Southern Jura synclines in between the the subalpine sediments of the Aar External Crystalline Massif (ECM) and the folded Mesozoic series of the Jura. At the time of phase 2 (18 – 12 Ma) the zone was affected by several transgression and regressions: continental deposits of the Lower Fresh Water Molasse (USM) last until ~20 Ma (Burdigalian), when a marine transgression yields to the deposition of  
900 the Upper Marine Molasse (OMM-I) until ~18.3 Ma (Homewood 1981; Allen 1984; Kempf et al. 1999; Garefalakis and Schlunegger 2019). After a sedimentation iatus until ~17.8 a new transgression yields to the deposition of the Upper Marine Molasse (OMM-II), until a final regression at ~16.5 Ma yielding to depositon of the Upper Fresh marine molasse (OSM) until at least 14 Ma, time after which sediments have not been preserved (Kempf et al. 1999; Garefalakis and Schlunegger 2019). Drainage directions in the USM and OMM-I are towards the north-east while in the OSM they are towards the south-west  
905 (Berger et al. 2005; Garefalakis and Schlunegger 2019). Based on apatite (U–Th–Sm)/He thermochronometry, Mock et al. (2020) infer exhumation of the Molasse between 12 and 4 Ma. These oscilations result from the interplay of eustatism and surface and/or deep-seated tectonic processes the detail of which are still discussed. From apatite and fission track data, exhumation of the Aar MCE started at ~22 Ma at a rate of 1.3–1.6 km/Myr in the southeast and 0.1 km/Myr in the northwest, and lasted until today in two phases with uniform exhumation rates of 0.5-0.9 km Myr<sup>-1</sup> between 13 and 5 Ma and 0.6- 0.8 km  
910 Myr<sup>-1</sup> until then (Herwegh et al., 2020). From these data it has been proposed that thrusting toward the NW below the Aar started at ~22 Ma and that it propagated from Aar to Jura at ~13 Ma along a NW verging flat decollement level (Mock et al., 2020 and reference therein). Such timing fits well with the U/Pb calcite ages of calcite veins in the footwall of that decollement at the eastern tip of the Jura (SHA trust), that suggest it has been active at least between 14.3 and 13.2 Ma (Looser et al., 2021). Similar ages from calcite slickenside suggest that frontal thrusts of the Jura have been active between  $11.3 \pm 0.9$  and  $4.5 \pm 1.5$   
915 Ma (Looser et al., 2021). Similar ages are documented further west from the inner to the external Jura:  $11.4 \pm 1.1$  Ma,  $10.6 \pm 0.5$  Ma and  $7.5 \pm 1.1$  Ma for the Montlebon, Fuans and Arguel thrusts respectively (Smeraglia et al., 2021). Such age are also in good condordance with those from the southwest Jura (see above). This NW verging deformation is locally characterized by SE verging backthrusts, including one close to the southern boundary of the NMB west of the Aar valley that was active

between ca. 13 and 4 Ma and has contributed to the exhumation of the molasse at that time (Looser et al., 2021 and references therein). In the Vercors and Chartreuse we have interpreted the thrusts of the Phase 2, starting at  $\sim 18.05 \pm 0.25$  Ma (GF), to be rooted below the Belledonne external cristaline massif. This would imply a start of the exhumation of that range slightly before 18 Ma. Such age is close to that proposed for the onset of the exhumation of the Aar range ( $\sim 22$  Ma). In front of the Aar cristaline range the thrust front appear to have stayed stable between 22 and  $\sim 13$  Ma at  $\sim 30$  km from the edge of the range. In front of central Belledonne the thrust front migrated from 20 km to 40 km away from the cristaline range between  $\sim 18$  and  $\sim 15$  Ma. Both structural histories are quite similar suggesting that similar mechanisms were active along strike of that part of the alpine belt, with a slight diachronism from north (22 Ma) to south (18 Ma) :  $\sim$ NW-SE shortening rooted below the ECM. To the South, in the Rhodano-Provençal Molasse basin (RPMB, Fig. 1A), Middle Miocene syn-tectonic deposits (Upper Burdigalian-Langhian;  $\sim 18$ -14 Ma) are described in the Digne (Gigot et al., 1974; Beaudoin et al., 1975; Crumeyrolle et al., 1991), the Lubéron (Clauzon, 1974), the Alpilles (Colomb, 1982) and the Vaison-la-Romaine (Brasseur, 1962) areas. These syn-tectonic sediments were deposited in response to the first Miocene alpine tectonic phase of the RPMB (Gigot et al., 1974) which is coeval to the onset of the phase 2 in our study area. Thus, the upper Burdigalian tectonic phase (phase 2 in this paper) was recorded at the western Alpine foreland basin scale suggesting a major tectonic event, as it is highlighted by new Miocene paleogeographical reconstructions at the foreland basin scale (Kalifi et al., 2021).

The following structural history however strongly differ between the north and the south: at  $\sim 13$  Ma in the Aar the deformation front appears to have quickly migrated more than 50 km to the NW to form the Jura, while it ended at  $\sim 12$  Ma in front of central Belledonne. However, some observations suggest that the Bas Dauphiné experienced uplift after 12 Ma. In the western and southern parts of the Bas-Dauphiné basin and the Crest basin (respectively, J, K, L zones, Fig. 3) the Miocene final sea retreat is recorded during deposition of sequence S7 ( $\sim 10$  Ma, Fig. S13, 14, 15, 16). The absence of marine deposits during S8 ( $\sim 9.5$  to  $\sim 8$  Ma) is unexpected, as it corresponds to an eustatic transgression corresponding to a higher sea level (+40 m) than that of sequence S7 (+5-10 m, Miller et al., 2005, Fig. 4B). This implies that the  $\sim 10$  Ma Miocene sea-retreat was induced by a basin-scale event. In the north-eastern part of the Bas-Dauphiné basin (F, H zones, Fig. 5), the uppermost marine deposits (sequence S6 regressive deposits,  $\sim 11$  Ma, Fig. S10, 12) outcrop today at elevation of  $\sim 350$  m a.s.l. (Fig. 14B; Fig. 15A). The sequence S6 transgression involved a +25 m sea-level rise which suggests a post-sequence S6 (12 Ma) minimum uplift of ca. 325 m. This is in agreement with Deville et al. (1994)'s observations implying a post-Langhian uplift. These authors interpreted this uplift as the result of a crustal thickening due to a crustal imbrication under the molasse basins, implying the activation of out-of-sequence thrusts in an internal position of the subalpine massifs. However, these thrusts have not been clearly identified and it is unclear how such thrusts could induce uplift of the Bas Dauphiné. Other possible interpretations are that this uplift would be linked to the activation of late backthrusts such as those described along section C (bkt1 & bkt2, Fig. 11), or to a yet unclear deeper process.

This study focused on the Miocene molasse of the western Alpine foreland basin (Subalpine massifs, southern Jura, the Bas-Dauphiné, the la Bresse and the Crest basins). The combination of chemiostratigraphy, biostratigraphy and magnetostratigraphy applied on sedimentological sections and well logs from the Miocene succession across the entire area allowed the establishment of a new chronostratigraphic framework. The Miocene is characterized by 11 depositional sequences dated between the late Aquitanian and the Tortonian. The spatial distribution of these sequences defines 12 depositional zones grouped into 4 domains. These domains are bounded by the main thrust fault zones, therefore implying a strong interplay between active tectonics and sedimentation during the Miocene, and lead us to propose three main tectonic phases (Fig. 17).

- (i) Phase 1 started prior to 21Ma, possibly since the early Oligocene ( $29 \pm 2$  Ma), and until the early Miocene ( $\sim 17.8$  Ma). During this phase, the southern Jura synclines were affected by flexural subsidence induced by the alpine tectonic front to the east. The maximum depositional thickness recorded to the east of the Rumilly syncline, as well as the absence of early Miocene marine deposits to the east of the FZ1 most probably indicate that the tectonic activity along FZ1 rooted east of the Belledonne external range.
- (ii) Phase 2 took place between the late Burdigalian ( $18.05 \pm 0.25$  Ma) and the Serravalian ( $\sim 12$  Ma). In the Chartreuse massif, the shortening rate related to that phase averages  $\sim 1.2$  km Ma<sup>-1</sup>. At  $18.05 \pm 0.25$  Ma, the development of a depocenter at the footwall of the SAL thrust along with the occurrence of seismites (of regional extent) together suggest the activation of the SAL fault. Subsequently, at  $17.35 \pm 0.15$  Ma, an angular unconformity characterized by westward-directed onlaps is recorded. This angular unconformity discloses a rapid westward migration of the depocenter at the footwall of GF fault and thereby points to its activation. At  $\sim 16.2$  Ma, growth strata relationships in S3 sequence (+S2b?) in the hangingwall of FZ3, combined with the occurrence of a sequence S3 depocenter in the footwall of FZ2 argue for the quasi-synchronous activation of FZ2 and FZ3 thrusts. Subsequently, at  $\sim 15.0$  Ma, sequence S4 growth strata geometries and the development of a sequence S4 depocenter in the footwall of the FZ4 document the onset of FZ4. Finally, at  $\sim 14.0$  Ma, the sequence S5 depocenter occurs in the footwall of FZ5, and probably dates the activation of the FZ5 thrust. The end of the Phase 2 took place at  $\sim 12.0$  Ma, as the S6 deposits have a constant thickness in the Bas-Dauphiné basin, and sequence S6 seals the underlying growth strata (S2 to S5 sequences). We interpret this phase as corresponding to the activation of the Belledonne basal thrust, rooted below the external Belledonne massif, and to the propagation at an average rate of  $\sim 2.9$  km Ma<sup>-1</sup> of the surface deformation toward the west within the subalpine ranges (successively SAL fault, GF fault, FZ2, FZ3, FZ4 and FZ5 thrusts). This appear quite similar with the Serravalian and Langhian thrusting at the base of the Aar range, and is coeval with to the first Miocene alpine tectonic phase of the Rhodano Provencal Molasse Basin implying a tectonic phase affecting the whole Western Alps.

(iii) In the north of the study area, deformation migrated NW in the Jura after 13 Ma, but stopped in Vercors and Chartreuse at ~12 Ma. Thick accumulation of continental sequences S7 and S8 deposits at the footwall of the Jura frontal thrust is coeval with thrusting of Mesozoic series atop sequences S6 and S7 marine deposits (~12 to ~10 Ma) indicating that the Jura front initiated during the Tortonian (~10 Ma, phase 3). Synchronously, to the south in the Bas-Dauphiné zones and the Crest basin no thrust activity is recorded after deposition of sequence S5 (~12 Ma). A post ~12 Ma mild uplift ( $\leq 325$  m) is probably linked with the ~10 Ma (Lower Tortonian) sea retreat and possibly to late backthrusts east of the Chartreuse.

990 *Data availability.* The research data are included in this paper and in the Supplement and can be freely accessed.

*Supplement.* The supplementary materials related to this manuscript are available in the attached .pdf file.

*Authors contribution.* This study was performed by AK in the framework of his Ph.D, co-supervised by TOTAL (CSTJF, Pau, France) and the LGL-TPE (University Lyon 1). JLR conceptualized the original research topic of this study, with the support of VS, in the EXPLOR/EP/GTS/ISS entity of TOTAL. Fieldwork and interpretations related to the chronostratigraphical study were performed by AK under the supervision of PS, BP, JLR, and by BH under the supervision of JLR and AK, for the northern part of the Bas-Dauphiné basin. Fieldwork and interpretations related to the structural study were performed by AK under the supervision of PHL, and the helpful support of VS. Restoration of the structural cross-sections were conducted by KL supervised by PHL and AK. The sampling and the sample preparation for the chemostratigraphical study was achieved by AK, and the analysis and interpretations were conducted by AG. The sampling for the paleomagnetic study was carried out by FD, PS, RG and AK. AK prepared the samples and the interpretations were conducted by FD. The sampling for the biostratigraphical study was conducted by AK, BH and RG, and the interpretations were performed by FQ for the planktonic foraminifera, by DM for the dinoflagellate cysts and by FR for the calcareous nannofossils. AK wrote the paper, with major contributions of PHL, PS and BP, and corrections from all other all co-authors.

*Competing interests.* The authors declare that no competing interest are present.

*Acknowledgments.* The authors would like to thank TOTAL for the financement of this PhD study. We would like to thank Andrea-Lopez Vega, Thomas Pichancourt, Hawoly Bass, Astrid Jonet, Antoine Mercier, Alessandro Menini, Pierre and Thomas Courier, Daniel Fournier, Ludovic Mochain, Sidonie Revillon, Hugues Fenies, Gilles Escarguel, Loïc Costeur, Jonathan Pelletier, Edouard Le-Garzik, Xavier Du-Bernard, Jean-Pierre Girard and Francois Lafont for their precious help in the field and/or for fruitful discussions. Constructive reviews by Thierry Dumont and Fritz Schlunegger helped to clarify the manuscript.

## 1015 **References**

- Aguilar, J.-P., Berggren, W. A., Aubry, M.-P., Kent, D. V., Clauzon, G., Benammi, M., and Michaux, J.: Mid-Neogene Mediterranean marine–continental correlations: an alternative interpretation, *Palaeogeogr. Palaeoclimatol. Palaeoecol.*, 204, 165–186, 2004.
- Allen, P. A. and Bass, J. P.: Sedimentology of the upper marine molasse of the Rhône-Alp Region, Eastern France: implications of basin evolution, *Eclogae Geol. Helv.*, 86, 121–172, 1993.
- Allen, P.A.: Reconstruction of ancient sea conditions with an example from the Swiss Molasse. *Marine Geology*, 60, 455–473, 1984.
- Arnaud, H., Combier, J., and Monjuvent, G.: Notice explicative, Carte géol. France (1/50 000), feuille Romans-sur-Isère (795), BRGM, Orléans, 30 pp., 1975.
- 1025 Barféty, J.-C., Antoine, P., Girod, J.-P., Bellamy, J., Chabod, J.-C., Boullud, C., Bullière, J., Debelmas, J., Sarrot-Reynaud, J., and Goguel, J.: Carte géol. France (1/50 000), feuille Vif (796), BRGM, Orléans, 1967.
- Barféty, J.-C. and Barbier, R.: Carte géologique (1/50 000), feuille La Rochette (750), BRGM, Orléans, 1983.
- Barféty, J.-C. and Gidon, M.: La structure des Collines bordières du Grésivaudan et des secteurs adjacents, à l’est de Grenoble (Isère, France), *Géologie Alp.*, 72, 5–22, 1996.
- 1030 Bass, J. P.: The sedimentology and basin evolution of the upper marine molasse of the Rhône-Alp region, France, Ph.D. Thesis, Department of Earth sciences, University of Oxford, 1991.
- Beaudoin B., Campredon R., Cotillon P. and Gigot P.: Alpes Méridionales Françaises : Reconstitution du bassin de sédimentation, Excursion N°7, IX Congrès International de Sédimentologie, Nice, IAS Publ, 1975.
- Beaumont, C.: Foreland basins, *Geophys. J. Int.*, 65, 291–329, 1981.
- 1035 Beck, C., Deville, E., Blanc, E., Philippe, Y., and Tardy, M.: Horizontal shortening control of Middle Miocene marine siliciclastic accumulation (Upper Marine Molasse) in the southern termination of the Savoy Molasse Basin (northwestern Alps/southern Jura), *Geol. Soc. London, Spec. Publ.*, 134, 263–278, 1998.
- Becker, A.: The Jura Mountains—an active foreland fold-and-thrust belt?, 321, 381–406, 2000.
- Bellahsen, N., Jolivet, L., Lacombe, O., Bellanger, M., Boutoux, A., Garcia, S., Mouthereau, F., Le Pourhiet, L., and Gumiaux, C.: Mechanisms of margin inversion in the external Western Alps: Implications for crustal rheology, 560, 62–83, 2012.
- 1040 Bellahsen, N., Mouthereau, F., Boutoux, A., Bellanger, M., Lacombe, O., Jolivet, L., and Rolland, Y.: Collision kinematics in the western external Alps, 33, 1055–1088, 2014.
- Berger, J.-P.: La transgression de la molasse marine supérieure (OMM) en Suisse occidentale, *Munchn. geowiss. Abh. R. A.*, 5, 206, 1985.
- 1045 Berger, J.-P.: Paléontologie de la Molasse de Suisse occidentale, Th. d'habilitation sci., University of Fribourg, 452 pp., 1992.



- Berger, J.P., Reichenbacher, B., et Becker, D., Grimm, M., Grimm, K., Picot, L., Storni, A., Pirkenseer, C., Derer, C., Schaefer, A.: Eocene-Pliocene time scale and stratigraphy of the Upper Rhine Graben (URG) and the Swiss Molasse Basin (SMB). *International Journal of Earth Sciences*, 94, 711–731, 2005.
- Bergerat, F.: Paléo-champs de contrainte tertiaires dans la plate-forme européenne au front de l’orogène alpin, *Bull. la Société géologique Fr.*, 3, 611–620, 1987.
- Bergerat, F., Mugnier, J.-L., Guellec, S., Truffert, C., and Cazes, M.: Extensional tectonics and subsidence of the Bresse basin: an interpretation from ECORS data, *Mémoires la Société géologique Fr.*, 156, 145–156, 1990.
- Debelmas, J.: *Géologie de la France, Tome 2: Les Chaînes plissées du cycle alpin et leur avant-pays*, Ed. Doin, 296–540, 1974.
- Blanc, E.: Evolution sédimentaire syntectonique au front d’une chaîne de collision en environnement littoral, *Mem. DEA.*, Université de Savoie (Chambéry), 35 pp., 1991.
- Blanchet, F. and Chagny, E.: Le promontoire de la Porte de France près de Grenoble: Analyse tectonique détaillée-Massif de la Chartreuse, *Bull. Serv. Carte Geol. Fr.*, 149, 253–276, 1923.
- Bocquet, J.: Le delta miocène de Voreppe. Etude des faciès conglomératiques du Miocène des environs de Grenoble, *Trav. du Lab. Géologie l’Université Grenoble*, 42, 53–75, 1966.
- Bolliger, T., Engesser, B., and Weidmann, M.: Première découverte de mammifères pliocènes dans le Jura neuchâtelois, *Eclogae Geol. Helv*, 86, 1031–1068, 1993.
- Bonnet, C., Malavieille, J., and Mosar, J.: Interactions between tectonics, erosion, and sedimentation during the recent evolution of the Alpine orogen: Analogue modeling insights, *Tectonics*, 26, TC6016, doi:10.1029/2006TC002048, 2007.
- BouDagher-Fadel, M. K.: *Biostratigraphic and Geological Significance of Planktonic Foraminifera (Updated 2nd Edition)*, UCL Press, London, doi: 10.14324/111.9781910634257, 2015.
- Brasseur R. : *Etude Géologique du Massif de Suzette (Vaucluse)*, PhD Thesis, Université de Lyon, 195p, 1962.
- Burkhard, M. and Sommaruga, A.: Evolution of the western Swiss Molasse basin: structural relations with the Alps and the Jura belt, *Geol. Soc. London, Spec. Publ.*, 134, 279–298, 1998.
- Butler, R. W. H.: The geometry of crustal shortening in the Western Alps, in: *Tectonic evolution of the Tethyan region*, Springer, 43–76, 1989a.
- Butler, R. W. H.: The influence of pre-existing basin structure on thrust system evolution in the Western Alps, *Geol. Soc. London, Spec. Publ.*, 44, 105–122, 1989b.
- Butler, R. W. H.: Structural evolution of the western Chartreuse fold and thrust system, NW French Subalpine chains, in: *Thrust tectonics*, edited by: McClay, K.R., Chapman and Hall, London, 287–298, 1992a.
- Butler, R. W. H.: Thrusting patterns in the NW French Subalpine chains, in: *Annales Tectonicae*, 150–172, 1992b.
- Butler, R. W. H.: Basement-cover tectonics, structural inheritance, and deformation migration in the outer parts of orogenic belts: A view from the western Alps, *Linkages Feed. Orog. Syst.*, 213, 55, 2017.
- Butler, R. W. H. and Bowler, S.: Local displacement rate cycles in the life of a fold-thrust belt, *Terra Nov.*, 7, 408–416, 1995.

- Cardozo, N., and Allmendinger, R. W.: Spherical projections with OSXStereonet: Computers & Geosciences, v. 51, no. 0, p. 193–205, doi: 10.1016/j.cageo.2012.07.021, 2013.
- Charollais, J. and Jamet, M.: Principaux résultats géologiques du forage Brizon 1 (BZN 1) Haute-Savoie, France, Mémoires la Société géologique Fr., 156, 185–202, 1990.
- Clauzon G. : Quel age le Lubéron a-t-il ? Etudes Vauclusiennes, XI, 1-16, 1974
- Colomb E. : Relation plate-forme carbonatée – continent dans le cas de la transgression Miocène dans les Alpilles (Bouches-du-Rhône). Géologie Méditerranéenne, 9, 3, 213-215, 1982.
- Couëffé, R. and Tourlière, B.: Modélisation géologique multicouche Bresse, Dombes, Bas-Dauphiné, Couloir rhodanien - Méthodologie de réalisation, guide d'utilisation des produits numériques - Rapport final, REP-57712-, 62, 2008.
- Crumeeyrolle, P., Rubino, J. and Clauzon, G.: Miocene depositional sequences within a tectonically controlled transgressive–regressive cycle. In: MacDonald, D.I.M. (ed.), Sedimentation, Tectonics and Eustasy: Sea-Level Changes at Active Margins, Spec. Publ. int. Ass. Sediment., 12, 371–390, 1991.
- Debelmas, J.: Etude tectonique de la bordure orientale du Massif du Vercors entre Grenoble et le Mont-Aiguille, Thèse de 3<sup>e</sup> cycle, University of Grenoble, 44 pp., 1953.
- Debelmas, J.: Quelques observations sur l'extrémité N-orientale du massif du Vercors, Trav. Lab. Géol. Fac. Sci. Grenoble., 41, 275–281, 1965.
- Debelmas, J.: Structure géologique du massif du Moucherotte, Géol. Alp., 42, 109–116, 1966.
- DeCelles, P. G. and Giles, K. A.: Foreland basin systems, Basin Res., 8, 105–123, 1996.
- De Graciansky, P.C. de, Roberts D.G., Tricart P. : The Western Alps, from rift to passive margin to orogenic belt, an intergated overview. Developments in Earth Surface Processes, 14, Elsevier, 398p., ISBN 9780444537249, 2011.
- Demarcq, G.: Etude stratigraphique du Miocène rhodanien, Mém. BRGM, 61, 257 pp., 1970.
- Demory, F., Conesa, G., Oudet, J., Mansouri, H., Münch, P., Borgomano, J., Thouveny, N., Lamarche, J., Gisquet, F., and Marié, L.: Magnetostratigraphy and paleoenvironments in shallow-water carbonates: the Oligocene-Miocene sediments of the northern margin of the Liguro-Provençal basin (West Marseille, southeastern France), Bull. la Société géologique Fr., 182, 37–55, 2011.
- Deville, E.: Structure of the Tectonic Front of the Western Alps: Control of Fluid Pressure and Halite Occurrence on the Decollement Processes, Tectonics, 40, 4, 2021.
- Deville, E. and Sassi, W.: Contrasting thermal evolution of thrust systems: An analytical and modeling approach in the front of the western Alps, Am. Assoc. Pet. Geol. Bull., 90, 887–907, 2006.
- Deville, E., Mascle, A., and Deronzier, J. F.: Etude non exclusive Chartreuse-Vercors 91. Rapport d'interprétation (Atlas, 52 planches), 1992.
- Deville, E., Blanc, E., Tardy, M., Beck, C., Cousin, M., and Ménard, G.: Thrust propagation and syntectonic sedimentation in the Savoy Tertiary Molasse Basin (Alpine foreland), in: Hydrocarbon and petroleum geology of France, Springer, 269–280, 1994.

- Deville, É. and Chauvière, A.: Thrust tectonics at the front of the western Alps: constraints provided by the processing of seismic reflection data along the Chambéry transect, *Comptes Rendus l'Académie des Sci. IIA-Earth Planet. Sci.*, 331, 725–732, 2000.
- Dickinson, R. W.: Plate tectonics and sedimentation, in: *Tectonics and Sedimentation*, vol. 22, edited by: Dickinson, R. W., Special Publications of SEPM, 1–27, <https://doi.org/10.2110/pec.74.22.0001>, 1974.
- Donzeau, M., Gamond, J.-F., and Mugnier, J.-L.: Evolution latérale et amortissement d'une structure chevauchante, un exemple du Nord Vercors, *Comptes rendus l'Académie des Sci. Série 2, Mécanique, Phys. Chim. Sci. l'univers, Sci. la Terre*, 317, 1675–1682, 1993.
- Doudoux, B., de Lepinay, B. M., and Tardy, M.: Une interprétation nouvelle de la structure des massifs subalpins savoyards (Alpes occidentales): nappes de charriage oligocènes et déformations superposées, *CR Acad. Sci*, 295, 63–68, 1982.
- Doudoux, B., Rosset, J., Barfèty, J.-C., Carfantan, J.-C., and Pairis, J.-L.: Carte géologique (1/50 000), feuille Annecy-Ugine (702), BRGM, Orléans, 1992a.
- Doudoux, B., Barfèty, J. C., Carfantan, J. C., Tardy, M., and Nicoud, G.: Notice explicative, Carte géol. France (1/50000), feuille Annecy-Ugine (702), BRGM, Orléans, 62 pp., 1992b.
- Doudoux, B., Barfèty, J.-C., Vivier, G., Carfantan, J.-C., Nicoud, G., Colletta, B., and Tardy, M.: Carte géologique (1/50 000), feuille Albertville (726), BRGM, Orléans, 1999.
- Dumont, M.: Etude stratigraphique et sédimentologique du Miocène supérieur de la région de Jujurieux (Ain, France), Ph.D. Thesis, University Lyon 1, 155 pp., 1983.
- Dumont, T., Champagnac, J.-D., Crouzet, C., and Rochat, P.: Multistage shortening in the Dauphiné zone (French Alps): the record of Alpine collision and implications for pre-Alpine restoration, *Swiss J. Geosci.*, 101, 89–110, 2008.
- Dumont, T., Simon-Labric, T., Authemayou, C., and Heymes, T.: Lateral termination of the north-directed Alpine orogeny and onset of westward escape in the Western Alpine arc: Structural and sedimentary evidence from the external zone, 30, 2011.
- Dumont, T., Schwartz, S., Guillot, S., Simon-Labric, T., Tricart, P., and Jourdan, S.: Structural and sedimentary records of the Oligocene revolution in the Western Alpine arc, *J. Geodyn.*, 56, 18–38, 2012.
- Dumont, T. and S.P.I.A.: Échaillon stone from France: a Global Heritage Stone Resource proposal, *Geol. Soc. London, Spec. Publ.*, 486, 115–128, 2020.
- Embry, A. F.: Transgressive–regressive (T–R) sequence analysis of the Jurassic succession of the Sverdrup Basin, Canadian Arctic Archipelago, *Can. J. Earth Sci.*, 30, 301–320, 1993.
- Embry, A. F.: Sequence boundaries and sequence hierarchies: problems and proposals, *Seq. Stratigr. Northwest Eur. Margin*, 5, 1–11, 1995.
- Enay, R., Gidon, P., Caillon, M., and Doudoux, B.: Carte géologique de la France à 1/50000: Rumilly (701), BRGM, Orléans, 1970.
- Ford, M. and Lickorish, W. H.: Foreland basin evolution around the western Alpine Arc, *Geol. Soc. London, Spec. Publ.*, 221, 39–63, 2004.

- Garefalakis, P. and Schlunegger, F.: Tectonic processes, variations in sediment flux, and eustatic sea level recorded by the 20 Myr old Burdigalian transgression in the Swiss Molasse basin. *Solid Earth*, 10(6), 2045-2072, 2019.
- Gaudant, J., Weidmann, M., Berger, J.-P., Bolliger, T., Kalin, D., and Reichenbacher, B.: Recherches sur les dents pharyngiennes de Poissons Cyprinidae de la Molasse d'eau douce oligo-miocène de Suisse (USM, OSM) et de Haute-Savoie (France), *Rev. Paléobiologie*, 21, 371–389, 2002.
- Gidon, M.: Nouvelle contribution à l'étude du massif de la Grande-Chartreuse et de ses relations avec les régions avoisinantes, *Trav. du Lab. Géologie Alp.*, 40, 187–205, 1964.
- Gidon, M.: Carte géologique (1/50 000), feuille Annecy-Ugine (748), BRGM, Orléans, 1970a.
- 1155 Gidon, M.: La structure de l'extrémité méridionale du massif de la Chartreuse aux abords de Grenoble et son prolongement en Vercors, *Géologie Alp.*, 57, 93–107, 1981.
- Gidon, M.: L'anatomie des zones de chevauchement du massif de la Chartreuse (Chaînes subalpines septentrionales, Isère, France), *Géologie Alp.*, 27–48, 1988.
- Gidon, M.: Les décrochements et leur place dans la structuration du massif de la Chartreuse (Alpes occidentales françaises),  
1160 *Géologie Alp.*, 66, 39–55, 1990.
- Gidon, M.: Quelques aspects des rapports entre l'histoire tectonique et la morphogenèse dans le massif de la Chartreuse, *Géologie Alp.*, 70, 13–27, 1994.
- Gidon, M.: Tectonique et origine de la cluse de Grenoble (France), *Géologie Alp.*, 71, 175–192, 1995.
- Gidon, M.: Tectoniques superposées dans le synclinal des Aillons et ses abords (massif des Bauges, Savoie, France), *Géologie*  
1165 *Alp.*, 75, 91–102, 1999.
- Gidon, M.: Les massifs cristallins externes des Alpes occidentales françaises sont-ils charriés, *Géologie Alp.*, 77, 23–38, 2001.
- Gidon, M.: Voreppe, cours inférieur de la Roize: [http://www.geol-alp.com/chartreuse/6\\_localites\\_ch/voreppe.html](http://www.geol-alp.com/chartreuse/6_localites_ch/voreppe.html), last access: 17 August 2018, 2018.
- Gidon, M.: Ugine, gorges de l'Arly: [http://www.geol-alp.com/bornes/\\_lieux\\_aravis/Ugine\\_NE.html](http://www.geol-alp.com/bornes/_lieux_aravis/Ugine_NE.html), last access: 23 November  
1170 2019, 2019.
- Gidon, M.: Comboire, Claix, Rochefort: [http://www.geol-alp.com/drac/\\_draclieuxN/comboire.html](http://www.geol-alp.com/drac/_draclieuxN/comboire.html), last access: 13 January 2020, 2020a.
- Gidon, M.: Seyssins - Fontaine: [http://www.geol-alp.com/h\\_vercors/lieux\\_vercors/seyssins.html](http://www.geol-alp.com/h_vercors/lieux_vercors/seyssins.html), last access: 13 January 2020, 2020b.
- 1175 Gidon, M. and Arnaud, H.: Carte géologique détaillée de la France à 1/50.000, feuille Grenoble (2<sup>e</sup> édition), BRGM, Orléans, 1978.
- Gidon, M. and Barféty, J.-C.: Carte géologique (1/50 000), feuille Montmélian (749), BRGM, Orléans, 1969.
- Gidon, M., Arnaud, H., and Montjuvent, A.: Notice explicative, Carte géol. France (1/50000), feuille Grenoble (772), BRGM, Orléans, 37 pp., 1978.
- 1180 Gidon, P.: Notice explicative, Carte géologique de France (1/50000), feuille Vif (701), BRGM, Orléans, 11p, 1970b.

- Gignoux, M. and Moret, L.: *Géologie dauphinoise: initiation à la géologie par l'étude des environs de Grenoble*, 2<sup>e</sup> édition, 2nd editio., Masson et Cie, Paris, 391 pp., 1952.
- Gigot P., Grandjacquet C. and Haccard D.: Evolution tectono-sédimentaire de la bordure septentrionale du bassin tertiaire de Digne depuis l'Eocène, *Bull. Soc. Géol. Fr., Sér. 7*, 16, 2, 128-139, 1974.
- 1185 Giot, P. R.: Contribution à l'étude des terrains tertiaires du Royans (Isère et Drôme), *Trav. Lab. Géol. Grenoble*, 24, 49–68, 1943.
- Gorin, G., Signer, C., and Amberger, G.: Structural configuration of the western Swiss Molasse Basin as defined by reflection seismic data, *Eclogae Geol. Helv.*, 86, 693–716, 1993.
- Guellec, S., Mugnier, J.-L., Tardy, M., and Roure, F.: Neogene evolution of the western Alpine foreland in the light of ECORS data and balanced cross-section, *Mémoires la Société géologique Fr.*, 156, 165–184, 1990.
- 1190 Heller, P. L., Angevine, C. L., Winslow, N. S., and Paola, C.: Two-phase stratigraphic model of foreland-basin sequences, *Geology*, 16, 501–504, 1988.
- Herwegh, M., Berger, A., Glotzbach, C., Wangenheim, C., Mock, S., Wehrens, P., Baumberger, R., Egli, D., and Kissling, E.: Late stages of continent-continent collision: Timing, kinematic evolution, and exhumation of the Northern rim (Aar Massif) of the Alps, *Earth-science Rev.*, 200, 102959, 2020.
- 1195 Homewood, P. : Faciès et environnements de dépôt de la Molasse de Fribourg. *Eclogae Geologicae Helvetiae*, 74, 29–36, 1981.
- Hardenbol, J. A. N., Jacquin, T., Farley, M. B., Jacquin, T., De Graciansky, P.-C., and Vail, P. R.: Mesozoic and Cenozoic Sequence Chronostratigraphic Framework of European Basins, in: *Mesozoic and Cenozoic sequence chronostratigraphic framework of European basins*, edited by: Graciansky, P.-C., Hardenbol, J. A. N., Jacquin, T., Vail, P. R., SEPM Society for Sedimentary Geology, 60, 1998.
- 1200 Hayes, J.M., Strauss, H. and Kaufman, A.J.: The abundance of <sup>13</sup>C in marine organic matter and isotopic fractionation in the global biogeochemical cycle of carbon during the past 800 Ma. *Chem. Geol.*, 161, 103–125, 1999.
- Hudson, J. D.: Carbon isotopes and limestone cement, *Geology*, 3, 19–22, 1975.
- 1205 Hudson, J. D.: Stable isotopes and limestone lithification, *J. Geol. Soc. London.*, 133, 637–660, 1977.
- Kalifi, A.: Caractérisation sédimentologique et distribution des dépôts syn-orogéniques Miocènes des chaînes subalpines septentrionales (Royans-Vercors-Chartreuse-Bauges), du sud du Jura et du Bas-Dauphiné. Cadre chronostratigraphique et tectonostratigraphique, Ph.D. Thesis, University of Lyon 1, 578 pp., 2020.
- Kalifi, A., Sorrel, P., Leloup, P.-H., Spina, V., Huet, B., Galy, A., Rubino, J.-L., and Pittet, B.: Changes in hydrodynamic process dominance (wave, tide or river) in foreland sequences: The subalpine Miocene Molasse revisited (France), *Sedimentology*, 63, 2455–2501, <https://doi.org/10.1111/sed.12708>, 2020.
- 1210 Kalifi, A., Sorrel, P., Leloup, P.H., Galy, A., Spina, V., Huet, B., Russo, S., Pittet, B., and Rubino, J.-L.: Tectonic control on the paleogeographical evolution of the Miocene seaway along the Western Alpine foreland basin, *Geological Society of London Special Publication*, in review, 2021.



- 1215 Kälın, D.: Litho-und Biostratigraphie der mittel-bis obermiozänen Bois de Raube-Formation (Nordwestschweiz), *Eclogae Geol. Helv.*, 90, 97–114, 1997.
- Kempf, O., Matter, A., Burbank, D.W. and Mange, M.: Depositional and structural evolution of a foreland basin margin in a magnetostratigraphic framework: the eastern Swiss Molasse Basin. *International Journal of Earth Sciences*, 88, 253–275, 1999.
- Klein, C.: Le Piemont rhodanien, in: *Génèse et évolution du piémont néogène subalpin du Bas-Dauphiné*, edited by: Clauzon, G., Travaux-Centre national de la recherche scientifique, 78, 1990.
- 1220 Kwasniewski, A., Rubino, J.-L., Gariteai, T., Lescanne, M., and Mascle, A.: Stratigraphic Variability of tide dominated depositional systems within Miocene sandy succession of Bas Dauphiné basin (Miocene Peri-Alpine foreland basin) SE France, in: IAS congress, Geneva, Switzerland, 18-22 August, 2014.
- Lacassin, R., Tapponnier, P., and Bourjot, L.: Culminations anticlinales d'échelle crustale et imbrication de la lithosphère dans les Alpes, apports du profil ECORS-CROP, *Comptes rendus l'Académie des Sci. Série 2, Mécanique, Phys. Chim. Sci. l'univers, Sci. la Terre*, 310, 807–814, 1990.
- 1225 Lamiroux, C.: Géologie du Miocène des chainons jurassiens méridionaux et du Bas-Dauphiné nord oriental entre Chambéry et La Tour du Pin: étude stratigraphique, sédimentologique et tectonique, Ph.D. Thesis, Université Scientifique et Médicale de Grenoble, 174 pp., 1977.
- 1230 Latreille, G.: La sédimentation détritique au Tertiaire dans le Bas-Dauphiné et les régions limitrophes, Ph.D. Thesis, University of Lyon 1, 340 pp., 1969.
- Laubscher, H.: Jura kinematics and the Molasse Basin, *Eclogae Geol. Helv.*, 85, 653–675, 1992.
- Lickorish, W. H., Ford, M., Burgisser, J., and Cobbold, P. R.: Arcuate thrust systems in sandbox experiments: A comparison to the external arcs of the Western Alps, *Geol. Soc. Am. Bull.*, 114, 1089–1107, 2002.
- 1235 Lirer, F., Maria, F. L., Maria, I. S., Gianfranco, S., Elena, T., Claudia, C., Javier, S. F., and Antonio, C.: Mediterranean Neogene planktonic foraminifer biozonation and biochronology, *Earth-Science Rev.*, 196, <https://doi.org/10.1016/j.earscirev.2019.05.013>, 2019.
- Looser, N., Madritsch, H., Guillong, M., Laurent, O., Wohlwend, S., and Bernasconi, S. M.: Absolute Age and Temperature Constraints on Deformation Along the Basal Décollement of the Jura Fold-and-Thrust Belt From Carbonate U-Pb Dating and Clumped Isotopes, 40, e2020TC006439, <https://doi.org/10.1029/2020TC006439>, 2021.
- 1240 Mastrangelo, B. and Charollais, J.: Nouvelle conception de la structure du Salève, *Arch. des Sci.*, 70, 43–50, 2018.
- McArthur, J. M., Howarth, R. J., and Shields, G. A.: Strontium isotope stratigraphy, in: *Geol. time scale*, edited by: Gradstein, F. M., Ogg, J. G., Schmitz, M. D., & Ogg, G. M., Elsevier, 1, 127–144, 2012.
- Mein, P.: A new direct correlation between marine and continental scales in rhodanian Miocene, in: VIII Congr. RCMNS., Hungar. Geol. Survey., Budapest, 377–379, 1985.
- 1245 Menard, G. and Thouvenot, F.: Balanced cross-sections at crustal scale-methods and application to the western Alps, *Geodin. Acta*, 1, 35–45, 1987.

- Miller, K. G., Kominz, M. A., Browning, J. V., Wright, J. D., Mountain, G. S., Katz, M. E., Sugarman, P. J., Cramer, B. S., Christie-Blick, N., and Pekar, S. F.: The phanerozoic record of global sea-level change, *Science*, 310, 1293–1298, 1250 <https://doi.org/10.1126/science.1116412>, 2005.
- Mock, S., Von Hagke, C., Schlunegger, F., Dunkl, I., and Herwegh, M.: Long-wavelength late-Miocene thrusting in the north Alpine foreland: implications for late orogenic processes, *Solid Earth*, 11, 1823–1847, 2020.
- Monjuvent, G., Combier, J., Michel, R., and Fournier, D.: Notice de la carte géologique de la France à 1/50000, feuille de La Côte-st-André (747), BRGM, Orléans, 34 pp., 1980.
- 1255 Mortaz-Djalili, D.: Sédimentologie des formations détritiques du Néogène du plateau de Chambaran (Bas-Dauphiné, France), Ph.D. Thesis, Université Scientifique et Médicale de Grenoble, 153 pp., 1977.
- Mortaz-Djalili, D. and Perriaux, J.: Le Néogène du Plateau de Chambaran (Bas-Dauphiné, France), *Géologie Alp.*, 55, 133–152, 1979.
- Mugnier, J.-L., Guellec, S., Menard, G., Roure, F., and Tardy, M.: A crustal scale balanced cross-section through the external 1260 Alps deduced from the ECORS profile, *Mémoires la Société géologique Fr.*, 156, 203–216, 1990.
- Mugnier, J. and Marthelot, J.: Crustal Reflections Beneath the Alps and the Alpine Foreland: Geodynamic Implications, *Geodynamic*, 177–183, 1991.
- Mugnier, J., Arpin, R., and Thouvenot, F.: Balanced cross-sections through the subalpine massif of the Chartreuse, *Geodin. Acta*, 1, 125–137, 1987.
- 1265 Mujito, S.: Les sédiments tertiaires dans le Jura méridional et les Bauges occidentales: Savoie, Haute Savoie (France)-Alpes françaises, Ph.D. Thesis, Université Scientifique et Médicale de Grenoble, 221 pp., 1981.
- Nelson, C. S. and Smith, A. M.: Stable oxygen and carbon isotope compositional fields for skeletal and diagenetic components in New Zealand Cenozoic nontropical carbonate sediments and limestones: a synthesis and review, *New Zeal. J. Geol. Geophys.*, 39, 93–107, 1996.
- 1270 Nicolas, A., Polino, R., Hirn, R., Nicolich, R., and Group, E.-C. working: ECORS-CROP traverse and deep structure of the western Alps: a synthesis., in: A synthesis, in *Deep structure of the Alps*, edited by: Roure, F., Heitzmann, P., and Polino, R., *Mém. Soc. Geol. France*, NS, 15–27, 1990.
- Nicolet, C.: Le Bas-Dauphiné septentrional: étude stratigraphique et sédimentologique, Ph.D. Thesis, Université Scientifique et Médicale de Grenoble, 150 pp., 1979.
- 1275 Ogg, J. G. and Lowrie, W.: Magnetostratigraphy, in: *The Geologic Time Scale 2012*, edited by Gradstein, F. M., Ogg, J. G., Schmitz, M., Ogg, G., Elsevier, 85–114, 2012.
- Ogg, J. G., Ogg, G. M., and Gradstein, F. M.: A concise geologic time scale: 2016, Elsevier, 2016.
- Ori, G. G. and Friend, P. F.: Sedimentary basins formed and carried piggyback on active thrust sheets, *Geology*, 12, 475–478, 1984.
- 1280 Pelin, S.: Etude géologique du bassin de Pont-en-Royans Vercors-Alpes françaises., Ph.D. Thesis, Université Scientifique et Médicale de Grenoble, 68 pp., 1965.

- Pfiffner, O.-A., Lehner, P., Heitzmann, P., Mueller, S., and Steck, A.: Deep structure of the Swiss Alps: results of NRP 20, Birkhäuser, Basel, 380 pp., 1997.
- Pfiffner, O. A.: Geology of the Alps, John Wiley & Sons, Wiley-Blackwell, 368 pp., 2014.
- 1285 Philippe, Y.: Rampes latérales et zones de transfert dans les chaînes plissées: géométrie, condition de formation et pièges structuraux associés, Ph.D. Thesis, Université de Savoie (Chambéry), 1995.
- Philippe, Y., Colletta, B., Deville, E., and Mascle, A.: The Jura fold-and-thrust belt: a kinematic model based on map-balancing, *Mémoires du Muséum Natl. d'histoire Nat.*, 170, 235–261, 1996.
- Philippe, Y., Deville, E., and Mascle, A.: Thin-skinned inversion tectonics at oblique basin margins: example of the western
- 1290 Vercors and Chartreuse Subalpine massifs (SE France), *Geol. Soc. London, Spec. Publ.*, 134, 239–262, 1998.
- Posamentier, H. W. and Allen, G. P.: Siliciclastic sequence stratigraphy: concepts and applications, SEPM (Society for Sedimentary Geology) Tulsa, Oklahoma, 7, <https://doi.org/10.2110/csp.99.07>, 1999.
- Rangheard, Y., Demarcq, G., Muller, C., Poignant, A., and Pharissat, A.: Données nouvelles sur le Burdigalien du Jura interne; paleobiologie, biostratigraphie et evolution structurale, *Bull. la Société Géologique Fr.*, 6, 479–486, 1990.
- 1295 Ricketts, B. D. and Evenchick, C. A.: Evidence of different contractional styles along foredeep margins provided by Gilbert deltas: examples from Bowser Basin, British Columbia, Canada, *Bull. Can. Pet. Geol.*, 55, 243–261, 2007.
- Rigassi, D.: Le Tertiaire de la région genevoise et savoissienne, *Bull. der Vereinigung Schweizerisches Pet. und-Ingenieur*, 24, 19–34, 1957.
- Roure, F., Howell, D. G., Guellec, S., and Casero, P.: Shallow structures induced by deep-seated thrusting, *Pet. Tectonics*
- 1300 *Mob. Belts*, Technip Paris, 15–30, 1990.
- Rubino, J. L., Lesueur, J. L., and Clauzon, G.: Le Miocène inférieur et moyen du bassin rhodanien: stratigraphie séquentielle et sédimentologie, *Field Trip Guidebook: Special Publication of the Association des Sédimentologues Français, ASF*, 67 pp., 1990.
- Saltzman, M. R., and Thomas, E.: Carbon isotope stratigraphy, in: *The Geologic Time Scale 2012*, edited by Gradstein, F. M.,
- 1305 Ogg, J. G., Schmitz, M. D., and Ogg, G. M., Volume 1, Amsterdam, Elsevier, 207–232, 2012.
- Schlunegger, F. and Kissling, E.: Slab rollback orogeny in the Alps and evolution of the Swiss Molasse basin, *Nat. Commun.*, 6, 8605, 2015.
- Signer, C. and Gorin, G. E.: New geological observations between the Jura and the Alps in the Geneva area, as derived from reflection seismic data. *Eclogae Geologicae Helvetiae*, 88, 235–265, 1995.
- 1310 Simon-Labric, T., Rolland, Y., Dumont, T., Heymes, T., Authemayou, C., Corsini, M., and Fornari, M.:  $^{40}\text{Ar}/^{39}\text{Ar}$  dating of Penninic Front tectonic displacement (W Alps) during the Lower Oligocene (31–34 Ma), *Terra Nov.*, 21, 127–136, 2009.
- Sinclair, H. D.: Tectonostratigraphic model for underfilled peripheral foreland basins: An Alpine perspective, *Bull. Geol. Soc. Am.*, 109, 324–346, 1997.
- Sinclair, H. D. and Allen, P. A.: Vertical versus horizontal motions in the Alpine orogenic wedge: Stratigraphic response in
- 1315 the foreland basin, *Basin Res.*, 4, 215–232, <https://doi.org/10.1111/j.1365-2117.1992.tb00046.x>, 1992.

- Sissingh, W.: Tertiary paleogeographic and tectonostratigraphic evolution of the Rhenish Triple Junction, *Palaeogeogr. Palaeoclimatol. Palaeoecol.*, 196, 229–263, 2003.
- Smeraglia, L., Looser, N., Fabbri, O., Choulet, F., Guillong, M., and Bernasconi, S. M.: U-Pb dating of middle Eocene-middle Pleistocene multiple tectonic pulses in the Alpine foreland, *Solid Earth Discuss.*, [preprint], [https://doi.org/10.5194/se-2021-](https://doi.org/10.5194/se-2021-2)  
1320 2, 1–14, 2021.
- Steininger, F. F., Berggren, W. A., Kent, D. V., Bernor, R. L., Sen, S., and Agusti, J.: Circum-Mediterranean Neogene (Miocene and Pliocene) marine-continental chronologic correlations of European mammal units, in: *The Evolution of Western Eurasian Neogene Mammal Faunas*, edited by Bernor, R. L., Fahlbusch, V., Mittmann, H-W., Columbia Univ. Press, New York, 7-46, <https://doi.org/10.7916/D86D63B1>, 1996.
- 1325 Suppe, J., Chou, G. T., and Hook, S. C.: Rates of folding and faulting determined from growth strata, in: *Thrust tectonics*, edited by McClay, K. R., Springer, 105–121, 1992.
- Wade, B. S., Pearson, P. N., Berggren, W. A., and Pälike, H.: Review and revision of Cenozoic tropical planktonic foraminiferal biostratigraphy and calibration to the geomagnetic polarity and astronomical time scale, *Earth-Science Rev.*, 104, 111–142, 2011.
- 1330 Watkins, H., Butler, R. W. H., and Bond, C. E.: Using laterally compatible cross sections to infer fault growth and linkage models in foreland thrust belts, *J. Struct. Geol.*, 96, 102–117, 2017.
- Young, J. R., Bown, P. R., Lees, J. A.: Nannotax3 website. International Nannoplankton Association, <http://www.mikrotax.org/Nannotax3>, 2017.
- Ziegler, P. A.: Evolution of the Arctic-North Atlantic and the Western Tethys: A visual presentation of a series of  
1335 Paleogeographic-Paleotectonic maps, *AAPG Mem.*, 43, 164–196, 1988.
- Ziegler, P. A.: Geological atlas of western and central Europe, 1990.
- Ziegler, P. A.: Cenozoic rift system of Western and Central-Europe-an overview, *Geol. en Mijnb.*, 73, 99–127, 1994.
- Ziegler, P.A. and Dèzes, P.: Cenozoic uplift of Variscan Massifs in the Alpine foreland: Timing and controlling mechanisms. *Global and Planetary change*, 58, 237–269, 2007.

1340